AFWAL-TR-83-3006

LANN WING TEST PROGRAM: ACQUISITION AND APPLICATION OF UNSTEADY TRANSONIC DATA FOR EVALUATION OF THREE-DIMENSIONAL COMPUTATIONAL METHODS

J.B.Malone
S.Y.Ruo

LOCKHEED-GEORGIA COMPANY
86 South Cobb Drive
Marietta,Georgia 30063

February 1983
Report for Period May 1980 - February 1983

FLIGHT DYNAMICS LABORATORY
AIR FORCE WRIGHT AERONAUTICAL LABORATORIES
AIR FORCE SYSTEMS COMMAND
WRIGHT-PATTERSON AIR FORCE BASE,OHIO 45433

NOTICE

When Government drawings, specifications, or other data are used for any purpose other than in connection with a definitely related Government procurement operation, the United States Government thereby incurs no responsibility nor any obligation whatsoever; and the fact that the government may have formulated, furnished, or in any way supplied the said drawings, specifications, or other data, is not to be regarded by implication or otherwise as in any manner licensing the holder or any other person or corporation, or conveying any rights or permission to manufacture use, or sell any patented invention that may in any way be related thereto.

This report has been reviewed by the Office of Public Affairs (ASD/PA) and is releasable to the National Technical Information Service (NTIS). At NTIS, it will be available to the general public, including foreign nations.

This technical report has been reviewed and is approved for publication.

Lawrence J. Huttsell

LAWRENCE J. HUTTSELL
Aerospace Engineer
Aeroelastic Group
Analysis & Optimization Branch

Fred A. Picchioni

FREDERICK A. PICCHIONI, LT COL, USAF
Chief, Analysis & Optimization Branch
Structures & Dynamics Division

FOR THE COMMANDER

Olsen, for

RALPH L. KUSTER, JR, COL, USAF
Chief, Structures & Dynamics Division

"If your address has changed, if you wish to be removed from our mailing list, or if the addressee is no longer employed by your organization please notify AFWAL/FIBR, *W-PAFB, OH 45433 to help us maintain a current mailing list".*

Copies of this report should not be returned unless return is required by security considerations, contractual obligations, or notice on a specific document.

UNCLASSIFIED

SECURITY CLASSIFICATION OF THIS PAGE (When Data Entered)

REPORT DOCUMENTATION PAGE		READ INSTRUCTIONS BEFORE COMPLETING FORM
1. REPORT NUMBER AFWAL-TR-83-3006	2. GOVT ACCESSION NO. AD-A130 701	3. RECIPIENT'S CATALOG NUMBER
4. TITLE (and Subtitle) LANN WING TEST PROGRAM: ACQUISITION AND APPLICATION OF UNSTEADY TRANSONIC DATA FOR EVALUATION OF THREE-DIMENSIONAL COMPUTATIONAL METHODS		5. TYPE OF REPORT & PERIOD COVERED Final Report May 1980 - February 1983
		6. PERFORMING ORG. REPORT NUMBER LG83ER0075
7. AUTHOR(s) J. B. Malone S. Y. Ruo		8. CONTRACT OR GRANT NUMBER(s) F33615-80-C-3212
9. PERFORMING ORGANIZATION NAME AND ADDRESS LOCKHEED CORPORATION Lockheed-Georgia Company Marietta, Georgia 30063		10. PROGRAM ELEMENT, PROJECT, TASK AREA & WORK UNIT NUMBERS PE: 62201F PROJ/TASK/WU: 2401/04/37
11. CONTROLLING OFFICE NAME AND ADDRESS Air Force Wright Aeronautical Laboratories/FIBRC Wright Patterson Air Force Base, OH 45433		12. REPORT DATE February 1983
		13. NUMBER OF PAGES 125
14. MONITORING AGENCY NAME & ADDRESS(if different from Controlling Office)		15. SECURITY CLASS. (of this report) Unclassified
		15a. DECLASSIFICATION/DOWNGRADING SCHEDULE

16. DISTRIBUTION STATEMENT (of this Report)

Approved for public release; distribution unlimited

17. DISTRIBUTION STATEMENT (of the abstract entered in Block 20, if different from Report)

18. SUPPLEMENTARY NOTES

19. KEY WORDS (Continue on reverse side if necessary and identify by block number)

Unsteady Aerodynamics
Transonic Flow
Wind-Tunnel Test
Computational Aerodyuamics

20. ABSTRACT (Continue on reverse side if necessary and identify by block number)

This report describes the LANN (Lockheed, AFWAL, NASA-Langley, and NLR) wind tunnel test program. The objective of this program was to acquire a comprehensive experimental data base on a modern, transport type wing in steady and unsteady transonic flow. Details of the model geometry and structural properties are documented. Initial correlations of portions of this data base with numerical results generated by two state-of-the-art computational aerodynamics computer programs are presented.

DD FORM 1 JAN 73 1473 EDITION OF 1 NOV 65 IS OBSOLETE

UNCLASSIFIED

SECURITY CLASSIFICATION OF THIS PAGE (When Data Entered)

FOREWORD

This report was prepared by the Lockheed-Georgia Company for the Air Force Wright Aeronautical Laboratory, Flight Dynamics Laboratory, Wright-Patterson AFB, Ohio. The wind tunnel tests described herein were conducted by NLR of the Netherlands under AFOSR Grant No. 80-0136. The program coordination and the data correlation tasks were performed under Contract F33615-80-C-3212 and Work Unit 24010237. The AFWAL Program Monitor was Mr. L. J. Huttsell of the Analysis and Optimization Branch, Structures and Dynamics Division.

The research activities associated with the design, fabrication, and static measurements of the wind tunnel model were performed under Lockheed-Georgia's Independent Research and Development Program and have been included in this report for completeness.

This effort was jointly sponsored by NASA-Langley. Computer time for data correlations was also provided on the NASA-Langley Research Center Cyber 203 computer, through the Unsteady Aerodynamics Branch, Dr. John W. Edwards, Branch Chief. Mr. Robert Hess of the Unsteady Aerodynamics Branch was the NASA Program Monitor.

This report is also identified as LG83ER0075 for Lockheed internal control purposes.

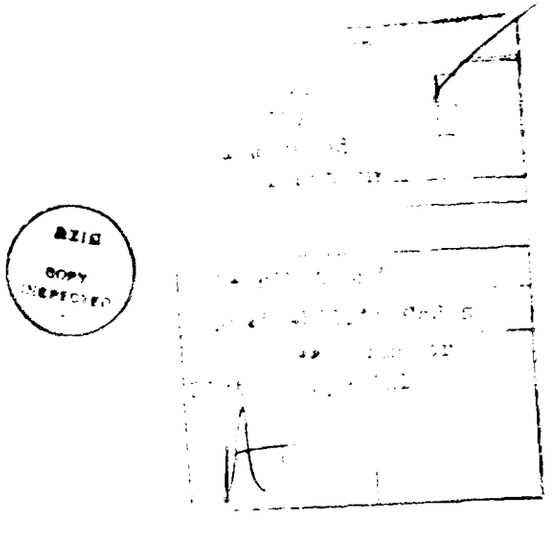

TABLE OF CONTENTS

LIST OF ILLUSTRATIONS (Continued)

LIST OF ILLUSTRATIONS (Continued)

LIST OF ILLUSTRATIONS (Continued)

LIST OF ILLUSTRATIONS (Continued)

LIST OF TABLES

LIST OF SYMBOLS

SYMBOL		DEFINITION
A.C.	-	aerodynamic center
ALPHA, α , α_o	-	mean angle of attack in degrees
AMP, $\Delta\alpha$	-	amplitude of oscillation in degrees
B-B	-	Bailey-Ballhaus steady flow computer program
B-B/M	-	Bailey-Ballhaus/McNally steady flow computer program with viscous effects
c	-	local chord
c_{AC}	-	mean aerodynamic chord
c_l	-	sectional lift coefficient
C_L	-	total lift coefficient based on model planform area
C_M	-	total moment coefficient about wing aerodynamic center based on model planform area
C_N	-	wing normal force coefficient based on model planform area
C_p	-	pressure coefficient
COMP	-	conditions used in numerical computations
EA	-	elastic axis
EI	-	model bending stiffness ($lb\text{-}in^2$)
f	-	frequency (Hertz)
FCR	-	fully conservative finite difference algorithm
GJ	-	model torsional stiffness ($lb\text{-}in^2$)
k	-	reduced frequency based on wing root chord
MACH, M_∞	-	freestream Mach number
REYN	-	Reynolds number
TEST	-	conditions used in experimental measurement
X	-	coordinate in freestream direction
XTRAN3S	-	Boeing/NASA-Langley steady/unsteady flow computer program

LIST OF SYMBOLS (Continued)

SYMBOL		DEFINITION
Y	-	coordinate in spanwise direction
Z	-	coordinate in direction normal to wing planform
η	-	spanwise station expressed as fraction of wing semi-span
ω	-	circular frequency (radians)

SECTION I
INTRODUCTION

Modern transport aircraft generally require the use of high-aspect-ratio wings and, as a result, can experience significant aeroelastic effects during flight. These effects range in severity from induced aeroelastic twists that modify rigid aircraft airload distributions to flutter phenomena which may cause the castastropic destruction of aircraft controls and lifting surfaces. Thus, the accurate prediction of potential aeroelastic problems, especially flutter instabilities, is an important factor in the production of safe, efficient flight vehicles.

The availability of accurate computational aerodynamics methods is critical to the successful development of reliable aeroelastic prediction techniques. In the past decade, the production of larger, high-speed computers and advances in computational fluid dynamics have led to the development of improved numerical aerodynamic analysis procedures. One of the major objectives of these research efforts has been the development of analysis methods for unsteady transonic flows. This emphasis is due, in part, to the potential performance improvements which can be obtained with transonic cruise aircraft.

New computational methods have recently been developed for calculating both two- and three-dimensional unsteady transonic flows. In two dimensions, these new codes include moderate- frequency extensions of LTRAN2 (Reference 1), full-potential equation solvers (References 2-6), and linear methods with shock-wave motion approximations (References 7, 8). For three-dimensional flow solutions, time-accurate computer programs are currently in the developmental stage at Boeing (Reference 9), the Lockheed-Georgia Company (Reference 10), NASA-Ames (Reference 11), and the NAL (Reference 12).

Because of these research programs, new codes are reaching a level of development which warrants correlation with test data. A systematic

correlation effort will help to establish code accuracies, efficiencies, and ranges of applicability. In addition, such correlations are necessary to provide the insight required for further code refinements.

Unfortunately, unsteady experimental data suitable for code correlation efforts are scarce, and are virtually non-existent for advanced-technology wings at transonic speeds. Although experiments (Reference 13) have been conducted at NASA-Langley for a supercritical transport wing with oscillating control surfaces, further experimental research is needed to investigate additional unsteady motions, such as wing pitching and bending oscillations.

To meet this need, a cooperative program was initiated in 1979 to produce unique unsteady transonic aerodynamic data on an aft-loaded 3-D transport aircraft type wing. This program resulted from common interest at Lockheed-Georgia, AFWAL, NASA-Langley and the NLR in the acquisition of high-quality test data to validate new computational methods and to provide insight into 3-D unsteady transonic flow phenomena. This cooperative effort has become known as the LANN program.

The major objectives of the LANN test program were to:

(1) Fabricate a model representative of a modern technology transport wing and suitable for unsteady testing in both the HST tunnel at the NLR Amsterdam and in the NTF facility at NASA-Langley.

(2) Acquire a set of high-quality, correlation-tailored, transonic test data for steady and unsteady flow conditions in the HST tunnel.

(3) Utilize selected portions of these data to correlate theoretical results from several 3-D transonic-flow computer programs.

Under the LANN program agreement, AFWAL monitored and controled the

program, and, together with NASA-Langley, provided partial funding to NLR and Lockheed. Lockheed received contract support for program coordination, data correlation, and preparation of the final program report. The design, fabrication, and static measurements of the model were funded under Lockheed-Georgia's Independent Research and Development program. The National Aerospace Laboratory designed and fabricated the wing mount, performed the wind tunnel tests, and prepared the final test data report. Finally, NASA-Langley provided computer time and made available to Lockheed an improved version of the Boeing Company's XTRAN3S code during the data correlation phase of the LANN program.

This report describes the work performed under the LANN program from May 1980 to February 1983. The first section describes the model design objectives, geometric details, instrumentation, and structural properties. The next two sections discuss the test facility, data acquisition and reduction methods, and the tunnel test program. Finally, correlations of selected test results with numerical computations obtained from several advanced, transonic-flow computer programs are presented to assess the accuracy and efficiency of the evaluated codes.

SECTION II
LANN MODEL DESCRIPTION

The wing geometry chosen for the LANN program was a large scale version of a wing previously designed and tested by the Lockheed-Georgia Company under funding from the AFOSR (Reference 14). This wing geometry, designated Wing A in Reference 14, was picked for the LANN unsteady tests for several reasons. First, Wing A was representative of a modern-technology transport wing (i.e. high aspect ratio, moderate wing sweep and twist, supercritical airfoil sections). Second, an extensive, steady transonic-flow data base for this geometry was available to guide planning of the unsteady test program. Finally, the simple planform used in the Wing A design would facilitate fabrication of the model and eliminate the question of geometric complexity when evaluating numerical results obtained from new transonic flow computer codes.

1. MODEL DESIGN

The LANN wing model was designed to satisfy several different test program objectives. Consideration of these objectives determined the structural materials, fabrication techniques, and types of instrumentation used in the final model design.

A major objective of the LANN program was to produce a wing model suitable for testing both in the High Speed Wind Tunnel (HST) at NLR and in the cryogenic National Transonic Facility (NTF) at NASA-Langley. This last requirement demands that the model be strong and stiff enough for unsteady tests at cryogenic temperatures. To be acceptable for NTF testing, NASA has specified certain minimum requirements for fracture toughness at cryogenic temperatures which cannot be met with steels ordinarily used for wind tunnel testing. Therefore, in order to meet NASA standards, the LANN model was fabricated from Nitronic 40 Stainless Steel. This material was chosen for the following reasons:

(1) acceptable strength at room temperatures
(2) good strength at cryogenic temperatures
(3) good toughness at cryogenic temperatures
(4) easier to machine than other materials considered
(5) better corrosion resistance than other materials considered

Also, since the NTF tunnel entry date is expected to occur after 1984, the possibility for retrofit of model instrumentation was an important design constraint. Therefore, to permit access to the wing instrumentation, the model was constructed with a lower cover plate attached to the upper half of the wing by taper pins and screws.

Finally, the possibility of future research applications for the LANN wing was considered in the design of the model. To satisfy this objective, the LANN model design incorporates provisions for active aileron,wing/pylon/nacelle, and wing/winglet configurations. These provisions include:

(1) a detachable aileron with space inside the model for an aileron oscillator and provision for static aileron deflection testing.
(2) hard points for future addition of a pylon and nacelle.
(3) hard points for future addition of wing tip devices (winglets, rails, etc.).

2. MODEL GEOMETRY

The LANN model planform is shown in Figure 1. The wing has straight leading and trailing edges. The planform aspect ratio, leading edge sweep, and wing taper ratio are typical of modern transport wing designs. Geometric parameters for the model are listed in Table 1.

The location and dimensions of the aileron cutout are also shown in Figure 1. For the present clean wing tests, an aileron was installed in

the wing cutout. This aileron was fixed at a zero degree deflection by two brackets attached to the upper portion of the wing model. The hardpoint locations for mounting a pylon or wing tip device are likewise indicated in Figure 1.

The model assembly is illustrated in Figure 2. The inside surfaces of the two wing halves were designed to provide space within the model for the necessary test instrumentation.

The airfoil sections used in this wing design are from a family of supercritical airfoils developed by the Lockheed-Georgia Company. The wing shape is defined by two control stations; one at the wing root and the other at the wing tip. The wing design ordinates for intermediate span stations were generated by linear loft between the wing root and tip. The control station airfoil shapes are shown in Figure 3.

To insure an accurate definition of the LANN wing model geometry, measured airfoil coordinates were obtained at eight span stations on the model. These data are given in Tables 2 thru 9. In the tables, measured ordinates and corresponding chordwise locations are non-dimensionalized with respect to local chord.

3. MODEL INSTRUMENTATION

In order to provide a data base which could be used to verify transonic-flow computer codes, the LANN model was instrumented to measure surface pressures at a large number of locations on the wing. A total of 240 static pressure orifices were positioned in chordwise rows at 6 wing span stations. One hundred and forty-four orifices were located on the wing upper surface, while the remaining 96 orifices were placed on the lower surface cover plate. The spanwise locations of the pressure orifice rows are shown in Figure 4. The chordwise locations of the pressure orifices are given in Table 10.

Two rows of static pressure orifices are located on the inboard region of the wing where a double shock formation was expected based on earlier Wing A tests (Reference 14). The first row is at 20-percent semispan and the second row is at 32.5-percent semispan. The pylon/nacelle hardpoint is located at the 40-percent semispan. Rows of pressure orifices would be desirable on either side of the pylon, so the 32.5-percent row was mirrored with a third row at the 47.5-percent semispan. A fourth orifice row was located at the center of the fixed wing aileron, while the 47.5-percent row was mirrored with a fifth row at the 82.5-percent location. Finally, the sixth static pressure orifice row was positioned near the wing-tip at 95-percent semispan.

Equal length stainless steel tubes were connected to each pressure orifice from inside the wing internal cavity. The tubes were soldered at the orifices with a material which is suitable for a cryogenic test environment. The tubes were then routed out of the wing root, along channels milled into the internal surfaces of both the upper and lower surface cover plates. Finally, the tubes were divided into several groups, each group being attached to an electronic scanning valve.

Additional pressure sensing instrumentation consisted of 22 individual Endevco dynamic pressure transducers. These pressure transducers were positioned along the wing span in two chordwise rows. The spanwise locations of these transducers is shown in Figure 4 and the chordwise locations are listed in Table II. Each transducer was located approximately .005 inch to one side of an existing pressure tube orifice and fastened by holders attached to the inside of the upper surface plate. The wire leads for each transducer were shielded by stainless steel tubing and routed out of the wing root.

Surface pressure measurements on the LANN model were made using the ESP measurement technique. This method is particularly well suited to handle a large number of pressure data at a relatively low cost. The principle of this technique is to use conventional static pressure

tube/scanning valve instrumentation for dynamic as well as static measurements. In the steady case the pressure at the surface orifice is recorded directly. For unsteady flow cases, however, the tube geometry, mean pressure level, compressibility effects, and frequency of the pressure fluctuation play a significant role in the dynamic response of the measuring system. Therefore, during unsteady testing, the pressure measured at the scanning valve had to be adjusted in magnitude and phase to correspond to the actual pressure at the model surface. To determine the necessary tube response corrections, the actual transfer functions of a few reference tubes were measured with the in-situ Endevco transducers. The measured transfer functions were then used to calibrate the remaining pressure tube responses. Further details of the NLR unsteady pressure measurement technique are given in Reference 15.

During unsteady testing, the model aeroelastic mode shape was measured using 12 accelerometers and one LVDT. The LVDT was positioned near the wing root station and was used to monitor the amplitude and frequency of the motion input to the model. The accelerometers were located in chordwise rows at 4 wing span stations. The placement of these accelerometers on the wing planform is shown in Figure 4 and the chordwise locations are listed in Table 12. The wire leads to each accelerometer were routed outside of the model through stainless steel tubing.

4. MODEL STRUCTURAL PROPERTIES

During unsteady tests, the aeroelastic mode shape of the LANN model was measured directly using in-situ accelerometers. However, for steady flow conditions, no similar direct measurement of the model static aeroelastic deformation was made. Therefore, in order to permit an estimation of static aeroelastic effects on the LANN wing, model stiffness distributions were measured after aerodynamic testing in the NST facility. This effort was funded under Lockheed's Independent Research and Development program. The model structural data is reported here to provide a more complete data base for the LANN test program.

For the model stiffness measurements, it was assumed that the gross structural properties of the LANN wing could be adequately modeled using a beam representation. This assumption is based upon a consideration of the following items:

(1) wing aspect ratio
(2) Nitronic 40 structural properties
(3) wing thickness distribution
(4) intended use of stiffness data (i.e. estimation of primary aeroelastic twist effects)

The elastic axis of this beam model was assumed to lie along the 38% chord line of the wing. This location for the elastic axis was chosen based on a graphical analysis of the wing sectional area distributions. This analysis also accounted for the internal model cavities along the wing span.

The stiffness properties of the LANN wing were measured using conventional force-deflection techniques. These measurements were obtained at wing span locations shown in Figure 5. A torque bar attached to the wing tip was used to apply known forces and moments at the elastic axis location. Rotation angles were then measured using a light beam which was reflected onto a fixed grid pattern from mirrors attached to the wing along the elastic axis. The laboratory setup for this test permitted slope measurements within .004 degree.

The wing EI and GJ distributions were obtained by first plotting the measured values of bending and torsional slopes versus span location, passing smooth curves through this data, and then determining, graphically, the derivatives of these curves at selected intervals. The resulting bending and torsional stiffness distributions, EI and GJ, are given in Table 13 and plotted in Figures 6 and 7.

The beam model representation for the LANN wing was verified by

comparison of computed and measured vibration characteristics of the model. The 10 lowest cantilever wing modes and frequencies were measured using an impact analyzer. The first four of these modes are shown in Figure 8. Next, mass and inertia distributions were calculated for the wing model. These data are given in Table 14. Finally, the measured EI and GJ distributions, together with the calculated mass properties, were used to compute an estimate of the lowest four wing modes. A comparison of measured and calculated natural frequencies is given in Table 15. Also shown in this table are the four lowest wing-in-mount modes measured by the NLR. A comparison of the NLR and Lockheed test results gives an indication of the effects of wing/mount flexibility on the wing vibration characteristics.

SECTION III
TEST FACILITY

Tests of the LANN wing model were performed in the transonic wind tunnel (HST) of the National Aerospace Laboratory (NLR), Amsterdam. This is a closed circuit wind tunnel with a test section of 1.6 x 2.0 meters and a velocity range of M_∞ = 0.0 to M_∞ = 1.28. Typical Reynolds numbers of 5×10^6 based on mean aerodynamic chord were attained on the model during testing.

The wing model was attached to a support that was mounted at the side wall of the tunnel test section. This support mechanism was designed and built by the NLR. The mean angle of attack of the model could be adjusted remotely over a ±3 degree range with respect to a preset reference angle. This reference angle for the wing mount was adjusted by rotating the mounting system with respect to the tunnel centerline.

The support also permitted wing oscillations in pitch about an axis normal to the tunnel side wall. The pitch axis intersected the wing root at a position 62.1% of chord aft of the leading edge. For unsteady testing the model was driven by a hydraulic exciter which was controlled by a variable frequency oscillator. The amplitude of oscillation could be varied by adjusting the travel distance of the hydraulic exciter shaft. The amplitude of oscillation could be adjusted up to ±1.0 degree, while the frequency could be varied between 0 and 72 Hertz. Figure 9 illustrates the wing/mount mechanism. The wing is shown installed in the HST facility in the photograph of Figure 10.

A schematic of the NLR's data acquisition and reduction system called PHAROS (Processor for Harmonic Analysis of the Response of Oscillating Surfaces) is shown in Figure 11. The PHAROS system is an accurate computer controlled multichannel transfer function analyzer. This system is capable of on-line analysis of incoming data from 40 channels, measured simultaneously. A complete description of the system can be found in Reference

16 from which Figure 11 is adapted to reflect the LANN test equipment configuration.

A unique feature of the PHAROS system is the capability for rapid on-line data reduction during testing. Output quantities from the PHAROS system are the zeroth (steady component) and the real and imaginary components of the first harmonic of the unsteady pressures. In addition, higher harmonic contributions can be measured when required. Section lift and moment coefficients are also obtained by integration of surface pressure distributions.

SECTION IV
LANN TEST PROGRAM

The wind tunnel tests of the LANN model were performed in the HST on December 14-17, 1981. The test schedule was chosen to provide aerodynamic data for variations of the following parameters:

(1) Mach number
(2) Mean angle-of-attack
(3) Amplitude of pitch oscillations
(4) Frequency of pitch oscillations

The tests covered a Mach number range between $M_\infty = 0.62$ and $M_\infty = .95$. Mean angles-of-attack of between -.4 to 6.0 degrees were examined. For unsteady tests, the amplitude of oscillation ranged between +.25 and +1.0 degrees. The reduced frequency, based on wing root chord, was varied between $k = 0.0$ and $k = 1.0$. A total of 217 steady and unsteady test runs were made in the HST facility. For these tests, transition was fixed by application of a grit strip on the upper and lower wing surfaces. To simulate the Wing A transition location, the grit strips were positioned .71 inches aft and parallel to the leading edge. Each grit strip was 2 mm in width and consisted of 62 micron diameter carborundum 220 grit.

The tunnel test conditions for the LANN wing are summarized in Figure 12. The Figure shows the lift coefficient versus Mach number variation for each mean angle-of-attack examined in the test program. Also shown in the figure are the conditions for which frequency sweep and quasi-steady data were obtained.

Values of the parameters used in each test run are indicated in Tables 16 through 21 which are adapted from Reference 17. Table 16 lists the test parameters and corresponding run ID numbers for the steady-flow conditions. Tables 17 and 18 list similar information for the unsteady test conditions. The basic unsteady schedule, shown in Table 17, was performed with a

constant ±.25 degree amplitude of oscillation. Additional unsteady data to examine the effects of amplitude variation and the significance of higher harmonics are itemized in Table 18. Finally, test run numbers and flow parameters are listed in Tables 19-21 for quasi-steady conditions and a number of miscellaneous unsteady test conditions.

A complete description of the experimental data obtained and data presentation formats for the LANN wing can be found in the NLR final test report (Reference 17). Among the data recorded in the report for each test condition are the following items:

(1) Reynold's number
(2) Mach number
(3) Mean angle-of-attack
(4) Frequency of oscillation
(5) Amplitude of oscillation
(6) Chordwise pressure distributions
(7) Sectional lift and moment coefficients
(8) Total wing lift and moment coefficients
(9) Unsteady aeroelastic mode shape

The majority of the LANN wing aerodynamic data was obtained for attached flow conditions. However, for steady flow, an angle of attack sweep was made at $M_\infty = .82$ to provide separated flow pressure data at transonic conditions. In addition, unsteady separated flow data was obtained for subcritical and supercritical conditions.

SECTION V
DATA CORRELATION

In 1977, the Air Force Systems Command initiated a program with the Boeing Military Aircraft Company to develop practical computational methods for the analysis of unsteady transonic flows over clean three-dimensional wings. As a result of this research effort, a pilot computer program, known as XTRAN3S (Reference 18), has recently been released to the Air Force and NASA laboratories.

The XTRAN3S computer program as well as the computer resources used in this data-correlation effort were provided by NASA-Langley. This program contains several improvements, namely a new computational grid distribution and code vectorization, made by the personnel of NASA-Langley. The latter improvement shortens the computer run time in comparison to the original program.

In addition to XTRAN3S, a computer program developed in 1979 under a Lockheed-Georgia IRAD project, which coupled a small disturbance steady flow wing code of Bailey-Ballhaus (Reference 19), with a two-dimensional boundary-layer code of McNally (Reference 20) was used for steady flow data correlation. This program allows the selection of any number of pre-determined span-stations where weak coupling of the boundary-layer is desired. Also, the program user may specify the number of times that boundary layer calculations are performed during the iterative solution procedure. This feature permits the user to reduce computer run times for cases where boundary layer effects are not expected to significantly modify the outer potential flow solution.

The airfoil-section geometry used in the XTRAN3S code was interpolated from polynomials fitted to the measured wing ordinates that are shown in Figure 13. This is regarded as the reference position of the wing. As can be seen in the figure, the static twist of the wing, which is a counter-clockwise twist from the root to the tip, is included in the wing

reference geometry. For Wing A, on the other hand, no wing twist is included in the wing reference geometry and the wing twist distribution needs to be included in the input data set for code correlation. The same geometry used in XTRAN3S was also used as input for Bailey-Ballhaus/McNally (B-B/M) code to maintain consistency of the ordinates used in computations.

A grid of 13 span stations by 39 points along each span station was used in the computation with XTRAN3S code and a grid of 25 by 33 was used in the B-B/M code.

In the XTRAN3S program, one of the options that a user can choose is the set of coefficients for the small disturbance equation used in the program. These coefficient sets are designated as NLR, Ames, classical and linear. Another option for the type of equation that a user can choose is either to include the second derivative term of velocity potential with respect to time for high frequency cases, or to neglect it for low frequency cases. Only limited effort was made in this study to examine the effects of these different options on the final solution due to the limitations in the available computer resources. With the exception of several analyses made using the NASA-Ames coefficients, all of the calculations made in this study were with NLR coefficients and low frequency options for steady flow and the high frequency option for unsteady flow.

The majority of the code correlations, both steady and unsteady, which are presented in this section are centered around the design conditions of Mach number = 0.82 and mean angle of attack = 0.60 degrees.

1. STEADY FLOW

In the following, the code correlation results using the test data of both the LANN Wing (Reference 17) and Wing A (Reference 14) and the computed results of XTRAN3S and B-B/M codes are presented. For steady flow calculations, the XTRAN3S program, which was developed using the unsteady form of the small disturbance equation, treats the flow as a transient

flow. The flow is impulsively started from rest at time zero and the computation is continued until all transients have either completely or nearly disappeared. For convenience, the term "chords-travelled" is used in this report to describe the state of numerical computation or the distance in terms of the wing root-chord that the wing has travelled during the computation. The number of chord lengths traveled refers to Δt * number of iterations. A good illustrative example of this is shown in Reference 21, page 285.

Two comparison runs for the steady flow design conditions were made with the XTRAN3S code to determine which coefficient set, either Ames or NLR, is more suitable for the LANN wing. The computed results along a number of selected span-stations, after 40 chords travelled, are shown in Figure 14. The time step sizes used were 0.04 and 0.025 for runs using Ames and NLR coefficients, respectively. The calculated results at mid semi-span station and the experimental data at 0.475 semi-span station are shown in Figure 15. As can be seen from these figures, the effect of using different coefficient-sets is mainly in the shock location on the wing. The shock location of the results obtained using NLR coefficients is downstream of that obtained from the Ames coefficients and is closer to the experimental results. Therefore, NLR coefficients were used in all other runs with the XTRAN3S code, including the unsteady runs.

The time histories of the wing normal force for several typical runs are shown in Figure 16. The numerical results seem to have converged after 500 time steps (approximately 20 to 40 chord lengths, dependent on time step); however, the results may show a low amplitude, low frequency numerical oscillation as time progresses further. Since the variation of the results with respect to time is so small, one may accept the results as converged at any point after the 500th time step without incurring a significant error.

Figures 16(a) and 16(b) respectively show the typical convergence pattern of a low and a high Mach number flow conditions. The time step sizes used were respectively 0.025 and 0.04. The low Mach number case

converged in less than 200 iterations whereas for the high Mach number it took about 400 iterations. The convergence pattern for these two cases is noticeably different. Whether the difference in the convergence pattern shown in these two figures was caused by the different time step size used in these two runs or the difference in the shock strength in the flowfield has not been investigated. However, one would suspect that the shock strength has more to do with the convergence pattern than the integration time step size used.

Figures 16(c) and 16(d) show the convergence pattern of one analysis (Mach number = 0.82 and mean angle of attack = 0.85 degrees) started from a uniform flow and the other from a set of convergent results for different flow conditions (Mach number = 0.82 and mean angle of attack = 0.6 degrees). The time step size used was 0.04 for both runs. The converged normal force for the wing shown in Figures 16(c) and 16(d) is 0.39 and 0.383, respectively. The numerical results differ slightly but the difference in the number of iterations required is quite significant, that is 800 versus 300. Therefore, it appears to be that if a slight error in the final solution is tolerable, a start from an already converged result may significantly reduce computer run costs.

The converged steady flow results from the XTRAN3S code for the design conditions are shown in Figure 17 which also includes the LANN wing experimental data. The computation was made with a time step size of 0.04 and iterated for 1200 time steps. The code tends to under-estimate the suction on the upper surface. However, there is good agreement in shock locations and pressure recovery behind the shock except near the wing tip. The agreement of the pressure distribution on the lower surface, in general, is fairly good, but the comparison, as on the upper surface, also deteriorates near the tip.

A similar comparison with the results obtained from the inviscid and viscid options of B-B/M code is shown in Figure 18. The boundary layer effects tend to lower the suction peak and move the shock wave forward.

When the flow is not separated, the boundary-layer effects do not appear to be very large. The correlation of the results obtained from the B-B/M code, as in the XTRAN3S case, is not very satisfactory near the tip. Although a strip boundary layer approximation is adequate in the mid span region of moderately swept high aspect ratio wings, an accurate prediction of viscous effects at the wing tip would require the use of a fully 3-D boundary-layer method.

The pressure coefficient distributions of the wing shown in Figures 17 and 18 are combined and shown in Figure 19 where the results from three methods are compared with the experimental data. In the figure, the B-B indicates the inviscid option of the B-B/M code. The suction peak of XTRAN3S code correlates better with the measured data near the wing tip. However, the B-B or B-B/M codes show better agreement with data away from the tip.

In order to calculate quasi-steady pressure distributions, two additional steady-flow conditions were computed using both the XTRAN3S and the B-B codes. For these analyses, the mean angle of attack was perturbed by ±0.25 degree from the design condition of 0.6 degree. Shown in Figures 20 and 21 are the results obtained respectively from the XTRAN3S and B-B codes for a Mach number of 0.82 and mean angles of attack of 0.35, 0.60 and 0.85 degree at span-stations where measured data are available. The results obtained from the XTRAN3S code showed a strong nonlinear effect, especially the shift of shock location. A smaller change in the mean angle of attack may be necessary to use XTRAN3S code for the quasi-steady analysis.

The effect of the mean angle of attack on the normal force and moment of the wing at a fixed Mach number ($M_\infty = 0.82$) is shown in Figures 22 and 23. A difference in the slope and zero lift angle of the measured normal force for LANN Wing and Wing A can be seen in Figure 22(a). The difference in the Wing A and LANN data are most likely due to wind tunnel wall interference effects or to the type of tunnel wall configuration used

during testing (porous versus slotted walls). This figure also shows that the slope remains nearly constant for both LANN Wing and Wing A until the angle of attack is greater than 3.0 degrees beyond which the flow starts to separate from the mid span.

Figure 22(b) shows the computed variation of the LANN wing normal force with the mean angle of attack at a fixed Mach number. The agreement with the experimental data at lower angle of attack was very good but the numerical methods failed to generate meaningful results when the strong flow separation took place. A similar comparison of the pitching moment coefficient, about the aerodynamic center (see Figure 1), is shown in Figure 23. The agreement of the viscid results of B-B/M code with the measured data is very good at lower angle of attack, while the agreement is only fair for the inviscid results of B-B and XTRAN3S codes.

The normal force and moment variation at a fixed mean angle of attack (0.6 degree) with respect to Mach number are shown in Figures 24 and 25, respectively. The agreement between the measured normal force and the results of B-B/M code is very good at lower Mach number. At higher Mach number, the comparison was not possible because of the flow separation. A similar comparison of the pitch moment coefficient, about the aerodynamic center, is shown in Figure 25. The correlation with the experimental data was quite good, as in Figure 23. The span loading at the design Mach number (0.85) for various angles of attack is shown in Figure 26. In general, the B-B/M code gives the best correlation. Finally, pressure distributions at a number of span-stations at 0.6 degree angle of attack at various Mach numbers calculated with XTRAN3S code is plotted in Figure 27. The nonlinear effects due to a change in Mach number seems to be stronger near the wing tip than near the wing root.

2. UNSTEADY FLOW

The data correlations for unsteady transonic flow were performed with XTRAN3S using the option labeled "dynamic analysis of a flexible wing with

specified modal motion". In addition to this, the B-B/M code was used to generate quasi-steady results.

An XTRAN3S run was made to simulate Test Run Number 73 (see Table 22), namely, Mach number = 0.82, mean angle of attack = 0.60 degree, and pitch amplitude = 0.25 degree at 24 cycles per second. The experimentally measured LANN Wing mode shape was used as input for the XTRAN3S run. The unsteady flow results using the converged steady state flow field as the initial conditions attained steady sinusoidal state in less than two cycles of computation. A rather small time step size (0.04265 for a reduced frequency of 0.2046, 720 steps/cycle), however, was required in this example to maintain numerical stability.

Other similar runs were also made at higher frequency, namely 48 Hz and 72 Hz, under the same flow conditions. These two runs were to simulate Test Run Numbers 85 and 87. The time step size for the 48 Hz case was 0.04293 (360 steps/cycle) and that for the 72 Hz case was 0.04283 (240 steps/cycle). The time history of the wing normal force is shown in Figures 28(a), (b) and (c) for Test Runs 73, 85, and 87, respectively. It is noted that the lower the reduced frequency, the fewer number of cycles are required for the computations to attain the converged steady sinusoidal results. This may be attributed to the fact that wave propagation is inversely proportional to the reduced frequency. At the lower frequency, the effects of boundary conditions, both wing surface and far-field, are fed into the numerical computation faster than the case at higher frequency. Thus, the solution to the boundary value problem is attained at a faster rate. By the same reason, the transient caused by the impulsive start of wing motion at time zero, decayed faster for the low frequency case than for the high frequency case.

The measured wing mode shape as given in Reference 17 consists of contributions from heave and pitch. The contribution from heave, however, is much smaller than that from pitch. A short run was made with the pitch alone by neglecting the contribution from heave. The effect of heave, as

was expected, is insignificant.

One cycle each of the measured normal force variation is shown in Figure 28(d). The mean values and amplitudes of the measured and the calculated data are summarized in Table 22. As can be seen, the agreement between the measured and the computed results is poor.

A comparison of the calculated and measured surface pressures during one cycle of pitch oscillation for Run 85 (reduced frequency 0.40657 or 48 Hz) at the various angular positions is shown in Figure 29, and a comparison of the pressure coefficient along various span-stations at different angular positions is shown in Figure 30. The fluctuation of pressure over the wing during one cycle of pitch oscillation is rather small and the experimental data hardly show any shock movement. The results of XTRAN3S, however, show a 5 to 10 percent shock excursion.

Quasi-steady results obtained from the steady flow data shown in Figures 20 and 21, (at design conditions) are presented in Figure 31. The mean angle of attack was perturbed positively and negatively from the design condition by 0.25 degree. The agreement between the computed and measured data on the lower surface, in general, is much better than that on the upper surface. This obviously is caused by the existence of the shock on the upper surface. The quasi-steady span-loading distribution is shown in Figure 32. None of the computational methods correlated well with the experimental data. The results of B-B/M code appeared to do better than the results obtained from the inviscid XTRAN3S and B-B codes.

SECTION VI
CONCLUSIONS

A high quality experimental data base has been established for a transport type advanced technology wing in the transonic flow regime. This data base has been obtained for both steady and unsteady flow conditions, and includes variations of Mach number, mean angle of attack, pitch oscillation frequency and amplitude. The experimental data contains a large number of attached flow conditions, and should be invaluable for evaluation of current computational methods. In addition, a limited amount of separated flow data, obtained for both steady and unsteady conditions, should provide guidance in developing more versatile computational methods in the future.

A limited number of correlations between the experimental data and computational results have been performed. A comparison of the steady flow results from the XTRAN3S and the inviscid Bailey-Ballhaus codes indicates that, even though both codes were based on the small disturbance assumptions, the Bailey-Ballhaus code gives better agreement with the experimental data than the XTRAN3S code. The inclusion of boundary-layer effects for attached flow conditions, although lowering the overall suction levels, definitely improved agreement with the test data in the region behind the shock.

The XTRAN3S code has a wide variety of options that a user can select. However, only a limited number of options provided in the code have been exercised in the study reported here. A more extensive study for the different user options available in this program, especially for unsteady flow analyses, needs to be performed before a more definitive assessment of XTRAN3S code capabilities can be made. However, there are a few improvements of a more basic nature that may be desirable. These are as follows:

1. Simplification of the restart data file - This modification would avoid

the possibility of either loading a wrong set of input data, or of inadvertently changing data that needs to remain constant throughout on the continuation runs.

2. Modification of spanwise grid input data - This modification would avoid the need of changing the grid distribution for different wings. If an adequate grid distribution is found and this grid is expressed in terms of semi-span instead of the reference chord, then the same data may be used for different wings without any changes.

3. Inclusion of an automatic convergence criterion - At the present time an automatic convergence criteria does not exist in XTRAN3S. Installation of this feature in XTRAN3S would very likely decrease the number of iterations actually performed in getting converged solutions.

REFERENCES

1. K. A. Hessenius and P. M. Goorjian, "A Validation of LTRAN2 with High Frequency Extensions by Comparisons with Experimental Measurements of Unsteady Transonic Flows," NASA TM 81307, July 1981.

2. K. Isogai, "Numerical Study of Transonic Flow Over Oscillating Airfoils Using the Full-Potential Equation," NASA TP1120, NASA-Langley, 1978.

3. I. C. Chang, "Unsteady Transonic Flow Fast Airfoils in Rigid Body Motion," R & D Report DOE/ER/03077-170, Courant Institute of Mathematical Sciences, New York University, March 1981.

4. R. Chipman and A. Jameson, "An Alternating-Direction Implicit Algorithm for Unsteady Potential Flow," presented at AIAA 19th Aerospace Sciences Meeting, Jan. 1981.

5. J. L. Steger and F. X. Caradonna, "A Conservative Implicit Finite Difference Algorithm for the Unsteady Transonic Full Potential Equation," AIAA Paper 80-1368, 13th Fluid & Plasma Dynamics Conference, Snowmass, Col., July 14-16, 1980.

6. J. B. Malone and N. L. Sankar, "Numerical Simulation of 2-D Unsteady Transonic Flows Using the Full-Potential Equation," AIAA Paper No. 83-233, AIAA 21st Aerospace Sciences Meeting, Reno, Nevada, Jan. 10-13, 1983.

7. M. H. Williams, "Unsteady Airloads in Supercritical Transonic Flows," AIAA Paper 79-0767, presented at the 20th Structures, Structural Dynamics and Materials Conference, St. Louis, MO, April 4-6, 1979.

8. M. H. L. Hounjet, "Transonic Panel Method to Determine Loads on Oscillating Airfoils with Shocks," AIAA Journal, Vol. 19, No. 5, May 1981, pp. 559-566.

9. D. P. Rizzetta and C. J. Borland, "Numerical Solution of Three-Dimensional Unsteady Transonic Flow Over Wings Including Inviscid/Viscous Interactions," AIAA Paper No. 82-0352, presented at the AIAA 20th Aerospace Meeting, Orlando, FL., Jan 11-14, 1982.

10. N. L. Sankar, J. B. Malone and Y. Tassa, "An Implicit Conservative Algorithm for Steady and Unsteady Three-Dimensional Transonic Potential Flows," AIAA Paper No. 81-1016, Proceedings of the 5th Computational Fluid Dynamics Conference, Palo Alto, CA., June 22-23, 1981.

REFERENCES (Continued)

11. J. O. Bridgeman, J. L. Steger, and F. X. Caradonna, "A Conservative Finite Difference Algorithm for the Unsteady Transonic Potential Equation in Generalized Coordinates," Paper No. 82-1388, presented at the AIAA 9th Atmospheric Flight Mechanics Conference, August 9-11, 1982.

12. K. Isogai, "Calculation of Unsteady Transonic Potential Flow Over Oscillating Three-Dimensional Wings," NAL-TR-706T, March 1982.

13. M. C. Sandford, et al., "Transonic Unsteady Airloads on an Energy Efficient Transport Wing with Oscillating Control Surfaces," AIAA Paper No. 80-7038, presented at the 21st Structures, Structural Dynamics, and Materials Conference, Seattle, WA., May 12-14, 1980.

14. B. L. Hinson and K. P. Burdges, "Acquisition and Application of Transonic Wing and Far-Field Test Data for Three-Dimensional Computational Method Evaluation," AFOSR-TR-80-0421, Lockheed-Georgia Company, March 1980.

15. H. Tijdeman, "Investigations of the Transonic Flow Around Oscillating Airfoils," NLR-TR-77090U, 1977.

16. J. J. Horsten, "Recent Developments in the Unsteady Pressure Measuring Technique at NLR," National Aerospace Laboratory, NLR MP 81055, 1981.

17. J. J. Horsten, R. G. Den Boer, and R. J. Zwaan, "Unsteady Transonic Pressure Measurements on a Semi-Span Wind Tunnel Model of a Transport-Type Supercritical Wing (LANN Model)," NLR TR82069U, Parts I & II and AFWAL-TR-83-3039 Parts I & II, March 1983.

18. C. J. Borland, and Rizzetta, "Transonic Unsteady Aerodynamics for Aeroelastic Applications. Volume I — Technical Development Summary," AFWAL-TR-80-3107, June 1982.

19. W. F. Ballhaus, F. R. Bailey, and J. Frick, "Improved Computational Treatment of Transonic Flow about Swept Wings," NASA CP-2001, Nov. 1976.

20. W. D. McNally, "Fortran Program for Calculating Laminar and Turbulent Boundary Layers in Arbitrary Pressure Gradients," NASA TN D-5681, May 1970.

21. R. L. Bisplinghoff, H. Ashley, and R. L. Halfman, Aeroelasticity, Addison-Wesley Publishing Company, 1955.

TABLE 1. LANN WING GEOMETRY

AR	7.92
C_r	0.361 m
λ	0.4
Λ_{LE}	27.493°
$\Lambda_{c/4}$	25.0°
Λ_{TE}	16.908°
b	1.0 m
S (SEMI-SPAN)	.253 m^2
MAC	.268 m
y_{MAC}	.429 m
θ_{TWIST}	-4.8°
t/c	.12
PITCH AXIS	62.1% C_r

TABLE 2. LANN WING MEASURED ORDINATES AT THE ROOT CHORD

Root chord $\eta = 0$

Local chord = 360.60 mm

upper side				lower side					
x/c	-z/c	x/c	-z/c	x/c	-z/c	x/c	-z/c	x/c	-z/c
0.00000	0.02072	0.67021	0.02644	0.00000	0.02072	0.01765	-0.00102	0.39998	-0.06824
0.00011	0.02465	0.70680	0.02166	0.00012	0.01631	0.01838	-0.00140	0.40512	-0.06832
0.00021	0.02525	0.75335	0.01526	0.00029	0.01543	0.01917	-0.00177	0.42387	-0.06643
0.00046	0.02606	0.79293	0.00954	0.00050	0.01476	0.01979	-0.00207	0.44041	-0.06839
0.00063	0.02663	0.83247	0.00361	0.00063	0.01434	0.02047	-0.00236	0.45038	-0.06795
0.00074	0.02683	0.85618	0.00000	0.00087	0.01371	0.02121	-0.00266	0.49747	-0.06709
0.00092	0.02722	0.88211	-0.00398	0.00099	0.01341	0.02205	-0.00310	0.53007	-0.06525
0.00120	0.02787	0.91717	-0.00939	0.00122	0.01298	0.02267	-0.00337	0.56550	-0.06251
0.00134	0.02795	0.95282	-0.01489	0.00135	0.01276	0.02335	-0.00368	0.60232	-0.05889
0.00204	0.02937	0.98323	-0.01955	0.00161	0.01228	0.02414	-0.00403	0.63587	-0.05477
0.00287	0.03089	1.00000	-0.02206	0.00170	0.01208	0.02467	-0.00423	0.67183	-0.04986
0.00361	0.03170			0.00194	0.01170	0.02645	-0.00499	0.70588	-0.04504
0.00464	0.03227			0.00216	0.01138	0.02834	-0.00578	0.74071	-0.03990
0.00500	0.03342			0.00237	0.01112	0.02999	-0.00646	0.77586	-0.03487
0.00609	0.03459			0.00247	0.01095	0.03192	-0.00722	0.81117	-0.03006
0.00673	0.03521			0.00282	0.01051	0.03351	-0.00785	0.84987	-0.02539
0.00753	0.03590			0.00311	0.00994	0.03541	-0.00859	0.88314	-0.02401
0.00858	0.03660			0.00334	0.00974	0.03709	-0.00918	0.88042	-0.02746
0.00952	0.03750			0.00363	0.00928	0.03890	-0.00985	0.89810	-0.02116
0.01150	0.04046			0.00382	0.00902	0.04059	-0.01045	0.91640	-0.02013
0.01231	0.04019			0.00402	0.00878	0.04235	-0.01107	0.93519	-0.01972
0.01708	0.04200			0.00425	0.00859	0.04608	-0.01243	0.95504	-0.01994
0.02166	0.04398			0.00459	0.00815	0.04943	-0.01356	0.98629	-0.02186
0.02477	0.04513			0.00499	0.00775	0.05294	-0.01472	0.98974	-0.02232
0.02819	0.04630			0.00533	0.00740	0.05646	-0.01586	0.99372	-0.02269
0.03240	0.04758			0.00565	0.00714	0.05999	-0.01698	0.99699	-0.02308
0.03530	0.04836			0.00602	0.00688	0.06344	-0.01803	1.00000	-0.02342
0.03914	0.04934			0.00642	0.00633	0.06697	-0.01909		
0.04283	0.05016			0.00678	0.00599	0.07052	-0.02017		
0.04627	0.05089			0.00710	0.00571	0.07775	-0.02222		
0.04935	0.05147			0.00740	0.00550	0.08485	-0.02422		
0.05640	0.05265			0.00776	0.00523	0.09168	-0.02605		
0.06372	0.05366			0.00814	0.00488	0.09894	-0.02796		
0.07053	0.05448			0.00852	0.00461	0.10599	-0.02977		
0.07834	0.05523			0.00885	0.00433	0.11285	-0.03149		
0.08503	0.05576			0.00916	0.00411	0.12029	-0.03332		
0.09967	0.05659			0.00953	0.00382	0.12722	-0.03498		
0.11279	0.05721			0.00995	0.00352	0.13426	-0.03663		
0.12695	0.05767			0.01059	0.00310	0.14121	-0.03821		
0.14162	0.05802			0.01090	0.00285	0.15656	-0.04203		
0.17966	0.05840			0.01131	0.00259	0.17722	-0.04582		
0.21579	0.05819			0.01167	0.00235	0.19374	-0.04889		
0.25344	0.05756			0.01207	0.00211	0.21247	-0.05205		
0.28613	0.05667			0.01243	0.00186	0.22897	-0.05459		
0.32399	0.05528			0.01278	0.00166	0.24773	-0.05718		
0.36076	0.05364			0.01310	0.00147	0.26472	-0.05932		
0.40032	0.05157			0.01351	0.00120	0.28495	-0.06156		
0.43068	0.04970			0.01385	0.00101	0.30013	-0.06301		
0.48496	0.04581			0.01412	0.00085	0.31759	-0.06440		
0.52728	0.04204			0.01486	0.00045	0.33512	-0.06557		
0.57015	0.03793			0.01568	-0.00001	0.35216	-0.06652		
0.60747	0.03443			0.01622	-0.00028	0.36988	-0.06734		
0.64598	0.03064			0.01694	-0.00066	0.38788	-0.06797		

TABLE 3. LANN WING MEASURED ORDINATES AT THE 20% SPAN STATION

Section 1 η = 0.200

Local chord = 317.65 mm

upper side				lower side					
x/c	-z/c	x/c	-z/c	x/c	-z/c	x/c	-z/c	x/c	-z/c
0.00000	0.01699	0.47915	0.02904	0.00000	0.01699	0.02840	-0.00856	0.39985	-0.06681
0.00060	0.02144	0.71651	0.02431	0.00020	0.01375	0.02916	-0.00887	0.41363	-0.06391
0.00072	0.02187	0.75558	0.01910	0.00063	0.01203	0.03015	-0.00928	0.43448	-0.06681
0.00094	0.02238	0.79784	0.01312	0.00081	0.01159	0.03103	-0.00964	0.47547	-0.06595
0.00154	0.02393	0.83404	0.00774	0.00100	0.01107	0.03191	-0.00997	0.51461	-0.06411
0.00170	0.02431	0.87604	0.00126	0.00129	0.01032	0.03276	-0.01029	0.55694	-0.06081
0.00206	0.02506	0.91421	-0.00476	0.00146	0.01016	0.03380	-0.01070	0.59506	-0.05697
0.00231	0.02551	0.95548	-0.01130	0.00188	0.00908	0.03586	-0.01115	0.63517	-0.05186
0.00245	0.02576	0.99395	-0.01698	0.00207	0.00880	0.03775	-0.01135	0.67346	-0.04638
0.00257	0.02559	1.00000	-0.01787	0.00236	0.00832	0.03979	-0.01299	0.71408	-0.04033
0.00317	0.02663			0.00245	0.00816	0.04186	-0.01367	0.75530	-0.03401
0.00406	0.02806			0.00277	0.00772	0.04383	-0.01435	0.79383	-0.02838
0.00447	0.02845			0.00311	0.00720	0.04579	-0.01491	0.81346	-0.02576
0.00526	0.02947			0.00326	0.00704	0.04787	-0.01562	0.83359	-0.02322
0.00561	0.02963			0.00366	0.00666	0.04994	-0.01631	0.85343	-0.02096
0.00611	0.03006			0.00384	0.00664	0.05177	-0.01679	0.87345	-0.01899
0.00733	0.03143			0.00437	0.00573	0.05381	-0.01750	0.88165	-0.01830
0.00824	0.03244			0.00464	0.00544	0.05583	-0.01813	0.88980	-0.01770
0.00856	0.03274			0.00510	0.00488	0.05789	-0.01874	0.89764	-0.01713
0.00937	0.03350			0.00530	0.00472	0.05976	-0.01932	0.90535	-0.01664
0.00976	0.03372			0.00569	0.00429	0.06189	-0.01993	0.91336	-0.01634
0.01063	0.03446			0.00627	0.00366	0.06385	-0.02051	0.92139	-0.01606
0.01214	0.03551			0.00643	0.00332	0.06608	-0.02117	0.92966	-0.01586
0.01378	0.03642			0.00701	0.00292	0.06785	-0.02167	0.93738	-0.01575
0.01619	0.03789			0.00724	0.00271	0.06985	-0.02224	0.94538	-0.01579
0.01782	0.03849			0.00772	0.00225	0.07180	-0.02279	0.95337	-0.01587
.01942	0.03945			0.00827	0.00180	0.07399	-0.02339	0.96145	-0.01603
0.02101	0.04025			0.00868	0.00151	0.07778	-0.02444	0.96959	-0.01632
0.02240	0.04084			0.00905	0.00118	0.08203	-0.02555	0.97739	-0.01671
0.02368	0.04137			0.00947	0.00089	0.08585	-0.02655	0.98557	-0.01730
0.02580	0.04214			0.00980	0.00068	0.09013	-0.02765	0.98940	-0.01754
0.02976	0.04344			0.01065	0.00001	0.09383	-0.02858	0.99343	-0.01800
0.03390	0.04467			0.01131	-0.00040	0.09799	-0.02959	0.99735	-0.01835
0.04184	0.04681			0.01212	-0.00095	0.10183	-0.03047	1.00000	-0.01858
0.04998	0.04865			0.01293	-0.00144	0.10612	-0.03153		
0.05812	0.05014			0.01378	-0.00190	0.11010	-0.03246		
0.06583	0.05130			0.01459	-0.00231	0.11376	-0.03331		
0.07393	0.05230			0.01539	-0.00282	0.12226	-0.03526		
0.09429	0.05413			0.01618	-0.00324	0.13003	-0.03698		
0.11535	0.05544			0.01696	-0.00359	0.13792	-0.03869		
0.15487	0.05697			0.01780	-0.00400	0.14591	-0.04037		
0.19378	0.05763			0.01882	-0.00448	0.15395	-0.04202		
0.23695	0.05765			0.01939	-0.00473	0.17059	-0.04583		
0.27537	0.05717			0.02019	-0.00507	0.19497	-0.04954		
0.31752	0.05613			0.02116	-0.00560	0.21414	-0.05250		
0.35529	0.05485			0.02197	-0.00595	0.23417	-0.05525		
0.39668	0.05306			0.02261	-0.00617	0.25386	-0.05771		
0.43402	0.05110			0.02340	-0.00645	0.27470	-0.06000		
0.47759	0.04838			0.02424	-0.00688	0.29386	-0.06177		
0.51703	0.04546			0.02496	-0.00720	0.31895	-0.06361		
0.55461	0.04228			0.02576	-0.00752	0.33651	-0.06453		
0.59686	0.03825			0.02675	-0.00789	0.35411	-0.06557		
0.63420	0.03434			0.02746	-0.00820	0.37371	-0.06622		

TABLE 4. LANN WING MEASURED ORDINATES AT THE 32.5% SPAN STATION

Section 2 $\eta = 0.325$

Local chord = 290.71 mm

upper side				lower side					
x/c	-z/c	x/c	-z/c	x/c	-z/c	x/c	-z/c	x/c	-z/c
0.00000	0.01168	0.07153	0.04993	0.00000	0.01168	0.02818	-0.01118	0.77772	-0.02853
0.00015	0.01245	0.07602	0.05048	0.00015	0.01090	0.03010	-0.01191	0.80290	-0.02476
0.00031	0.01559	0.09870	0.05269	0.00045	0.00986	0.03250	-0.01275	0.82381	-0.02201
0.00045	0.01661	0.12119	0.05426	0.00065	0.00931	0.03456	-0.01348	0.84819	-0.01910
0.00064	0.01663	0.14165	0.05534	0.00101	0.00832	0.03673	-0.01428	0.86682	-0.01716
0.00090	0.01853	0.16391	0.05622	0.00124	0.00769	0.03896	-0.01513	0.88459	-0.01569
0.00122	0.01946	0.18573	0.05684	0.00176	0.00657	0.04110	-0.01589	0.90635	-0.01432
0.00146	0.01980	0.20796	0.05721	0.00216	0.00591	0.04329	-0.01659	0.92796	-0.01358
0.00197	0.02121	0.25206	0.05744	0.00231	0.00571	0.04552	-0.01732	0.93718	-0.01346
0.00202	0.02153	0.29941	0.05688	0.00259	0.00521	0.04777	-0.01802	0.94135	-0.01345
0.00213	0.02140	0.34086	0.05588	0.00293	0.00496	0.04996	-0.01868	0.95000	-0.01350
0.00266	0.02278	0.38489	0.05443	0.00320	0.00419	0.05220	-0.01935	0.95865	-0.01365
0.00296	0.02331	0.42814	0.05255	0.00353	0.00411	0.05420	-0.01996	0.96722	-0.01391
0.00318	0.02357	0.47169	0.05020	0.00385	0.00389	0.05884	-0.02129	0.97610	-0.01432
0.00353	0.02424	0.51395	0.04741	0.00412	0.00322	0.06334	-0.02254	0.98489	-0.01493
0.00389	0.02440	0.55782	0.04398	0.00440	0.00292	0.06762	-0.02373	0.99363	-0.01575
0.00425	0.02520	0.60544	0.03966	0.00469	0.00286	0.07167	-0.02480	0.99796	-0.01620
0.00446	0.02547	0.64628	0.03546	0.00488	0.00249	0.07627	-0.02602	1.00000	-0.01642
0.00477	0.02585	0.69276	0.03014	0.00324	0.00190	0.08053	-0.02711		
0.00525	0.02652	0.73269	0.02515	0.00570	0.00139	0.08528	-0.02831		
0.00562	0.02694	0.77591	0.01934	0.00601	0.00108	0.08926	-0.02925		
0.00591	0.02713	0.82141	0.01270	0.00626	0.00086	0.09365	-0.03030		
0.00654	0.02787	0.86295	0.00633	0.00662	0.00054	0.09791	-0.03129		
0.00669	0.02822	0.90617	-0.00059	0.00702	0.00012	0.10243	-0.03232		
0.00735	0.02882	0.95054	-0.00779	0.00751	-0.00052	0.11145	-0.03433		
0.00777	0.02922	0.99507	-0.01450	0.00794	-0.00073	0.11973	-0.03615		
0.00837	0.02975	1.00000	-0.01525	0.00834	-0.00105	0.12874	-0.03808		
0.00875	0.03002			0.00877	-0.00140	0.13769	-0.03992		
0.00951	0.03073			0.00920	-0.00172	0.14593	-0.04158		
0.00993	0.03108			0.00973	-0.00213	0.15476	-0.04328		
0.01034	0.03129			0.01055	-0.00271	0.16345	-0.04490		
0.01085	0.03173			0.01144	-0.00330	0.17234	-0.04651		
0.01148	0.03224			0.01190	-0.00353	0.18526	-0.04868		
0.01198	0.03256			0.01235	-0.00385	0.20704	-0.05201		
0.01281	0.03311			0.01281	-0.00412	0.22512	-0.05497		
0.01374	0.03362			0.01325	-0.00435	0.25090	-0.05757		
0.01459	0.03411			0.01362	-0.00449	0.27265	-0.05984		
0.01578	0.03456			0.01410	-0.00471	0.29472	-0.06175		
0.01659	0.03520			0.01446	-0.00499	0.31643	-0.06325		
0.01762	0.03582			0.01487	-0.00514	0.33870	-0.06443		
0.01883	0.03624			0.01582	-0.00564	0.36021	-0.06529		
0.01966	0.03686			0.01667	-0.00611	0.38236	-0.06591		
0.02233	0.03807			0.01758	-0.00654	0.39996	-0.06618		
0.02408	0.03874			0.01844	-0.00688	0.42134	-0.06618		
0.02707	0.03990			0.01924	-0.00737	0.42682	-0.06613		
0.03002	0.04092			0.02006	-0.00779	0.47369	-0.06501		
0.03407	0.04224			0.02103	-0.00825	0.51291	-0.06304		
0.03901	0.04371			0.02210	-0.00872	0.55791	-0.05931		
0.04321	0.04480			0.02300	-0.00910	0.60082	-0.05464		
0.04864	0.04611			0.02384	-0.00946	0.64583	-0.04851		
0.05427	0.04721			0.02537	-0.01008	0.68572	-0.04217		
0.06026	0.04829			0.02645	-0.01051	0.71566	-0.03795		
0.06702	0.04933			0.02718	-0.01080	0.75486	-0.03179		

TABLE 5. LANN WING MEASURED ORDINATES AT THE 47.5% SPAN STATION

Section 3 η = 0.475

Local chord = 258.06 mm

upper side				lower side					
x/c	-z/c	x/c	-z/c	x/c	-z/c	x/c	-z/c	x/c	-z/c
0.00000	0.01001	0.02822	0.03617	0.00000	0.01001	0.0429	-0.02058	0.91418	-0.01005
0.00003	0.01043	0.03114	0.03717	0.00008	0.00589	0.0[illegible]	-0.02130	0.93428	-0.00963
0.00039	0.01308	0.03310	0.03784	0.00018	0.00515	0.04[illegible]	-0.[illegible]206	0.94849	-0.00974
0.00053	0.01281	0.03566	0.03868	0.00048	0.00394	0.05045	-0.02275	0.96149	-0.01006
0.00089	0.01444	0.03851	0.03957	0.00082	0.00305	0.05315	-0.02349	0.96965	-0.01042
0.00133	0.01589	0.04086	0.04025	0.00100	0.00282	0.05785	-0.02477	0.97750	-0.01089
0.00146	0.01658	0.04347	0.04095	0.00143	0.00203	0.06279	-0.02605	0.98324	-0.01133
0.00204	0.01741	0.04668	0.04176	0.00172	0.00142	0.06792	-0.02736	0.98728	-0.01169
0.00229	0.01784	0.04886	0.04227	0.00210	0.00083	0.07281	-0.02852	0.99289	-0.01224
0.00247	0.01835	0.05101	0.04276	0.00255	0.00014	0.07745	-0.02963	0.99589	-0.01255
0.00313	0.01933	0.05309	0.04321	0.00278	-0.00002	0.08323	-0.03098	1.00000	-0.01298
0.00318	0.01943	0.05520	0.04355	0.00328	-0.00078	0.08724	-0.03188		
0.00384	0.02013	0.05646	0.04392	0.00345	-0.00090	0.09256	-0.03303		
0.00438	0.02105	0.05776	0.04416	0.00391	-0.00150	0.09715	-0.03402		
0.00476	0.02150	0.06279	0.04512	0.00429	-0.00192	0.10215	-0.03507		
0.00494	0.02164	0.06762	0.04593	0.00469	-0.00237	0.10725	-0.03613		
0.00533	0.02207	0.07253	0.04670	0.00525	-0.00284	0.11690	-0.03807		
0.00563	0.02243	0.07749	0.04739	0.00560	-0.00326	0.12674	-0.03999		
0.00619	0.02312	0.08732	0.04861	0.00615	-0.00386	0.13650	-0.04185		
0.00657	0.02339	0.09770	0.04975	0.00644	-0.00412	0.14639	-0.04366		
0.00698	0.02392	0.10664	0.05065	0.00695	-0.00464	0.15625	-0.04541		
0.00723	0.02407	0.11705	0.05152	0.00716	-0.00483	0.16622	-0.04709		
0.00756	0.02469	0.12658	0.05224	0.00770	-0.00531	0.17611	-0.04866		
0.00821	0.02522	0.13716	0.05287	0.00815	-0.00563	0.18594	-0.05015		
0.00853	0.02552	0.14651	0.05339	0.00861	-0.00600	0.19641	-0.05163		
0.00901	0.02593	0.15061	0.05585	0.00907	-0.00635	0.20584	-0.05289		
0.00953	0.02638	0.22548	0.05640	0.00963	-0.00675	0.21521	-0.05407		
0.00964	0.02644	0.25834	0.05683	0.01011	-0.00702	0.22575	-0.05533		
0.01004	0.02672	0.31258	0.05615	0.01065	-0.00741	0.25009	-0.05794		
0.01068	0.02730	0.37718	0.05579	0.01110	-0.00769	0.27461	-0.06020		
0.01113	0.02761	0.42746	0.05418	0.01153	-0.00794	0.29886	-0.06197		
0.01195	0.02819	0.47585	0.[illegible]01	0.01249	-0.00848	0.32343	-0.06334		
0.01251	0.02858	0.52187	0.[illegible]329	0.01355	-0.00901	0.34891	-0.06433		
0.01324	0.02908	0.57990	0.04580	0.01456	-0.00951	0.37[illegible]	-0.06495		
0.01381	0.02947	0.62482	0.04129	0.01540	-0.00990	0.39978	-0.06522		
0.01442	0.02980	0.[illegible]7201	0.03658	0.01642	-0.01040	0.42228	-0.06507		
0.01492	0.[illegible]007	0.[illegible]1829	0.03122	0.01739	-0.01088	0.44635	-0.06452		
0.01546	0.03040	0.77926	0.02474	0.01841	-0.01135	0.47114	-0.06361		
0.01601	0.03076	0.81517	0.01771	0.01950	-0.01187	0.49612	-0.06232		
0.01630	0.03085	0.86493	0.01053	0.02041	-0.01230	0.52041	-0.06061		
0.01687	0.[illegible]3[illegible]9	0.91586	0.00224	0.02144	-0.01282	0.55624	-0.05725		
0.01745	0.03155	0.92894	0.00000	0.02235	-0.01321	0.58729	-0.05374		
0.01800	0.03182	0.94489	-0.00594	0.02342	-0.01368	0.62017	-0.04935		
0.01844	0.03204	1.00000	-0.01165	0.02434	-0.01405	0.65092	-0.04476		
0.01940	0.03256			0.02537	-0.01443	0.68218	-0.03987		
0.02026	0.03292			0.02659	-0.01487	0.71732	-0.03435		
0.02129	0.03341			0.02732	-0.01517	0.75083	-0.02898		
0.02227	0.03385			0.02843	-0.01556	0.76832	-0.02599		
0.02328	0.03426			0.03079	-0.01641	0.79117	-0.02259		
0.02428	0.03469			0.03318	-0.01719	0.81581	-0.01915		
0.02553	0.03518			0.[illegible]3541	-0.01804	0.84046	-0.01603		
0.[illegible]27	0.03552			0.03810	-0.01904	0.86483	-0.01340		
0.02[illegible]11	0.03587			0.[illegible]4044	-0.[illegible]1979	0.88946	-0.01136		

TABLE 6. LANN WING MEASURED ORDINATES AT THE 65.0% SPAN STATION

Section 4 $\eta = 0.650$

Local chord = 220.29 mm

upper side				lower side					
x/c	-z/c	x/c	-z/c	x/c	-z/c	x/c	-z/c	x/c	-z/c
0.00000	0.00273	0.05984	0.04008	0.00000	0.00273	0.07031	-0.03173	0.98140	-0.00322
0.00069	0.00348	0.06325	0.04078	0.00020	0.00197	0.07305	-0.03232	0.98692	-0.00373
0.00031	0.00514	0.06674	0.04145	0.00053	-0.00086	0.07569	-0.03291	0.99282	-0.00445
0.00055	0.00685	0.07026	0.04213	0.00081	-0.00178	0.07893	-0.03353	0.99834	-0.00513
0.00081	0.00769	0.07424	0.04317	0.00134	-0.00315	0.08170	-0.03408	1.00000	-0.00533
0.00121	0.00891	0.08170	0.04409	0.00156	-0.00355	0.08744	-0.03521		
0.00145	0.00957	0.08759	0.04500	0.00191	-0.00417	0.09334	-0.03634		
0.00166	0.01009	0.09378	0.04589	0.00225	-0.00482	0.09912	-0.03739		
0.00203	0.01096	0.09924	0.04663	0.00261	-0.00532	0.10475	-0.03843		
0.00231	0.01137	0.10515	0.04739	0.00295	-0.00567	0.11053	-0.03946		
0.00263	0.01207	0.11076	0.04808	0.00330	-0.00609	0.11652	-0.04049		
0.00310	0.01286	0.12208	0.04935	0.00371	-0.00657	0.12232	-0.04147		
0.00348	0.01346	0.13399	0.05055	0.00424	-0.00713	0.12815	-0.04245		
0.00401	0.01414	0.14592	0.05161	0.00447	-0.00729	0.13368	-0.04332		
0.00452	0.01482	0.15730	0.05253	0.00491	-0.00784	0.14002	-0.04433		
0.00493	0.01509	0.16826	0.05335	0.00541	-0.00846	0.15123	-0.04605		
0.00555	0.01562	0.17965	0.05404	0.00587	-0.00884	0.16750	-0.04770		
0.00615	0.01649	0.19136	0.05474	0.00628	-0.00913	0.17445	-0.04834		
0.00658	0.01710	0.22379	0.05632	0.00668	-0.00954	0.18573	-0.05078		
0.00730	0.01814	0.26734	0.05763	0.00721	-0.00999	0.19731	-0.05216		
0.00787	0.01871	0.29128	0.05812	0.00766	-0.01041	0.20897	-0.05344		
0.00851	0.01913	0.31485	0.05835	0.00821	-0.01100	0.22014	-0.05457		
0.00898	0.01975	0.34111	0.05846	0.00873	-0.01140	0.22537	-0.05514		
0.00967	0.02035	0.37006	0.05839	0.00917	-0.01174	0.25473	-0.05759		
0.01037	0.02093	0.39920	0.05810	0.00985	-0.01222	0.28149	-0.05953		
0.01099	0.02143	0.42853	0.05758	0.01035	-0.01254	0.31243	-0.06091		
0.01154	0.02185	0.45701	0.05684	0.01085	-0.01286	0.34120	-0.06178		
0.01220	0.02236	0.48610	0.05585	0.01146	-0.01320	0.37018	-0.06219		
0.01282	0.02281	0.51407	0.05462	0.01231	-0.01370	0.39992	-0.06215		
0.01342	0.02323	0.54285	0.05319	0.01301	-0.01404	0.42761	-0.06157		
0.01430	0.02381	0.57201	0.05143	0.01367	-0.01431	0.45643	-0.06065		
0.01538	0.02439	0.60050	0.04954	0.01478	-0.01493	0.48548	-0.05878		
0.01661	0.02512	0.62935	0.04740	0.01588	-0.01547	0.54662	-0.05379		
0.01765	0.02568	0.65815	0.04501	0.01719	-0.01605	0.57714	-0.04938		
0.01886	0.02637	0.68697	0.04231	0.01853	-0.01664	0.60718	-0.04499		
0.01997	0.02697	0.71647	0.03931	0.01958	-0.01698	0.63797	-0.04172		
0.02115	0.02759	0.74524	0.03619	0.02063	-0.01733	0.65825	-0.03682		
0.02279	0.02821	0.75069	0.03557	0.02185	-0.01801	0.68714	-0.03205		
0.02340	0.02877	0.75448	0.03417	0.02298	-0.01848	0.71622	-0.02713		
0.02458	0.02924	0.77376	0.03219	0.02417	-0.01894	0.74475	-0.02232		
0.02573	0.02979	0.80270	0.02816	0.02695	-0.01995	0.75095	-0.02122		
0.02748	0.03050	0.83148	0.02390	0.02982	-0.02090	0.75320	-0.02045		
0.02926	0.03118	0.86045	0.01924	0.03262	-0.02183	0.77360	-0.01746		
0.03093	0.03185	0.89056	0.01424	0.03830	-0.02373	0.80241	-0.01302		
0.03264	0.03243	0.91853	0.00970	0.04146	-0.02470	0.83136	-0.00911		
0.03438	0.03304	0.94933	0.00794	0.04363	-0.02552	0.86016	-0.00582		
0.03577	0.03354	0.94083	0.00606	0.04716	-0.02729	0.88857	-0.00326		
0.03848	0.03465	0.95230	0.00420	0.05010	-0.02772	0.91192	-0.00193		
0.04248	0.03574	0.96369	0.00232	0.05586	-0.02846	0.92379	-0.00150		
0.04607	0.03671	0.97624	0.00015	0.05901	-0.02919	0.93540	-0.00142		
0.04962	0.03767	0.98681	-0.00157	0.06159	-0.02975	0.94860	-0.00152		
0.05290	0.03852	1.00000	-0.00382	0.06473	-0.03051	0.95854	-0.00178		
0.05620	0.03926			0.06734	-0.03111	0.96984	-0.00234		

TABLE 7. LANN WING MEASURED ORDINATES AT THE 82.5% SPAN STATION

Section 5 $\eta = 0.825$

Local chord = 182.35 mm

upper side						lower side			
x/c	-z/c	x/c	-z/c	x/c	-z/c	x/c	-z/c	x/c	-z/c
0.00000	-0.00585	0.05110	0.03178	0.78232	0.04357	0.00000	-0.00585	0.07537	-0.03829
0.00010	-0.00403	0.05241	0.03217	0.81725	0.03880	0.00052	-0.01049	0.07894	-0.03885
0.00077	-0.00120	0.05376	0.03253	0.85259	0.03329	0.00111	-0.01185	0.08629	-0.03996
0.00145	0.00132	0.05519	0.03293	0.88690	0.02776	0.00182	-0.01293	0.09264	-0.04092
0.00144	0.00180	0.05556	0.03322	0.92244	0.02159	0.00259	-0.01386	0.09969	-0.04191
0.00244	0.00341	0.05790	0.03357	0.94248	0.01812	0.00312	-0.01447	0.10653	-0.04286
0.00293	0.00435	0.06131	0.03441	0.95669	0.01559	0.00366	-0.01515	0.11373	-0.04381
0.00334	0.00486	0.06492	0.03530	0.97038	0.01316	0.00419	-0.01573	0.12071	-0.04475
0.00404	0.00584	0.06834	0.03611	0.98427	0.01068	0.00462	-0.01620	0.12793	-0.04563
0.00461	0.00655	0.07040	0.03657	0.99812	0.00818	0.00554	-0.01717	0.14173	-0.04729
0.00518	0.00737	0.07332	0.03721	1.00000	0.00780	0.00609	-0.01765	0.15537	-0.04884
0.00564	0.00790	0.07605	0.03781			0.00680	-0.01821	0.17034	-0.05040
0.00666	0.00846	0.07883	0.03838			0.00745	-0.01879	0.18356	-0.05165
0.00655	0.00909	0.08218	0.03906			0.00809	-0.01931	0.19040	-0.05222
0.00726	0.00977	0.08569	0.03973			0.00896	-0.01990	0.22535	-0.05480
0.00770	0.01027	0.08917	0.04038			0.00944	-0.02010	0.24004	-0.05571
0.00833	0.01095	0.09274	0.04103			0.01017	-0.02074	0.25491	-0.05799
0.00905	0.01166	0.09612	0.04160			0.01109	-0.02130	0.32967	-0.05863
0.00983	0.01233	0.09960	0.04221			0.01113	-0.02131	0.36454	-0.05871
0.01029	0.01257	0.10313	0.04282			0.01170	-0.02151	0.39978	-0.05814
0.01114	0.01358	0.10655	0.04334			0.01230	-0.02190	0.43449	-0.05668
0.01176	0.01401	0.11013	0.04389			0.01279	-0.02213	0.46866	-0.05452
0.01259	0.01467	0.11352	0.04440			0.01330	-0.02247	0.50425	-0.05151
0.01336	0.01520	0.12094	0.04548			0.01387	-0.02282	0.53950	-0.04744
0.01404	0.01569	0.12859	0.04653			0.01478	-0.02323	0.57338	-0.04273
0.01459	0.01613	0.13461	0.04729			0.01541	-0.02347	0.60830	-0.03707
0.01530	0.01658	0.14151	0.04817			0.01624	-0.02390	0.64273	-0.03096
0.01619	0.01718	0.14839	0.04897			0.01752	-0.02446	0.67786	-0.02450
0.01683	0.01759	0.15530	0.04976			0.01915	-0.02516	0.71249	-0.01823
0.01741	0.01796	0.16249	0.05053			0.02024	-0.02559	0.74031	-0.01315
0.01907	0.01893	0.16928	0.05122			0.02176	-0.02617	0.76950	-0.00820
0.02030	0.01963	0.17739	0.05257			0.02300	-0.02666	0.79644	-0.00375
0.02136	0.02046	0.19738	0.05377			0.02439	-0.02713	0.82396	0.00028
0.02287	0.02108	0.21166	0.05490			0.02581	-0.02751	0.85175	0.00382
0.02434	0.02175	0.22545	0.05588			0.02753	-0.02798	0.88078	0.00660
0.02604	0.02257	0.23917	0.05677			0.02871	-0.02833	0.89456	0.00759
0.02730	0.02311	0.25334	0.05760			0.03014	-0.02875	0.90875	0.00831
0.02844	0.02375	0.26491	0.05830			0.03131	-0.02920	0.92202	0.00890
0.03030	0.02455	0.28101	0.05897			0.03275	-0.02957	0.93570	0.00905
0.03114	0.02492	0.29645	0.05955			0.03440	-0.02981	0.94944	0.00898
0.03295	0.02552	0.33001	0.06074			0.03587	-0.03042	0.96351	0.00862
0.03427	0.02606	0.36483	0.06152			0.03719	-0.03081	0.97755	0.00787
0.03552	0.02655	0.39923	0.06198			0.03872	-0.03119	0.99122	0.00670
0.03697	0.02711	0.43396	0.06213			0.04044	-0.03162	0.99816	0.00602
0.03829	0.02753	0.46903	0.06200			0.04399	-0.03237	1.00000	0.00585
0.03981	0.02810	0.50392	0.06153			0.04734	-0.03312		
0.04133	0.02871	0.53861	0.06067			0.05094	-0.03390		
0.04256	0.02913	0.57369	0.05941			0.05437	-0.03453		
0.04405	0.02962	0.60817	0.05790			0.05790	-0.03523		
0.04546	0.03008	0.64295	0.05601			0.06132	-0.03588		
0.04687	0.03051	0.67770	0.05377			0.06477	-0.03648		
0.04819	0.03088	0.71290	0.05089			0.06841	-0.03711		
0.04959	0.03133	0.74734	0.04771			0.07210	-0.03773		

TABLE 8. LANN WING MEASURED ORDINATES AT THE 95% SPAN STATION

Section 6 $\eta = 0.950$

Local chord = 155.34 mm .

upper side				lower side			
x/c	-z/c	x/c	-z/c	x/c	-z/c	x/c	-z/c
0.00000	-0.01515	0.09807	0.03590	0.00000	-0.01514	0.07407	-0.04529
0.00047	-0.01261	0.10630	0.03754	0.00043	-0.01753	0.08148	-0.04616
0.00119	-0.01062	0.11448	0.03916	0.00129	-0.01992	0.08979	-0.04706
0.00137	-0.01063	0.12254	0.04056	0.00186	-0.02119	0.09908	-0.04789
0.00182	-0.00842	0.13062	0.04195	0.00244	-0.02218	0.10679	-0.04873
0.00227	-0.00703	0.13895	0.04333	0.00298	-0.02312	0.11431	-0.04940
0.00280	-0.00640	0.14711	0.04455	0.00371	-0.02405	0.12252	-0.05012
0.00319	-0.00561	0.15598	0.04586	0.00425	-0.02463	0.13075	-0.05079
0.00397	-0.00523	0.16342	0.04688	0.00476	-0.02520	0.14900	-0.05218
0.00455	-0.00368	0.17155	0.04799	0.00531	-0.02570	0.16496	-0.05329
0.00525	-0.00270	0.18843	0.05003	0.00572	-0.02602	0.17939	-0.05421
0.00581	-0.00204	0.20429	0.05181	0.00628	-0.02651	0.19246	-0.05491
0.00636	-0.00180	0.22084	0.05355	0.00697	-0.02709	0.20647	-0.05558
0.00697	-0.00146	0.23699	0.05507	0.00764	-0.02757	0.22050	-0.05615
0.00788	-0.00049	0.25344	0.05451	0.00824	-0.02794	0.25320	-0.05710
0.00863	0.00008	0.27063	0.05787	0.00894	-0.02842	0.28619	-0.05757
0.00924	0.00155	0.28632	0.05898	0.00961	-0.02888	0.32482	-0.05764
0.01011	0.00237	0.30307	0.06009	0.01045	-0.02947	0.35174	-0.05733
0.01073	0.00319	0.31915	0.06103	0.01125	-0.02991	0.38459	-0.05640
0.01140	0.00383	0.33545	0.06191	0.01210	-0.03041	0.39957	-0.05578
0.01196	0.00427	0.36818	0.06345	0.01277	-0.03072	0.41675	-0.05488
0.01255	0.00481	0.40049	0.06462	0.01342	-0.03092	0.45809	-0.05201
0.01315	0.00527	0.43374	0.06556	0.01423	-0.03153	0.49886	-0.04809
0.01392	0.00590	0.46591	0.06616	0.01504	-0.03190	0.53977	-0.04268
0.01457	0.00640	0.49876	0.06647	0.01602	-0.03234	0.58603	-0.03499
0.01546	0.00703	0.53183	0.06647	0.01679	-0.03267	0.61996	-0.02860
0.01627	0.00747	0.54828	0.06641	0.01746	-0.03305	0.66283	-0.02024
0.01796	0.00833	0.56469	0.06629	0.01833	-0.03336	0.70479	-0.01187
0.01937	0.00950	0.58054	0.06608	0.01897	-0.03355	0.74429	-0.00427
0.02099	0.01055	0.61373	0.06534	0.01979	-0.03380	0.77654	0.00232
0.02264	0.01153	0.64583	0.06428	0.02073	-0.03403	0.80921	0.00755
0.02447	0.01258	0.67920	0.06273	0.02176	-0.03404	0.84198	0.01200
0.02614	0.01351	0.71190	0.06073	0.02304	-0.03400	0.87473	0.01540
0.02766	0.01431	0.74468	0.05815	0.02400	-0.03498	0.90765	0.01751
0.02916	0.01487	0.77690	0.05483	0.02464	-0.03558	0.92372	0.01805
0.03101	0.01585	0.81072	0.05054	0.02556	-0.03604	0.93217	0.01815
0.03276	0.01654	0.82703	0.04810	0.02747	-0.03674	0.94004	0.01815
0.03425	0.01726	0.84255	0.04567	0.02938	-0.03731	0.94815	0.01808
0.03625	0.01814	0.85886	0.04294	0.03131	-0.03787	0.95695	0.01794
0.03751	0.01868	0.87595	0.04009	0.03259	-0.03823	0.96468	0.01766
0.03930	0.01942	0.89123	0.03749	0.03429	-0.03869	0.97271	0.01723
0.04094	0.02012	0.90790	0.03461	0.03594	-0.03906	0.98126	0.01665
0.04280	0.02156	0.92452	0.03165	0.03759	-0.03960	0.98968	0.01593
0.04912	0.02308	0.94028	0.02880	0.03942	-0.04005	1.00000	0.01498
0.05293	0.02434	0.95695	0.02568	0.04103	-0.04032		
0.05723	0.02570	0.96505	0.02422	0.04399	-0.04081		
0.06127	0.02692	0.97362	0.02265	0.04745	-0.04153		
0.06520	0.02787	0.98130	0.02125	0.05048	-0.04197		
0.06937	0.02911	0.98978	0.01968	0.05389	-0.04253		
0.07349	0.03031	0.99756	0.01816	0.05730	-0.04304		
0.08157	0.03224	1.00000	0.01762	0.06114	-0.04359		
0.08564	0.03329			0.06532	-0.04417		
0.08975	0.03420			0.06949	-0.04474		

TABLE 9. LANN WING MEASURED ORDINATES AT THE TIP CHORD

Tip section $\eta = 1.0$

Local chord = 144.45 mm

upper side				lower side			
x/c	-z/c	x/c	-z/c	x/c	-z/c	x/c	-z/c
0.00000	-0.02163	0.09960	0.03237	0.00000	-0.02163	0.17946	-0.05566
0.00070	-0.01802	0.10853	0.03436	0.00051	-0.02379	0.19833	-0.05634
0.00135	-0.01621	0.11739	0.03649	0.00125	-0.02641	0.22271	-0.05696
0.00165	-0.01532	0.12643	0.03805	0.00186	-0.02770	0.26678	-0.05745
0.00229	-0.01400	0.13480	0.03962	0.00250	-0.02879	0.31064	-0.05729
0.00260	-0.01328	0.14416	0.04125	0.00299	-0.02954	0.35566	-0.05622
0.00320	-0.01213	0.15251	0.04266	0.00357	-0.03023	0.39981	-0.05416
0.00377	-0.01103	0.16164	0.04414	0.00429	-0.03097	0.44253	-0.05117
0.00459	-0.00958	0.17015	0.04544	0.00487	-0.03157	0.48658	-0.04674
0.00503	-0.00886	0.17977	0.04681	0.00535	-0.03199	0.53111	-0.04080
0.00594	-0.00747	0.19635	0.04904	0.00596	-0.03236	0.57495	-0.03341
0.00640	-0.00693	0.21404	0.05124	0.00623	-0.03253	0.61844	-0.02495
0.00760	-0.00543	0.23169	0.05323	0.00668	-0.03296	0.66244	-0.01602
0.00818	-0.00501	0.25012	0.05515	0.00770	-0.03376	0.70644	-0.00726
0.00913	-0.00373	0.26711	0.05676	0.00825	-0.03417	0.71354	-0.00563
0.01002	-0.00278	0.28452	0.05826	0.00883	-0.03454	0.75065	0.00130
0.01092	-0.00185	0.30231	0.05961	0.00927	-0.03482	0.79454	0.00909
0.01168	-0.00155	0.31068	0.06024	0.00955	-0.03517	0.83830	0.01562
0.01270	-0.00037	0.35558	0.06311	0.01062	-0.03552	0.88279	0.02031
0.01340	0.00026	0.39854	0.06522	0.01124	-0.03592	0.89174	0.02094
0.01474	0.00135	0.44252	0.06689	0.01229	-0.03646	0.90395	0.02161
0.01533	0.00172	0.48646	0.06796	0.01308	-0.03682	0.91765	0.02209
0.01655	0.00274	0.53040	0.06856	0.01389	-0.03719	0.92646	0.02224
0.01709	0.00317	0.56573	0.06865	0.01451	-0.03746	0.93516	0.02226
0.01815	0.00389	0.57442	0.06862	0.01512	-0.03770	0.94378	0.02223
0.01908	0.00440	0.61894	0.06823	0.01579	-0.03797	0.94814	0.02217
0.02012	0.00489	0.66303	0.06700	0.01657	-0.03832	0.95340	0.02164E
0.02129	0.00571	0.70781	0.06487	0.01722	-0.03857	0.96147	0.02142E
0.02228	0.00642	0.75032	0.06184	0.01803	-0.03886	0.97054	0.02093E
0.02395	0.00728	0.79431	0.05717	0.01894	-0.03920	0.97893	0.02043E
0.02585	0.00830	0.81199	0.05483	0.01975	-0.03946	0.98776	0.01973E
0.02741	0.00920	0.82983	0.05221	0.02045	-0.03959	0.99650	0.01895E
0.02931	0.01002	0.84958	0.04904	0.02163	-0.03990	1.00000	0.01861E
0.03088	0.01064	0.86460	0.04658	0.02237	-0.04008		
0.03299	0.01171	0.88213	0.04352	0.02469	-0.04071		
0.03494	0.01261	0.90133	0.04004	0.02611	-0.04108		
0.03636	0.01310	0.91941	0.03673	0.02773	-0.04150		
0.03839	0.01400	0.93587	0.03367	0.02942	-0.04192		
0.04036	0.01493	0.95301	0.03050E	0.03155	-0.04240		
0.04263	0.01581	0.97060	0.02725E	0.03324	-0.04279		
0.04394	0.01635	0.98795	0.02402E	0.03814	-0.04379		
0.04565	0.01706	1.00000	0.02155E	0.04233	-0.04451		
0.04727	0.01741			0.04592	-0.04525		
0.05121	0.01880			0.05128	-0.04586		
0.05581	0.02042			0.05601	-0.04648		
0.06016	0.02189			0.06477	-0.04755		
0.06487	0.02335			0.07419	-0.04857		
0.06895	0.02455			0.08227	-0.04938		
0.07342	0.02581			0.09087	-0.05014		
0.07830	0.02715			0.10938	-0.05161		
0.08219	0.02817			0.12653	-0.05287		
0.08660	0.02928			0.14417	-0.05392		
0.09111	0.03037			0.16221	-0.05487		

Note: "E" denotes "extrapolated"

TABLE 10. CHORDWISE LOCATION OF THE LANN WING PRESSURE ORIFICES

section:	1 (η = .200)		2 (η = .325)		3 (η = .475)		4 (η = .650)		5 (η = .825)		6 (η = .950)	
% c	upper	lower	upper	lower	upper	lower	upper	lower	upper	lower	upper	lower
.0	o		o		o		o		o		o	
.5	o	o	o	o	o	o	o	o	o	o		o
1.5	x	x	x	x	x	x	x	x	x		x	
3.0	x	x	x	x	x	x	x	x	x			
5.0	x	x	x	x	x	x	x		x		x	
7.5	o	o	o	o	o	o	o		o		o	x
10.0	x	x	x	x	x	x			x	x	x	
15.0	x	x	x	x	x		x	x	x		x	x
20.0	x	x	x	x	x	x	x	x	x	x	x	
25.0	x	o	x	o	x	o	x	o	x	o	x	x
30.0	x	x	x	x					x		x	x
35.0	x		x		x		x		x		x	
40.0	x	x	x	x	x		x	x	x		x	x
45.0	x		x		x		x		x		x	
50.0	x	x	x	x	x	x	x	x	x	x	x	x
55.0	x		x		x		x		x		x	
60.0	x	x	x	x	x	x	x	x	x		x	
65.0	x		x		x		x		x		x	
70.0	x	x	x	x	x	x	x	x	x		x	
75.0	x		x		x		x		x		x	
80.0	x	x	x	x	x	x	x	x	x	x	x	x
85.0	o		o		o		o		o		o	
90.0	x	x	x	x	x	x	x	x	x	x	x	x
95.0	o		o		o		o		o		o	

(o indicates inner diameter tube : 1.07 mm
x indicates inner diameter tube : 1.60 mm)
all orifices at model surface inner diameter : 0.79 mm

TABLE 11. LOCATION OF THE LANN WING PRESSURE TRANSDUCERS

section:	η = .189	η = .4625	η = .639	η = .814
% c				
5.0	x	x	x	x
10.0		x	x	
20.0		x	x	
30.0				
40.0		x	x	
50.0		x	x	
60.0		x	x	
70.0	x	x	x	x
80.0		x	x	
90.0		x	x	

TABLE 12. LOCATION OF THE LANN WING ACCELEROMETERS

section:	η = .100	η = .420	η = .700	η = .920
number	X = 73.7 (6.4 % c) 1	X = 236.4 (6.6 % c) 4	X = 376.2 (5.7 % c) 7	X = 492.2 (8.3 % c) 10
number	X = 175.8 (36.5 % c) 2	X = 325.7 (39.7 % c) 5	X = 447.2 (39.6 % c) 8	X = 542.3 (39.3 % c) 11
number	X = 300.3 (73.2 % c) 3	X = 414.2 (72.5 % c) 6	X = 512.9 (71.0 % c) 9	X = 593.1 (70.7 % c) 12

TABLE 13. LANN WING STIFFNESS DISTRIBUTIONS

EA	ELASTIC AXIS
EI	BENDING STIFFNESS, LB IN^2
GJ	TORSIONAL STIFFNESS, LB IN^2
WS	WING STATION
a	SWEEP ANGLE OF 38%, CHORD LINE, DEG

THE DISTRIBUTIONS OF EI AND GJ ARE RELATED TO WING SECTIONS NORMAL TO THE ASSUMED ELASTIC AXIS.

% SPAN ALONG EA	$GJ*10^{-6}$ (LB IN^2)	$EI*10^{-6}$ (LB IN^2)
0	115.6	82.6
12.5	61.7	49.0
25.0	36.8	31.9
37.5	23.0	22.9
50.0	14.3	15.6
62.5	2.39	11.0
75.0	3.55	6.76
87.5	1.81	3.77
100	.77	2.30

TABLE 14. LANN WING WEIGHT AND INERTIA DISTRIBUTIONS (ELASTIC AXIS COORDINATE SYSTEM)

PERCENT SPAN ALONG EA.	WEIGHT (LBS)	BENDING INERTIA ($LB-IN^2$)	TORSIONAL INERTIA ($LB-IN^2$)	STATIC MOMENT (LB - IN)
5	13.12	20.6	114	3.28
15	10.95	16.6	98.3	2.59
25	10.38	15.8	68.9	.78
35	8.92	13.6	51.6	.70
45	7.15	10.9	36.8	.60
55	5.83	8.4	16.3	.74
65	5.17	8.0	13.2	.87
75	4.11	6.7	9.0	.20
85	3.43	5.2	8.6	.13
95	2.90	4.5	5.4	.08

TABLE 15. COMPARISON OF MEASURED AND CALCULATED LANN WING NORMAL MODE FREQUENCIES

LOCKHEED (WING-ALONE MODES)			NLR (WING-IN-MOUNT MODES)
MODE SHAPE	MEASURED*	COMPUTED*	MEASURED*
1ST BENDING	31.93	32.01	30.56
2ND BENDING	115.75	117.60	104.46
3RD BENDING	249.07	271.60	229.39
1ST TORSION	292.12	291.70	292.95

* FREQUENCIES ARE IN HERTZ

TABLE 16. LANN WING STEADY TEST PROGRAM (RUN ID NUMBERS)

α \ M	0.62	0.72	0.77	0.82	0.87	0.95
-0.4	16	27	46	67	88	97
0.35	17			68		
0.60*)	15/19	28	47	69	89	98
0.85	18			70		
1.60	20	29	48	71	90	99
2.00	183			218		
2.35	235	238	240	132		155
2.50				219		
2.60*)	234	109	121	222/133		154
2.75				220	242	245
2.85	236	237	241	134		156
2.90				231		230
3.00*)	184			221	168	
3.25				223	244	247
3.50				224		
3.60	104/232	110	122	135		157
4.00				225	169	248
4.50				226		
4.75			201	205		
5.00*)	185	193	202	206		228
5.25			203	207		
5.50				227		
6.00	186	194	204	208		229

*) Steady incidences for which unsteady measurements were performed as well

TABLE 17. LANN WING UNSTEADY TEST PROGRAM (RUN ID NUMBERS)

τ		12	24	36	48	60	72
$\Delta\alpha$		1.0	0.25	0.25	0.25	0.25	.025
α	M						
0.6	0.62	36	129/22	23	24	25	26
	0.72		30		31	32	33
	0.77	117	118	119	120	65	66
	0.82	83	73	77	85	86	87
	0.87	91	92	93	94	95	96
	0.95		100		101	102	103
2.6	0.62		105		106	107	108
	0.72	111	112	113	114	115	116
	0.77	123	124	125	126		128
	0.82	139	143	150	151	152	153
3.0	0.72		165				
	0.77		166				
	0.82		167				
	0.87		170		171	172	173
	0.95	250	175	179	180	181	182
5.0	0.62	187	188	189	190	191	192
	0.72	195	196	197	198	199	200
	0.82	211	212	214	215	216	217

TABLE 18. LANN WING TEST PROGRAM FOR AMPLITUDE AND HIGHER HARMONICS (RUN ID NUMBERS)

M	α	f	Δα / harm	0.125	0.25	0.5	1.0
0.62	0.6	12	1	34	21	35	36
		24	1	37	22/39/129	42	
		24	2		40/130	43	
		24	3		41/131	44	
		36	1	45	23		
0.82	0.6	12	1		72	82	83
		24	1	78	73	79	
		24	2		74	80	
		24	3		75	81	
		36	1	76	77		
0.82	2.6	12	1	135	137	138	139
		24	1	140	143	146	
		24	2	141	144	147	
		24	3	142	145	148	
		36	1	149	150		
0.95	2.6	12	1		161	162	163
0.95	3.0	24	1		175	178	
		24	2		176		
		24	3		177		
0.82	5.0	12	1		209	210	211
		24	1		212	213	

TABLE 19. ADDITIONAL LANN WING QUASI-STEADY TEST RESULTS FOR UNSTEADY TEST PROGRAM (RUN ID NUMBERS)

Δα		0.25	0.50	0.75	1.00
α	M				
0.6	.62	260			261
	.72				262
	.77				263
	.82	264			265
	.87				266
	.95				267
2.6	.62	268			269
	.72	270			271
	.77	272			273
	.82	274			275
3.0	0.72				
	0.77				
	0.82	276	277		278
	0.87	279			
	0.95	280			
5.0	0.62				
	0.72				
	0.82	281	282		283

TABLE 20. LANN WING QUASI-STEADY TEST PROGRAM FOR ANGLE-OF-ATTACK EFFECTS (RUN ID NUMBER)

Δα		0.29	1.00
α	M		
1.60	.62		284
	.72		285
	.77		286
	.82		287
	.95		288
2.60	.95	289	290
2.75	.82	291	
3.25	.82	292	
3.50	.82		293
4.00	.82		294
	.95		295
4.50	.82		296
4.75	.82	297	
5.00	.77	300	
	.95		298
5.25	.82	299	

TABLE 21. MISCELLANEOUS TEST CONDITIONS FOR LANN WING

run number	α	M	t	Δα	harm
38	0.6	0.62	24.0	0.50	1
84	0.6	0.82	18.0	0.50	1
127	2.6	0.77	50.0	0.25	1
164	3.0	0.95	12.0	0.50	1
174	3.0	0.95	12.0	0.50	1
158	0.6	0.95	30.1	0.05	1
159	0.6	0.95	30.1	0.05	2
160	0.6	0.95	30.1	0.05	3
253	4.0	0.00	12.0	0.25	1
254	4.0	0.00	24.0	0.25	1
255	4.0	0.00	36.0	0.25	1
256	4.0	0.00	48.0	0.25	1
257	4.0	0.00	60.0	0.25	1
258	4.0	0.00	72.0	0.25	1

TABLE 22. COMPARISON OF CALCULATED AND MEASURED UNSTEADY TOTAL NORMAL FORCE

REDUCED FREQUENCY		MEAN VALUE	AMPLITUDE	PHASE ANGLE
0.20463 (RUN 73)	MEASURED	0.32027	0.02373	-16.20°
	XTRAN3S	0.35029	0.02964	9.59°
0.40657 (RUN 85)	MEASURED	0.3230	0.01598	-34.80
	XTRAN3S	0.35004	0.02183	-0.08°
0.61121 (RUN 87)	MEASURED	0.3228	0.01295	-37.90
	XTRAN3S	0.34998	0.01990	-9.70°

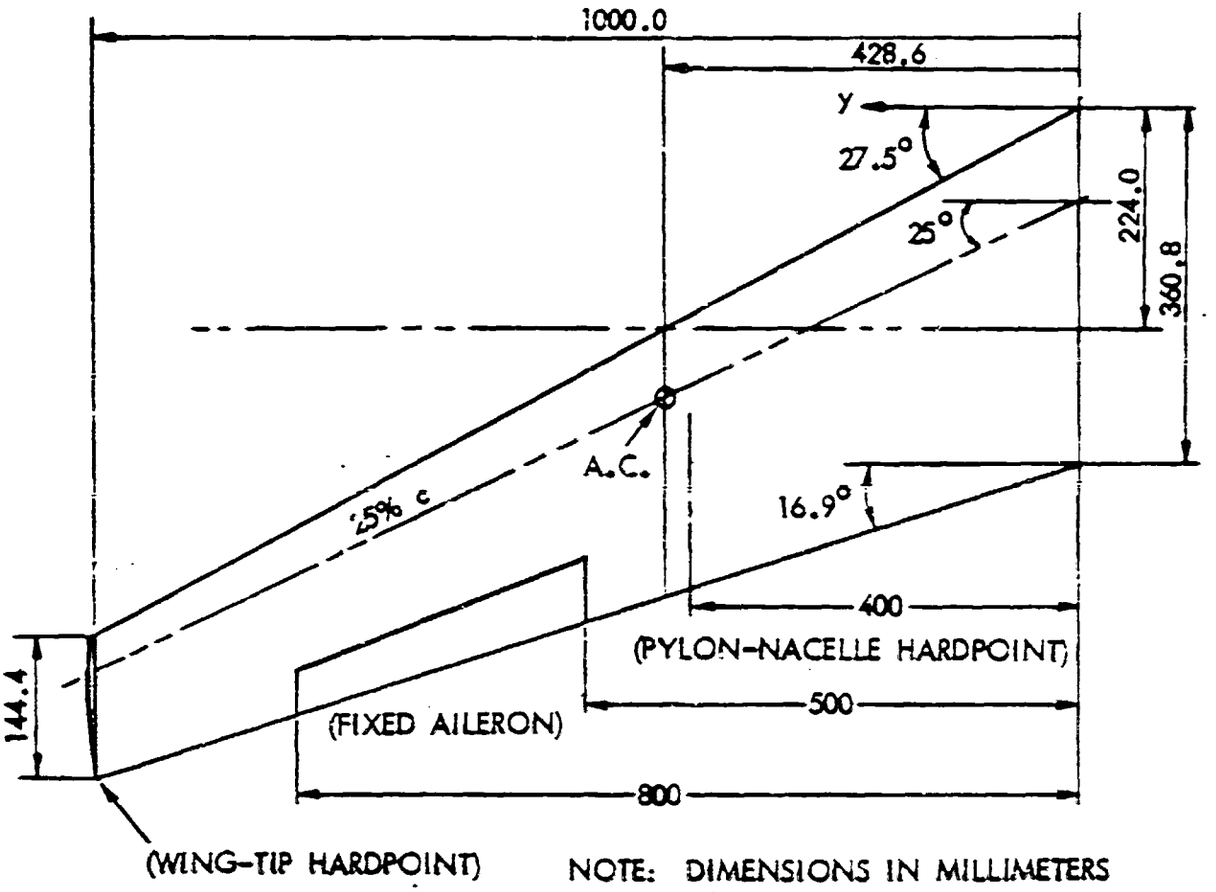

Figure 1. LANN Wing Planform Layout.

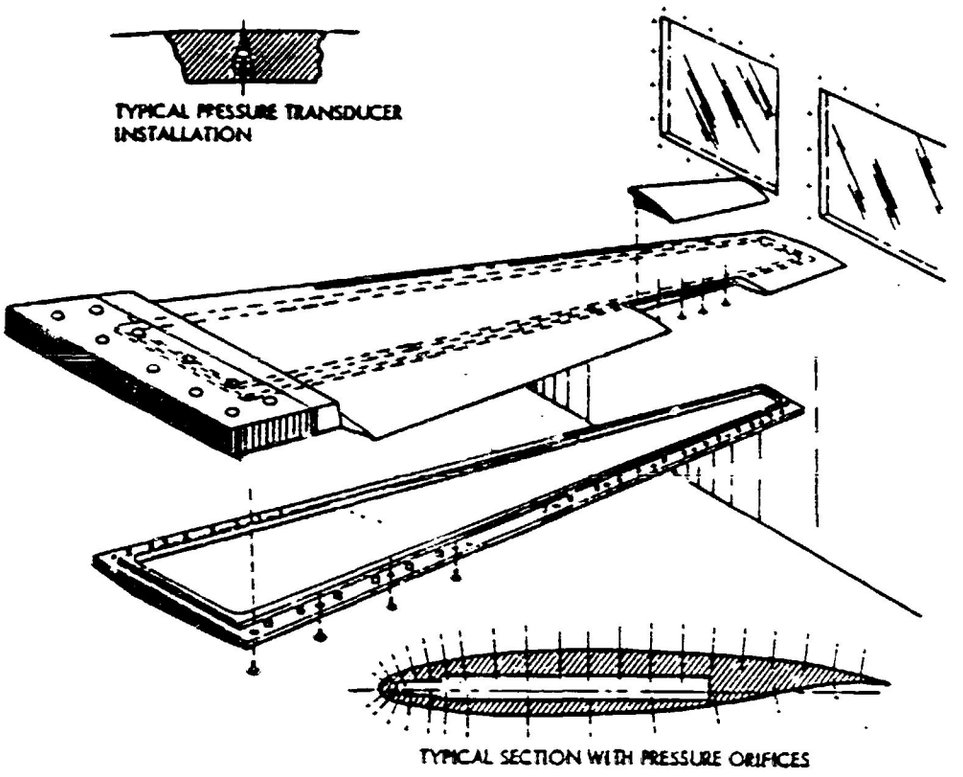

Figure 2. LANN Wing Assembly

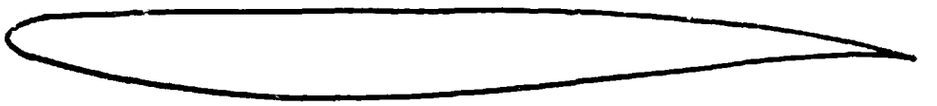

ROOT SECTION

BOTH SECTIONS
t/c 12%

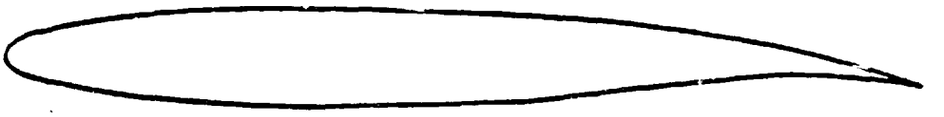

TIP SECTION

Figure 3. Airfoil Sections for LANN Wing

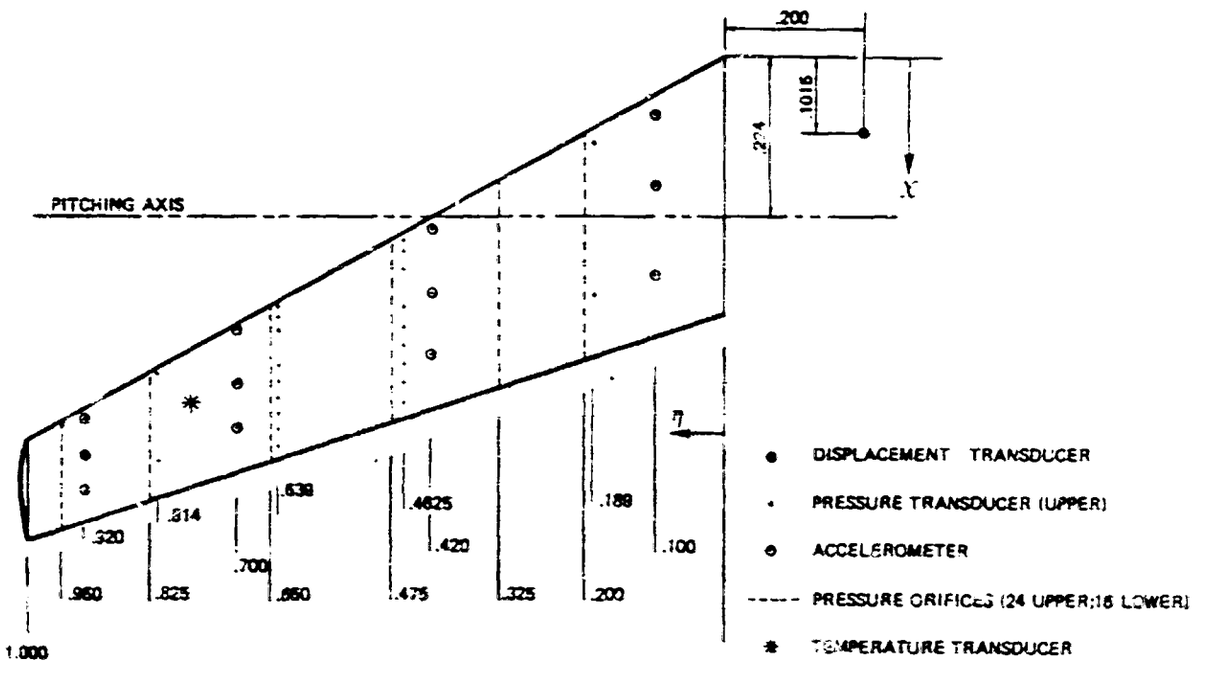

Figure 4. Position of Measuring Points on the LANN Wing

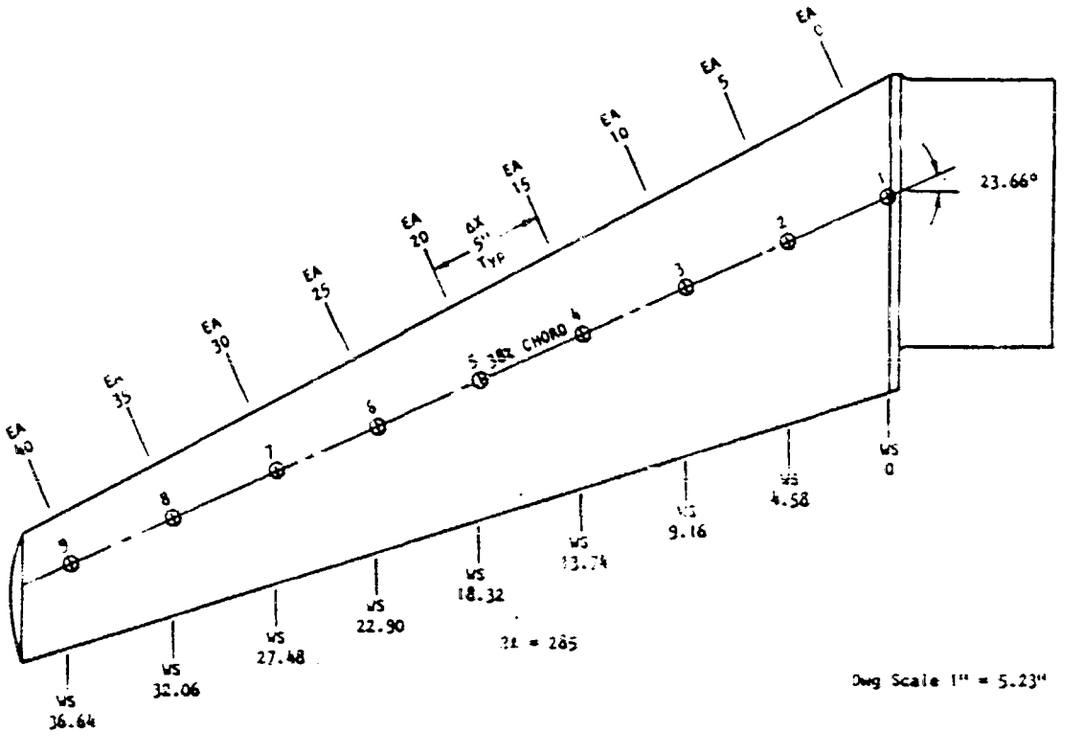

Figure 5. LANN Wing-Stiffness Test Mirror Locations

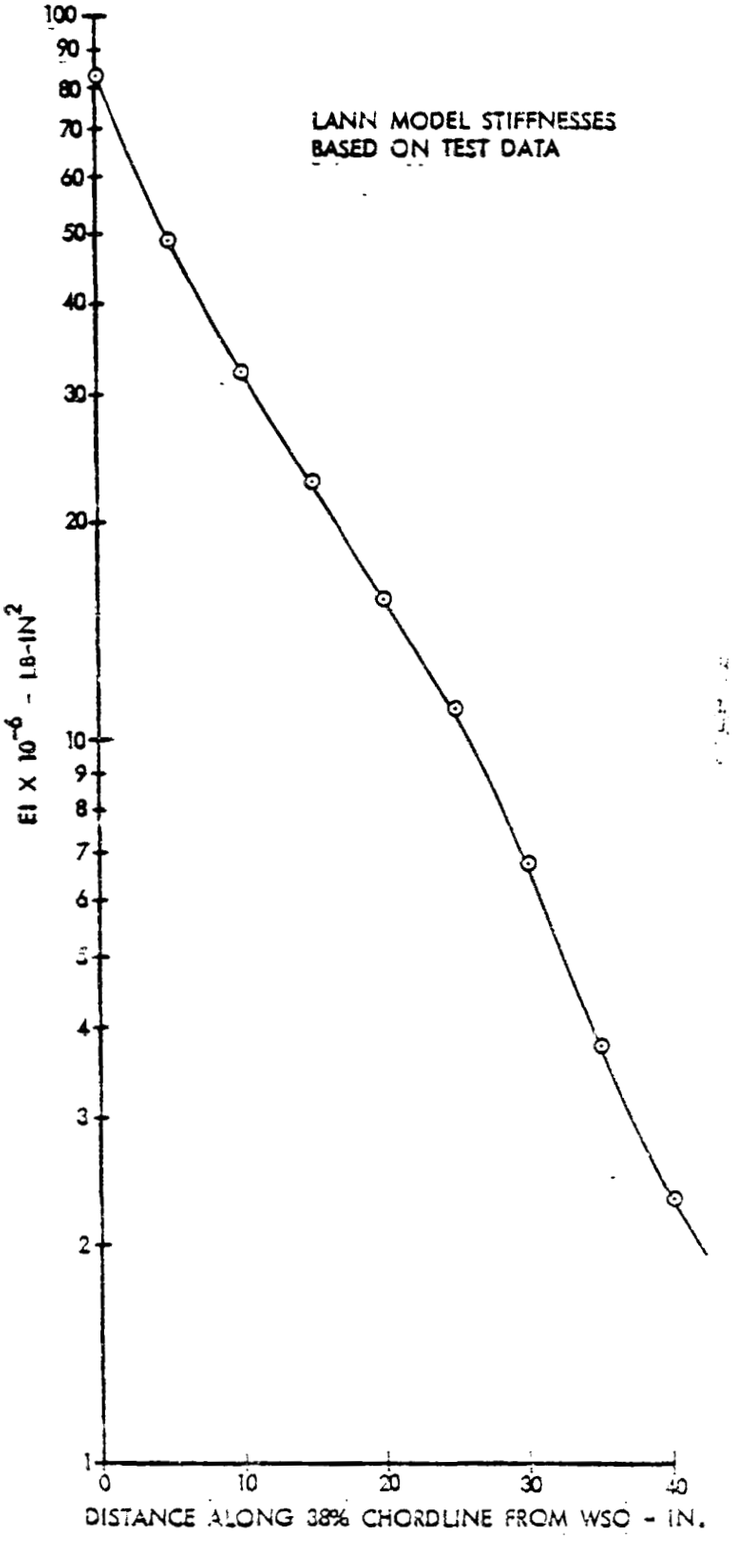

Figure 6. Bending Stiffness Distribution

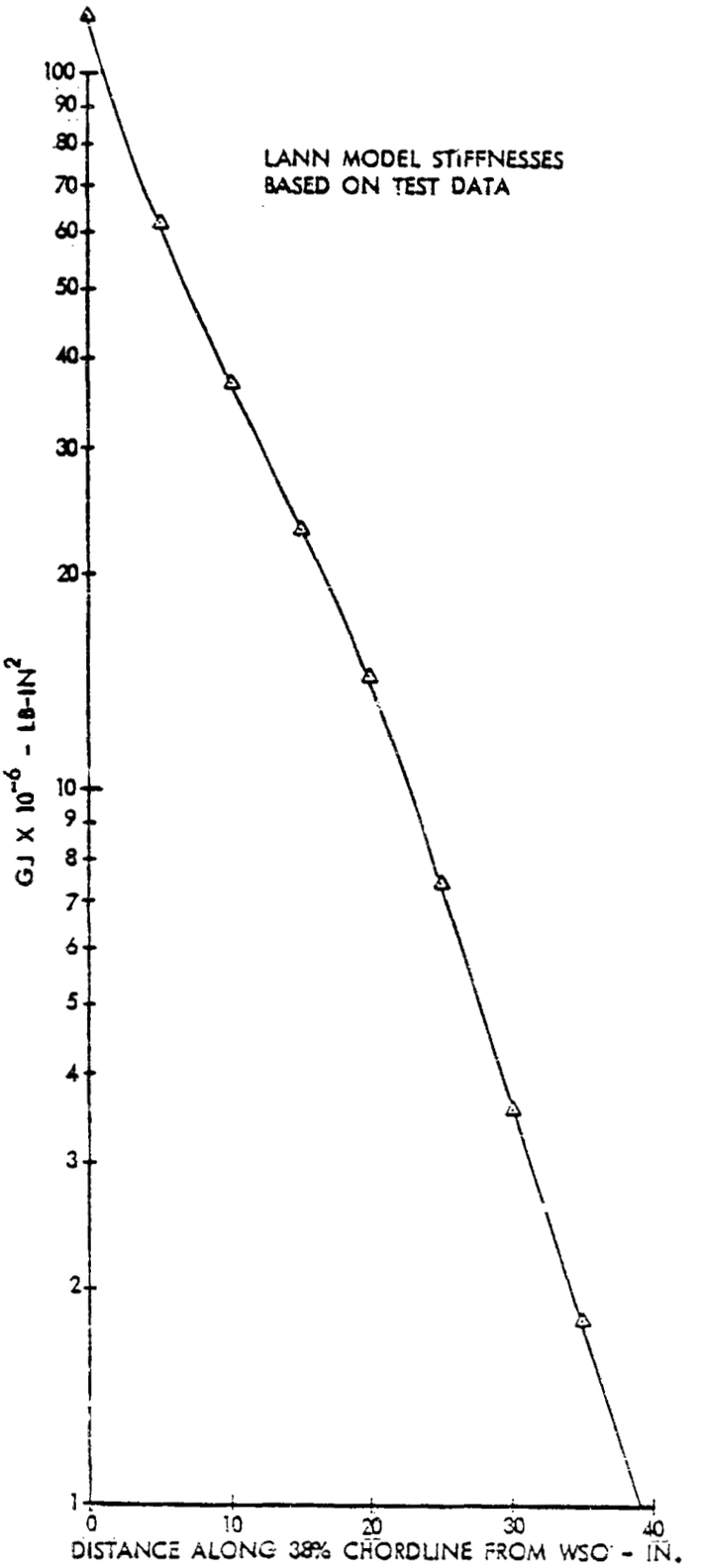

Figure 7. Torsional Stiffness Distribution

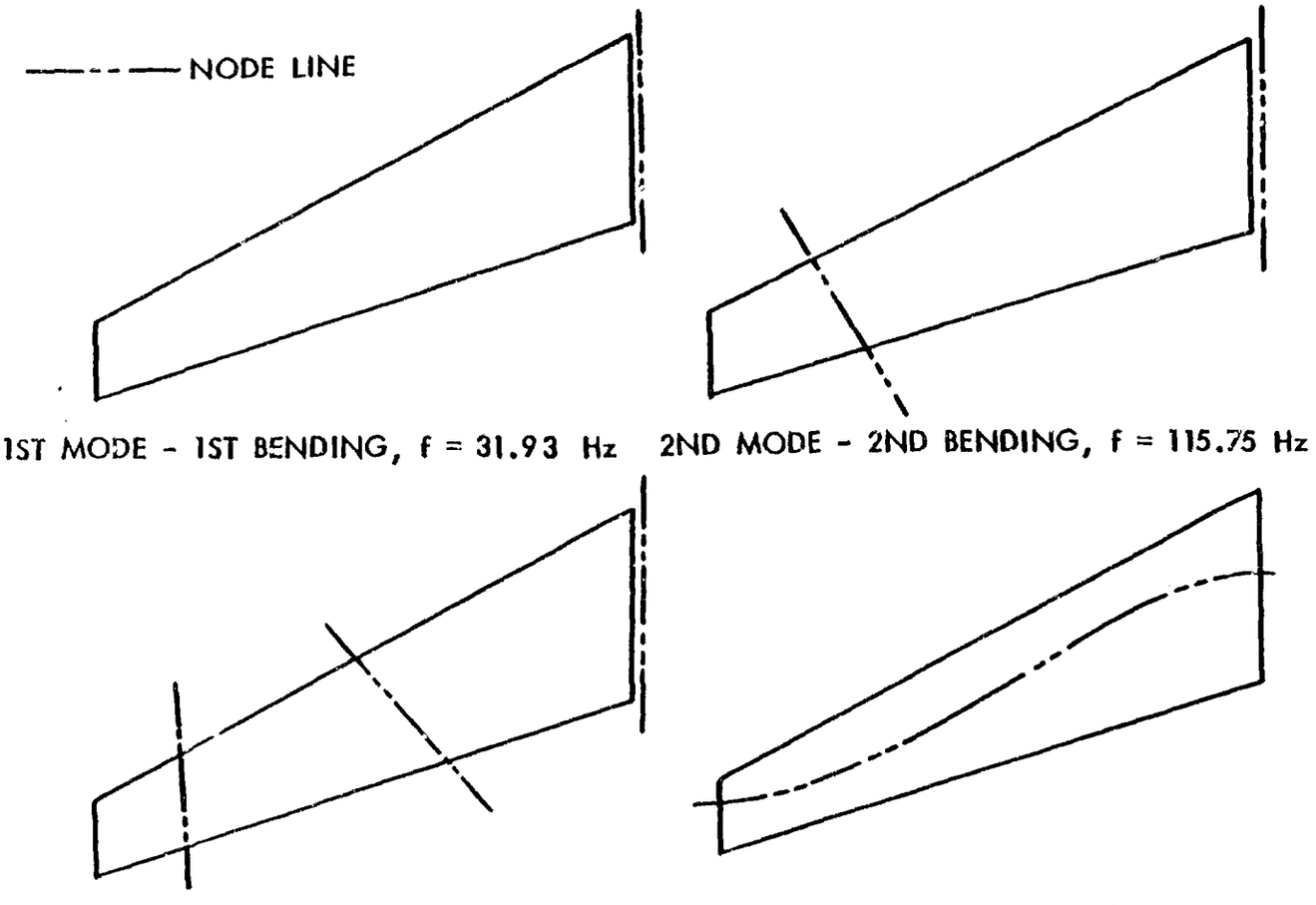

Figure 8. LANN Model Mode Shape Node Line Locations

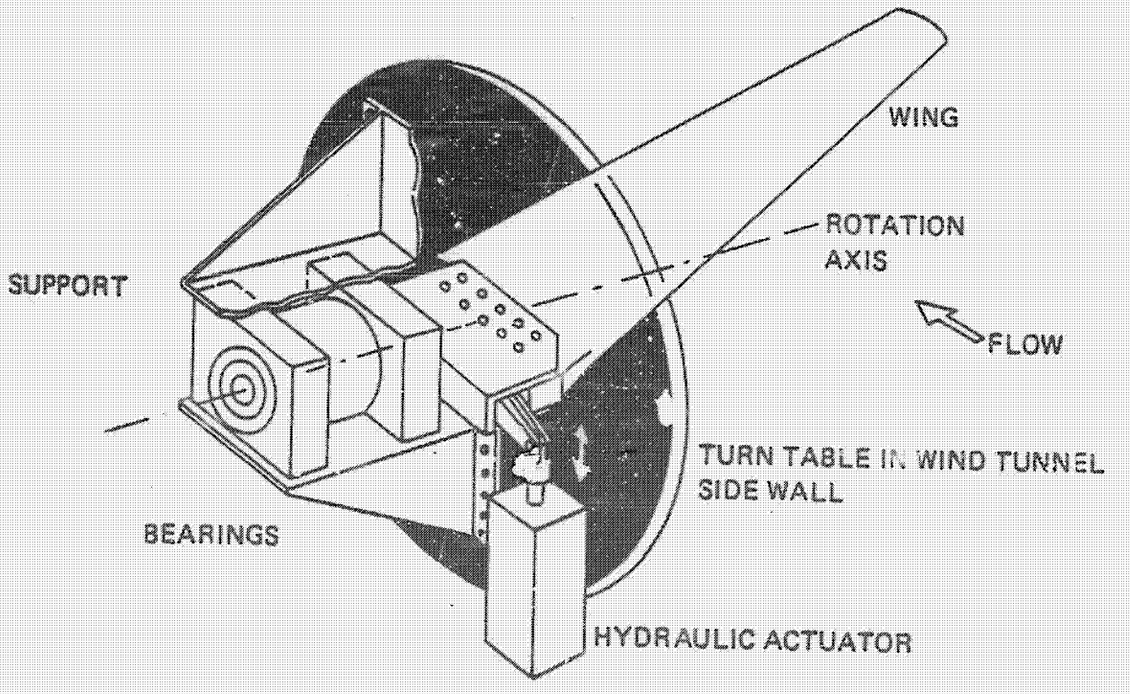

Figure 9. LANN Wing Mount Installation

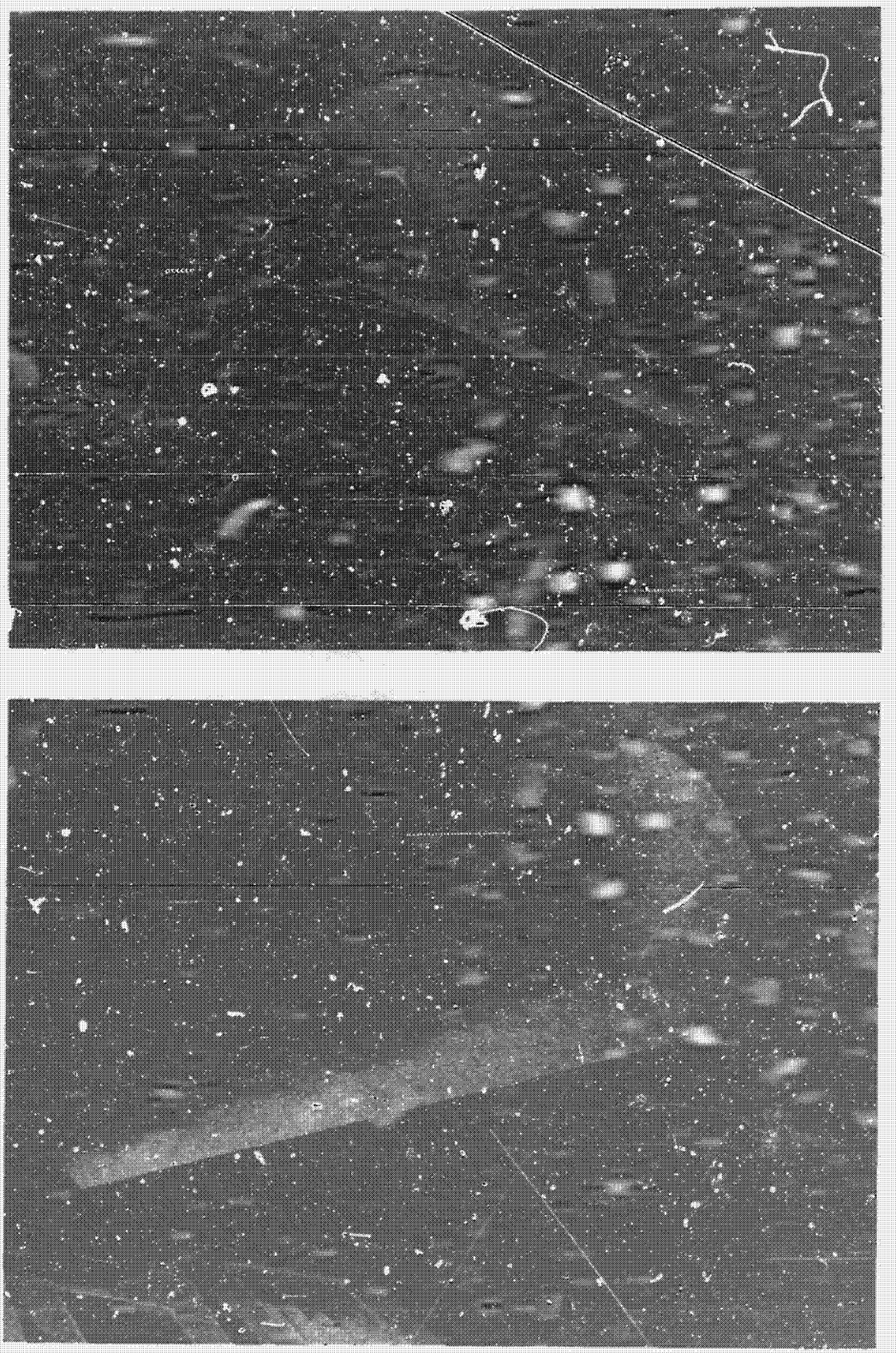

Figure 10. Views of LANN Model Installation in the HST

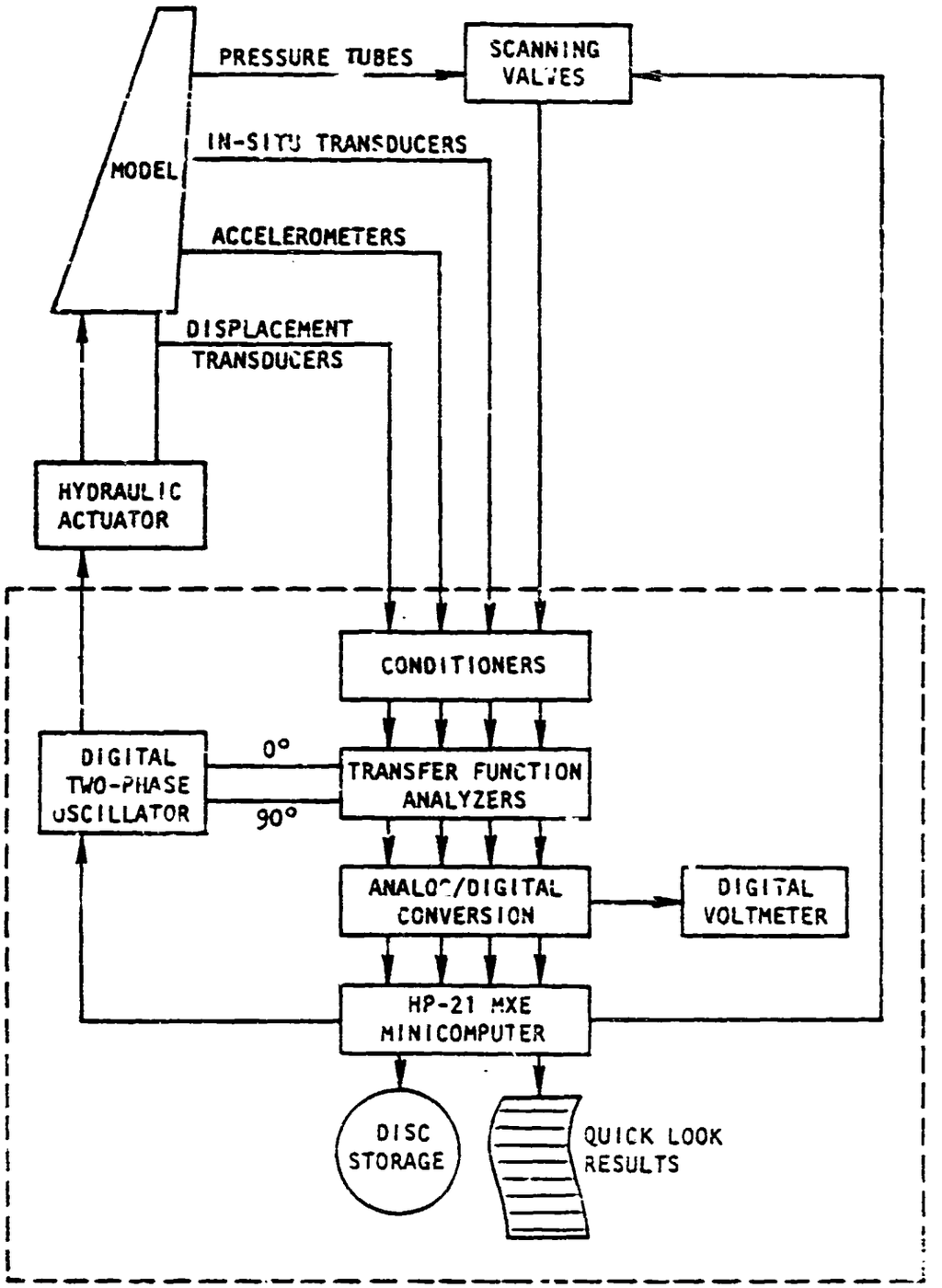

Figure 11. Block-Diagram of PHAROS Data Acquisition and Reduction System

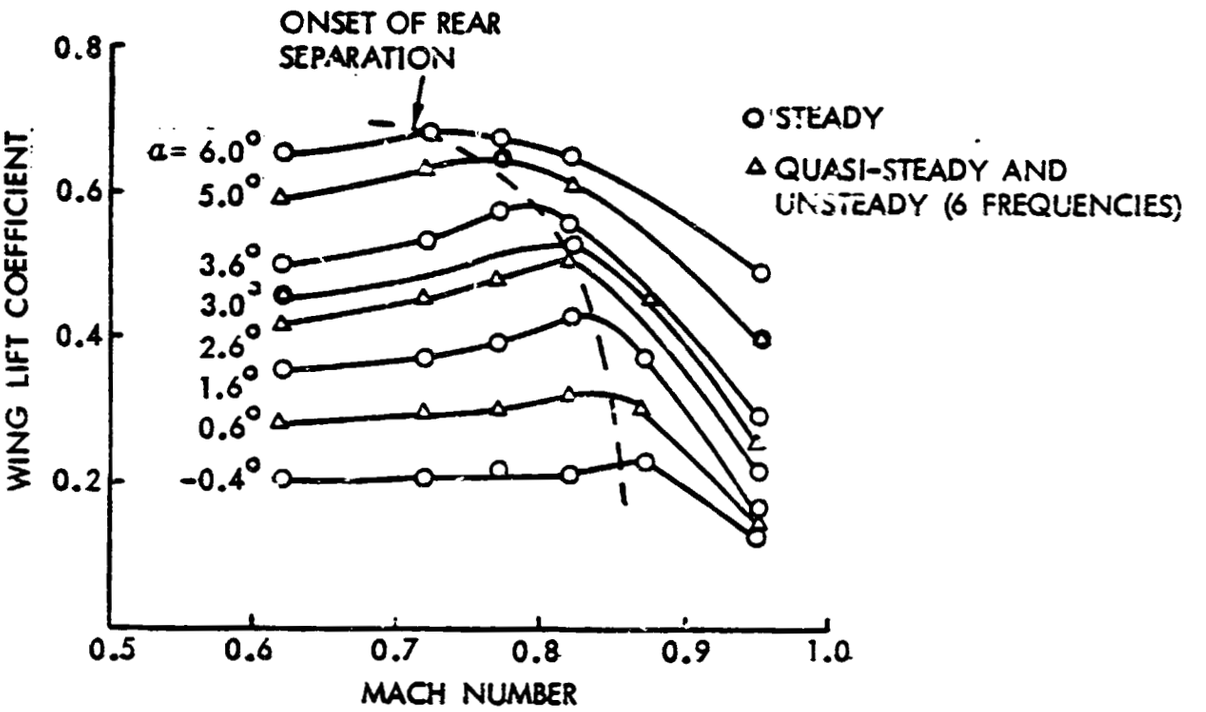

Figure 12. Measuring Program for LANN Model

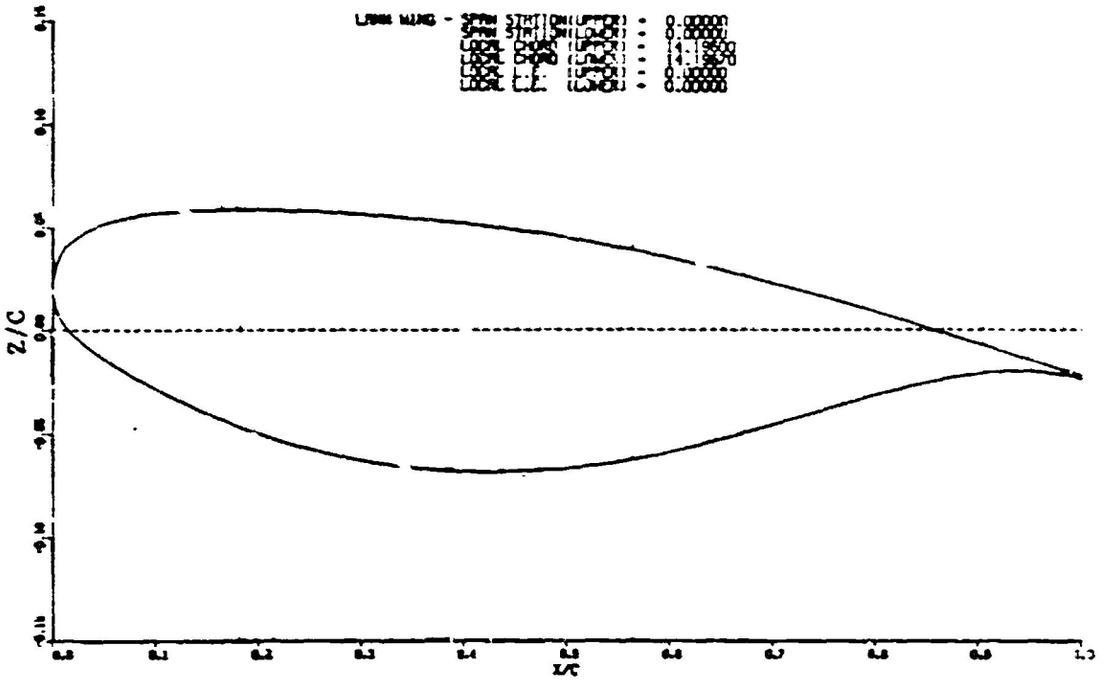

(a) SPAN-STATION = 0.00

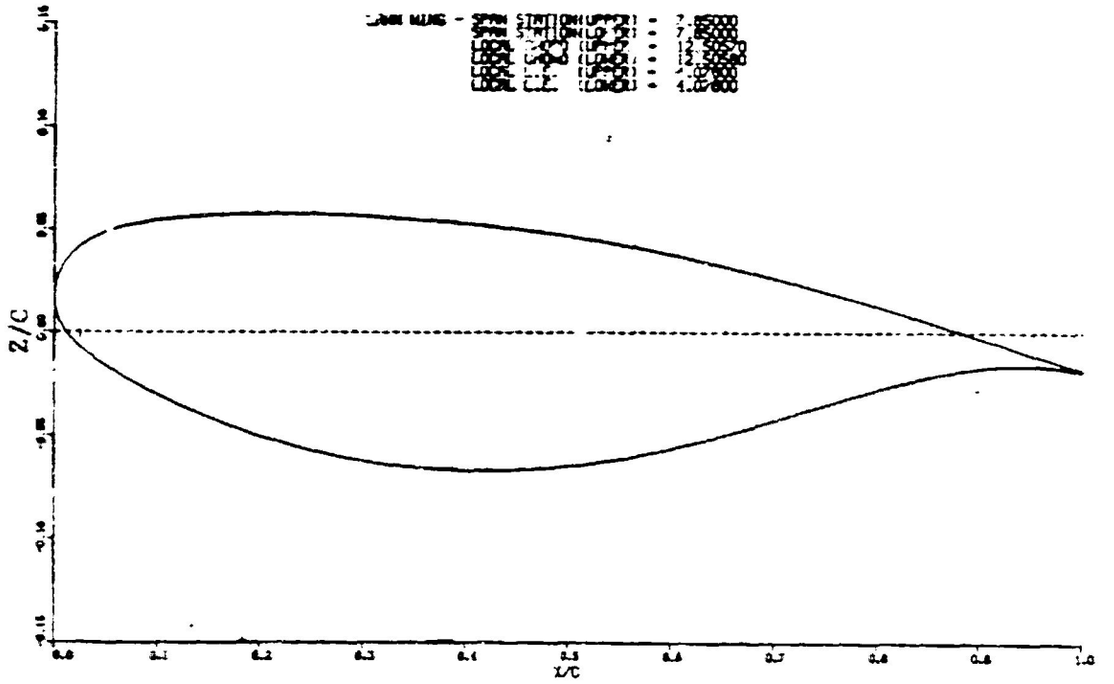

(b) SPAN-STATION = 0.20

Figure 13. Ordinates of LANN Wing Airfoil Sections (Sheet 1 of 4)

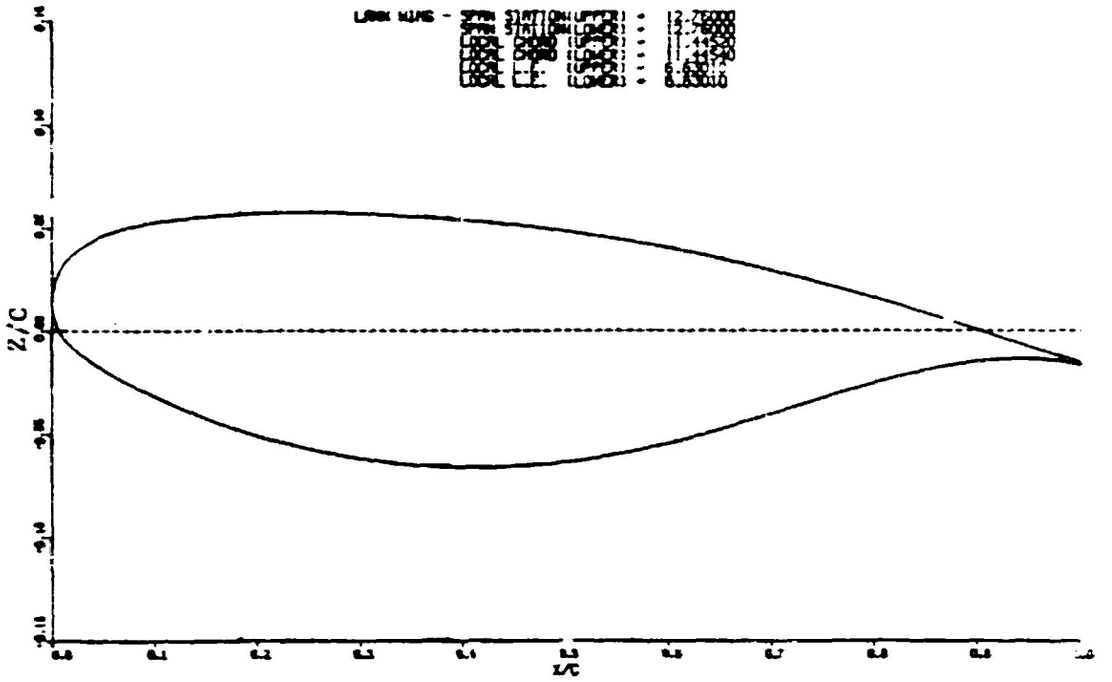

(c) SPAN-STATION = 0.32

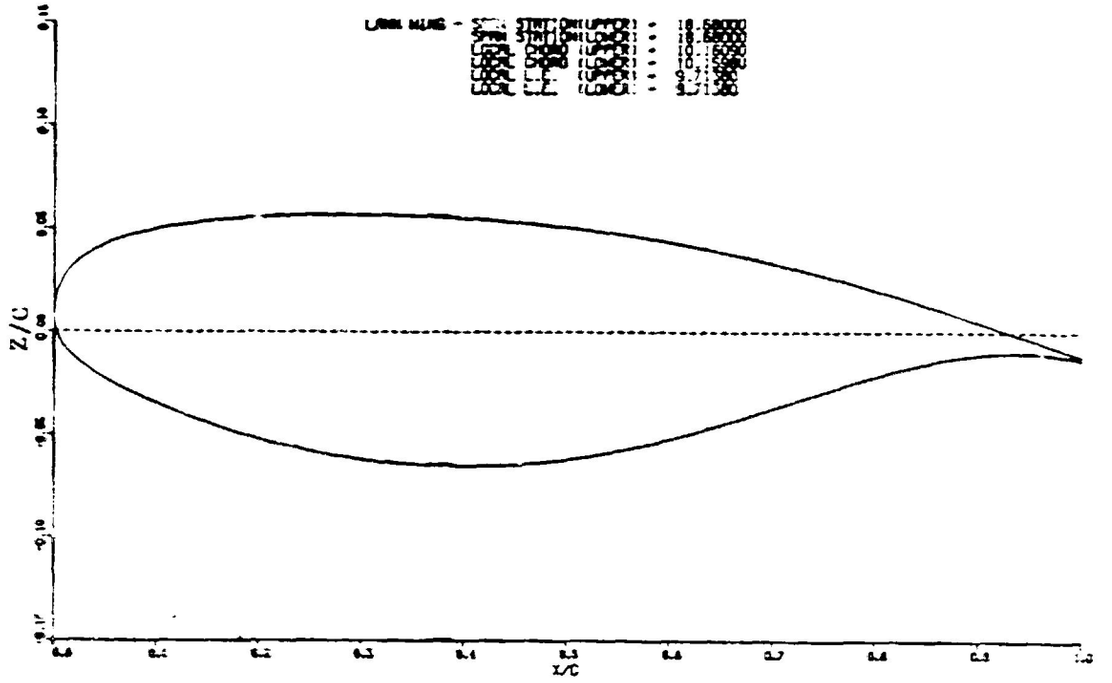

(d) SPAN-STATION = 0.47

Figure 13. Ordinates of LANN Wing Airfoil Sections (Sheet 2 of 4)

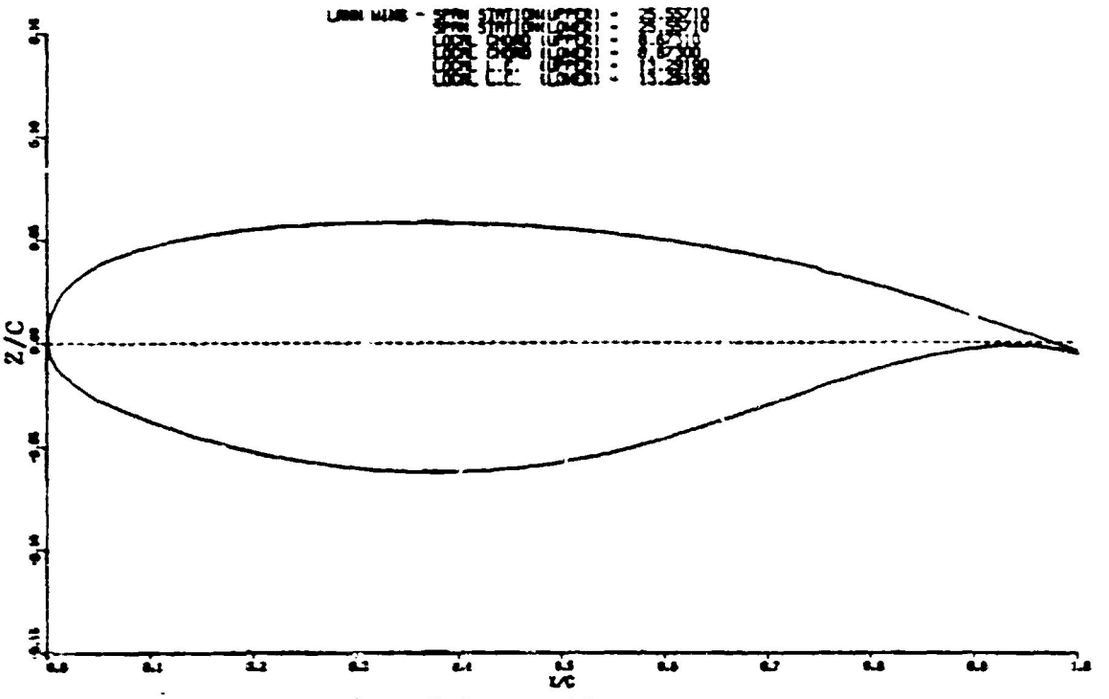

(e) SPAN-STATION = 0.65

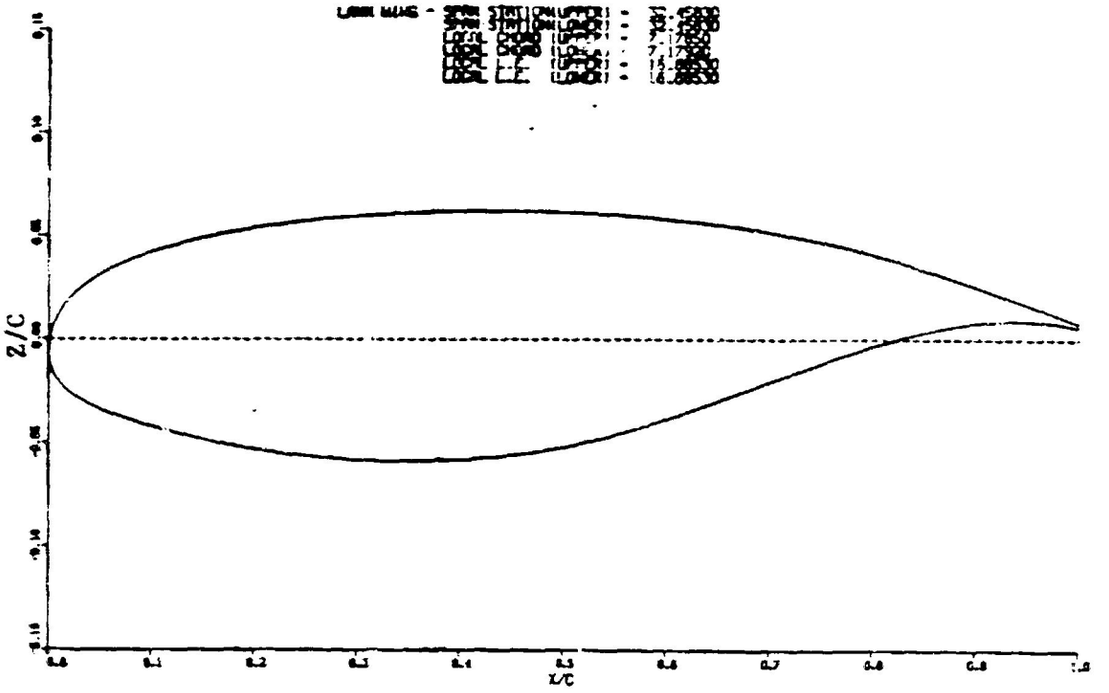

(F) SPAN-STATION = 0.82

Figure 13. Ordinates of LANN Wing Airfoil Sections (Sheet 3 of 4)

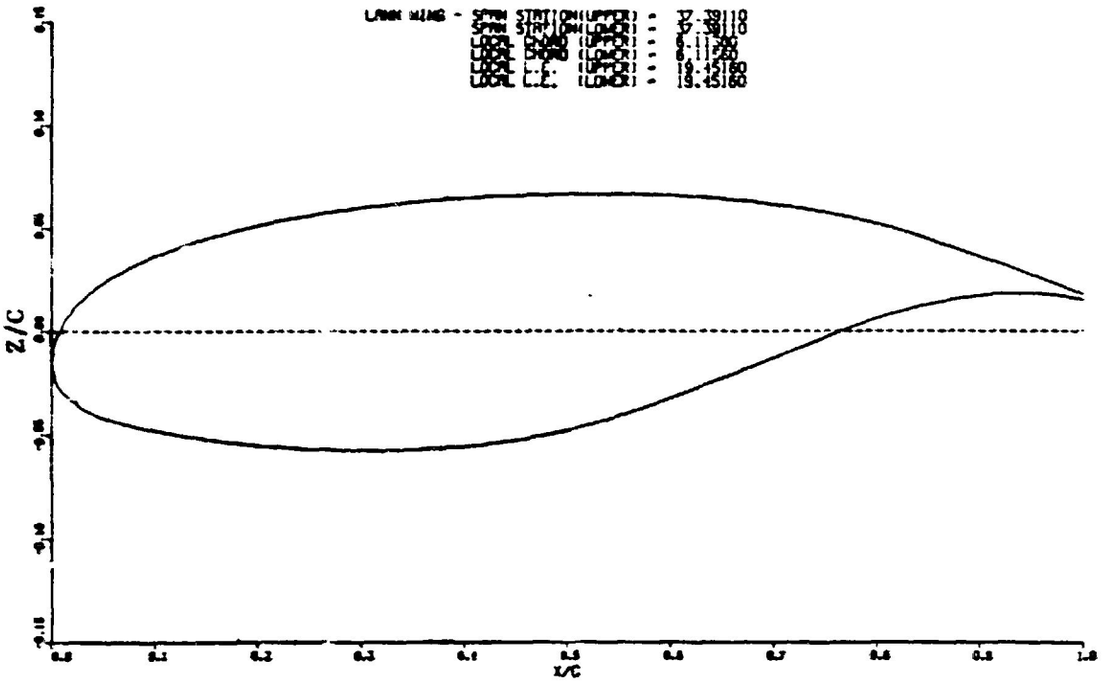

(g) SPAN-STATION = 0.95

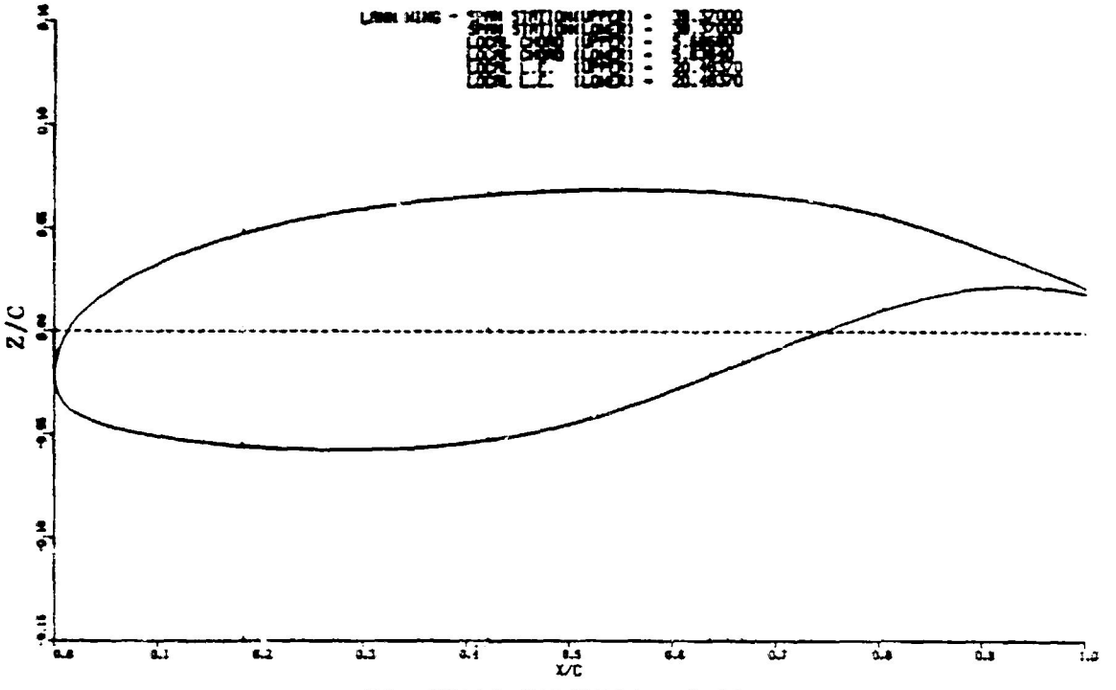

(h) SPAN-STATION = 1.00

Figure 13. Ordinates of LANN Wing Airfoil Sections (Sheet 4 of 4)

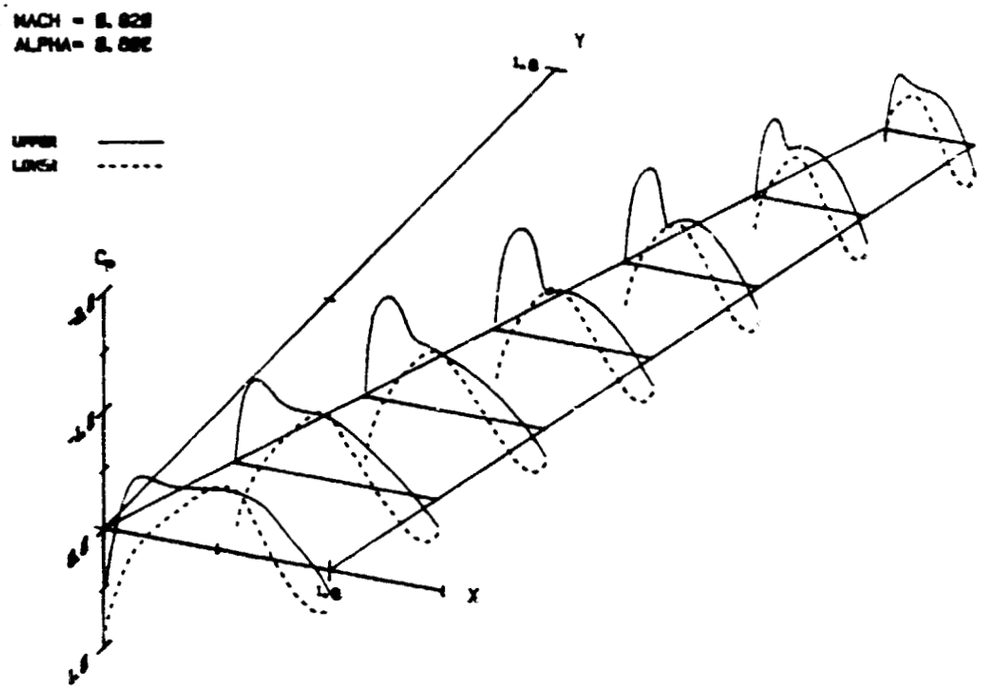

(a) AMES COEFFICIENTS

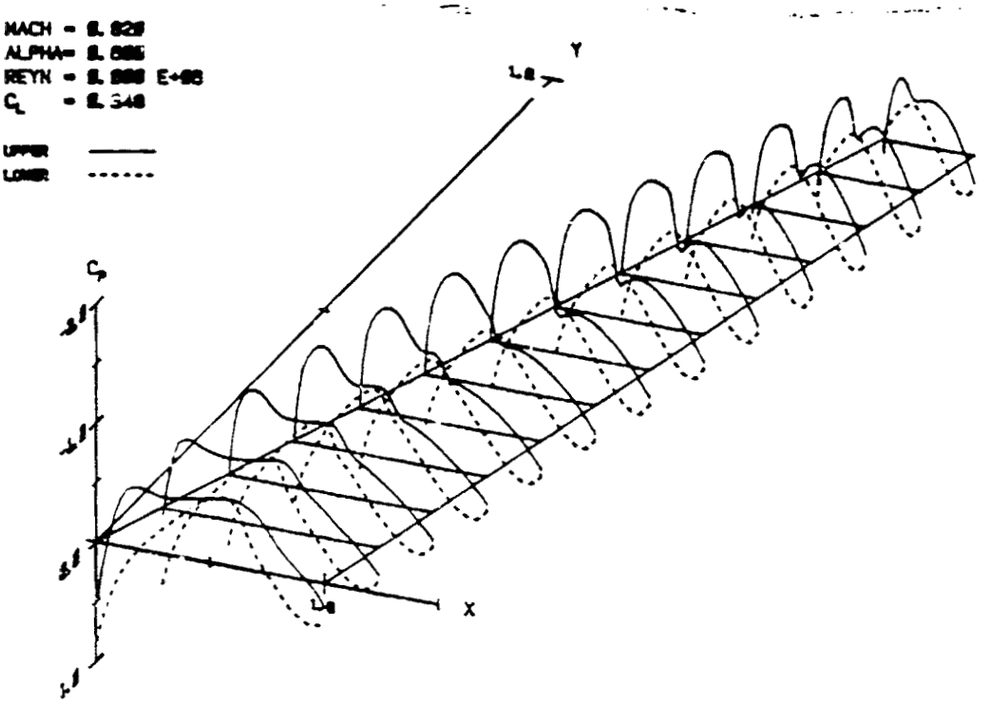

(b) NLR COEFFICIENTS

Figure 14. Computed Steady Flow Pressure Distributions on Wing with XTRAN3S Code

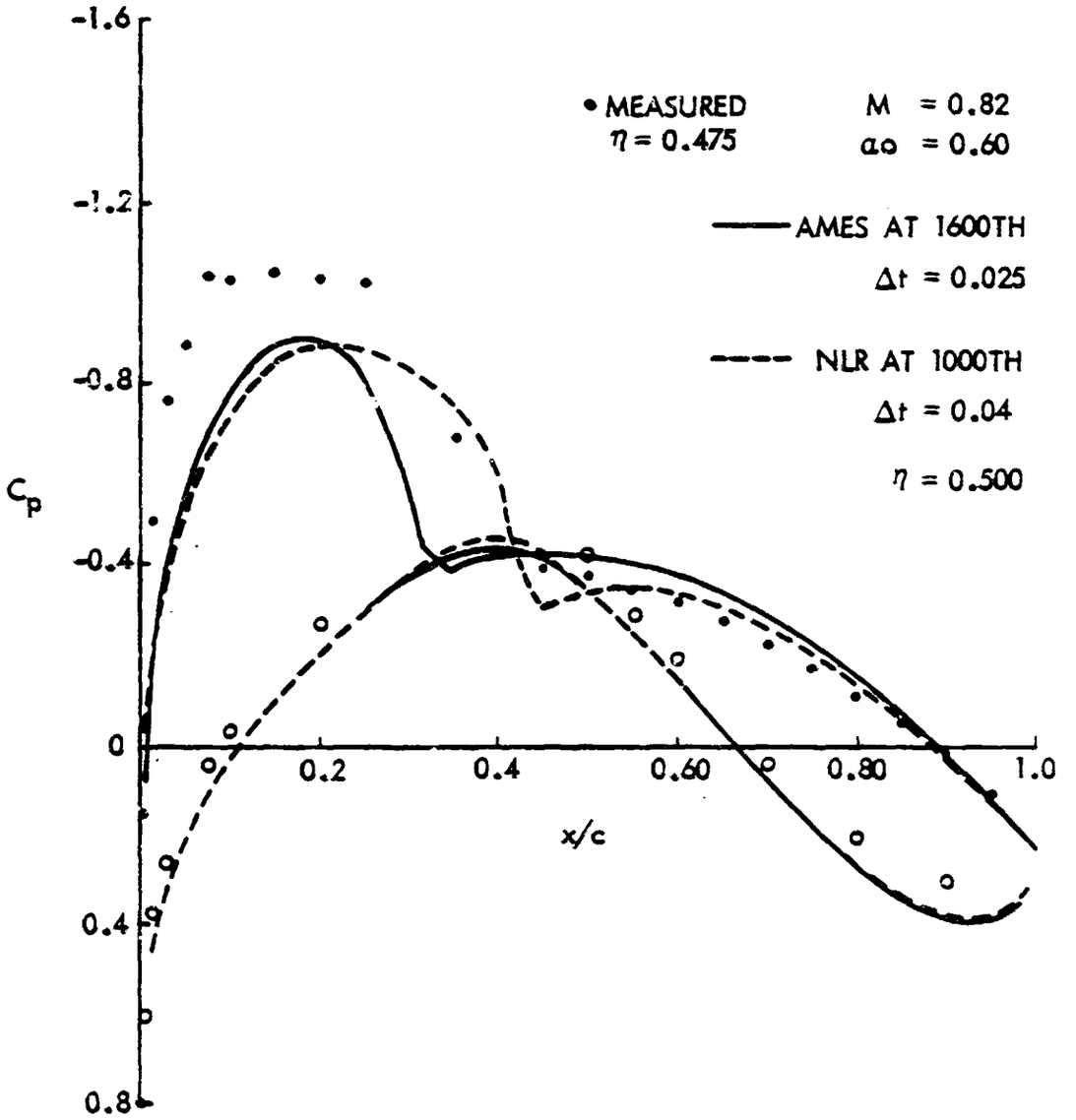

Figure 15. Pressure Distribution Comparison of XTRAN3S Code for Different Coefficients

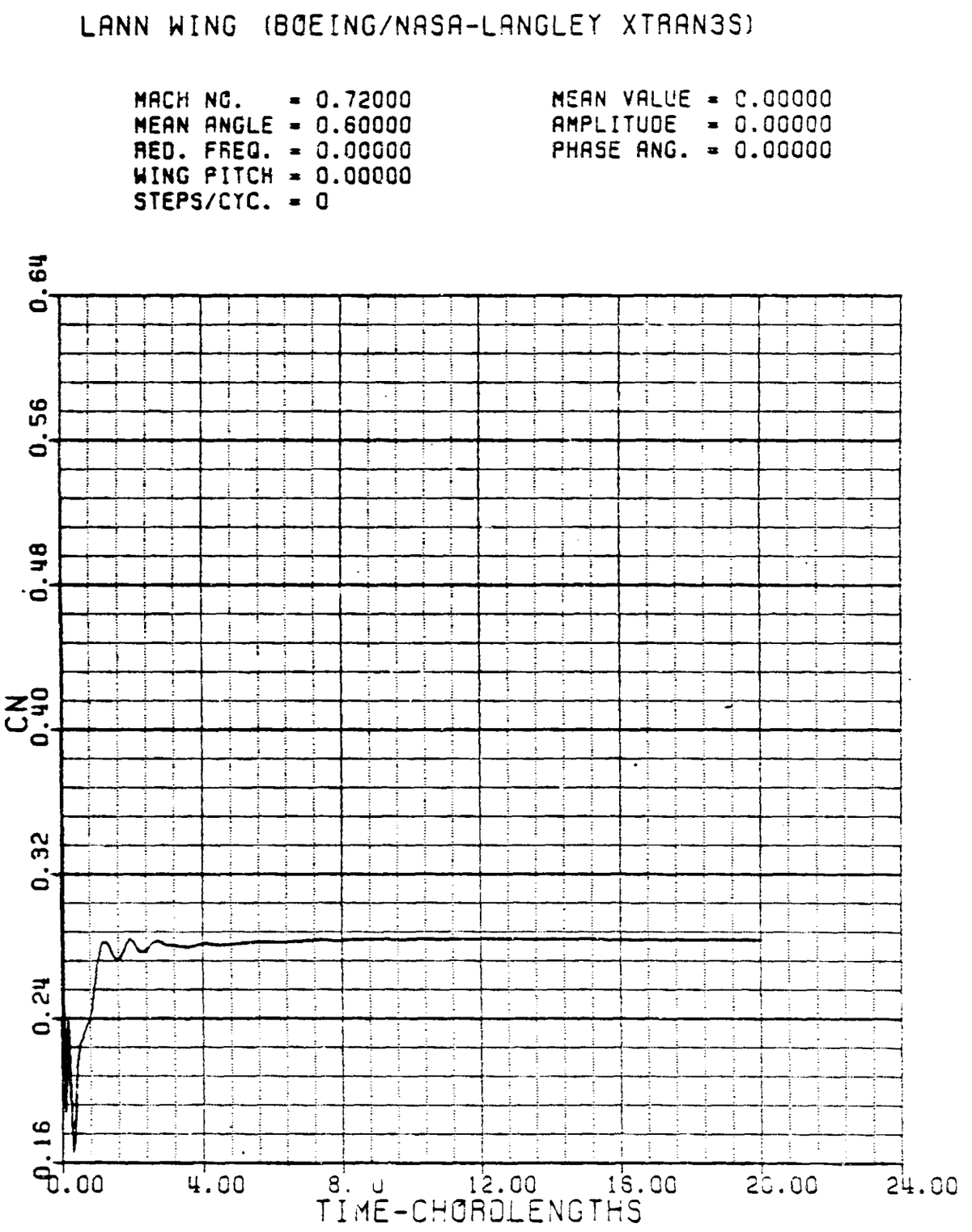

(a) MACH NUMBER = 0.72 AND MEAN ANGLE OF ATTACK = 0.60

Figure 16. Time History of Steady Flow Calculations with XTRAN3S Code (Sheet 1 of 4)

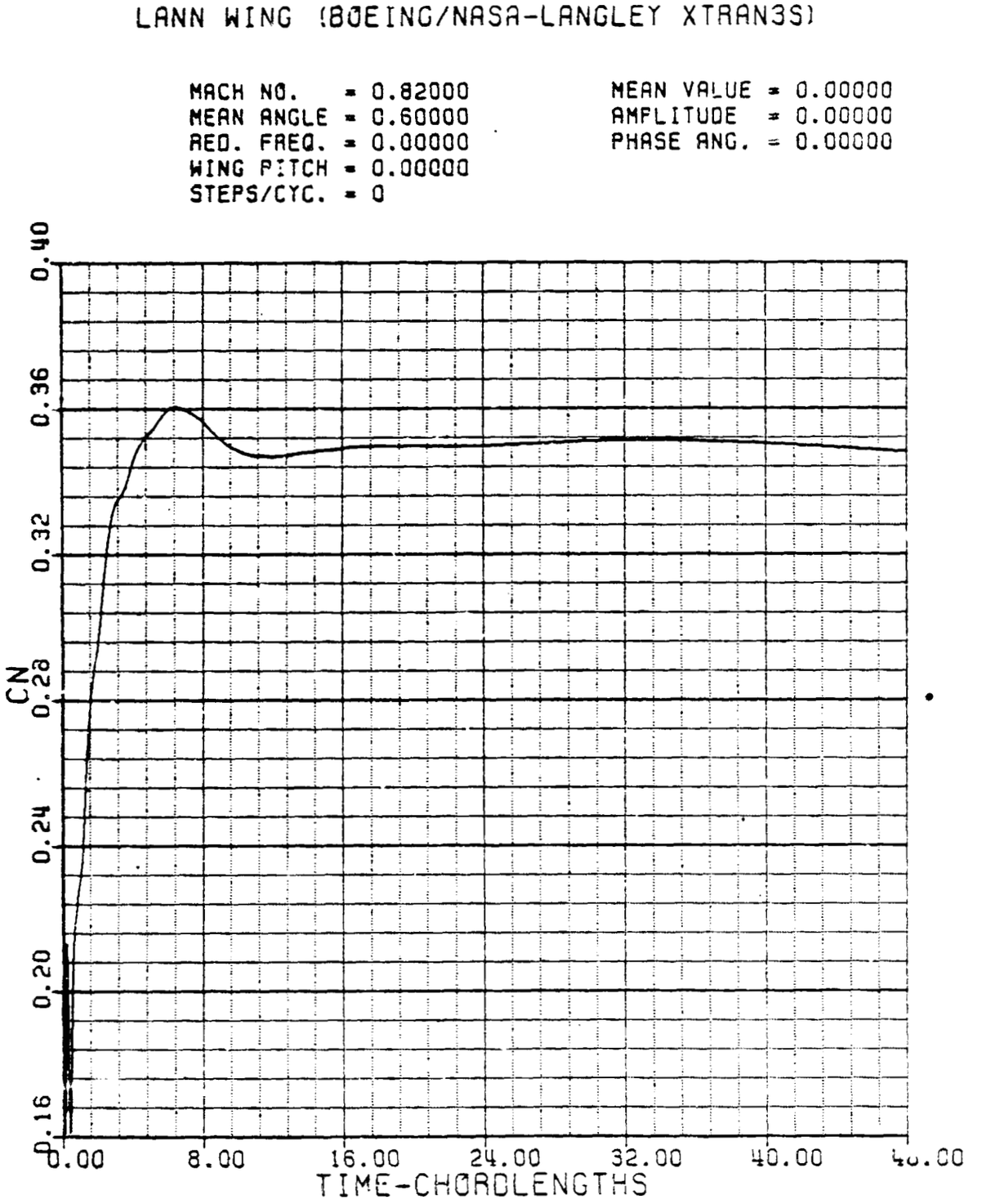

(b) MACH NUMBER = 0.82 AND MEAN ANGLE OF ATTACK = 0.60

Figure 16. Time History of Steady Flow Calculations with XTRAN3S Code (Sheet 2 of 4)

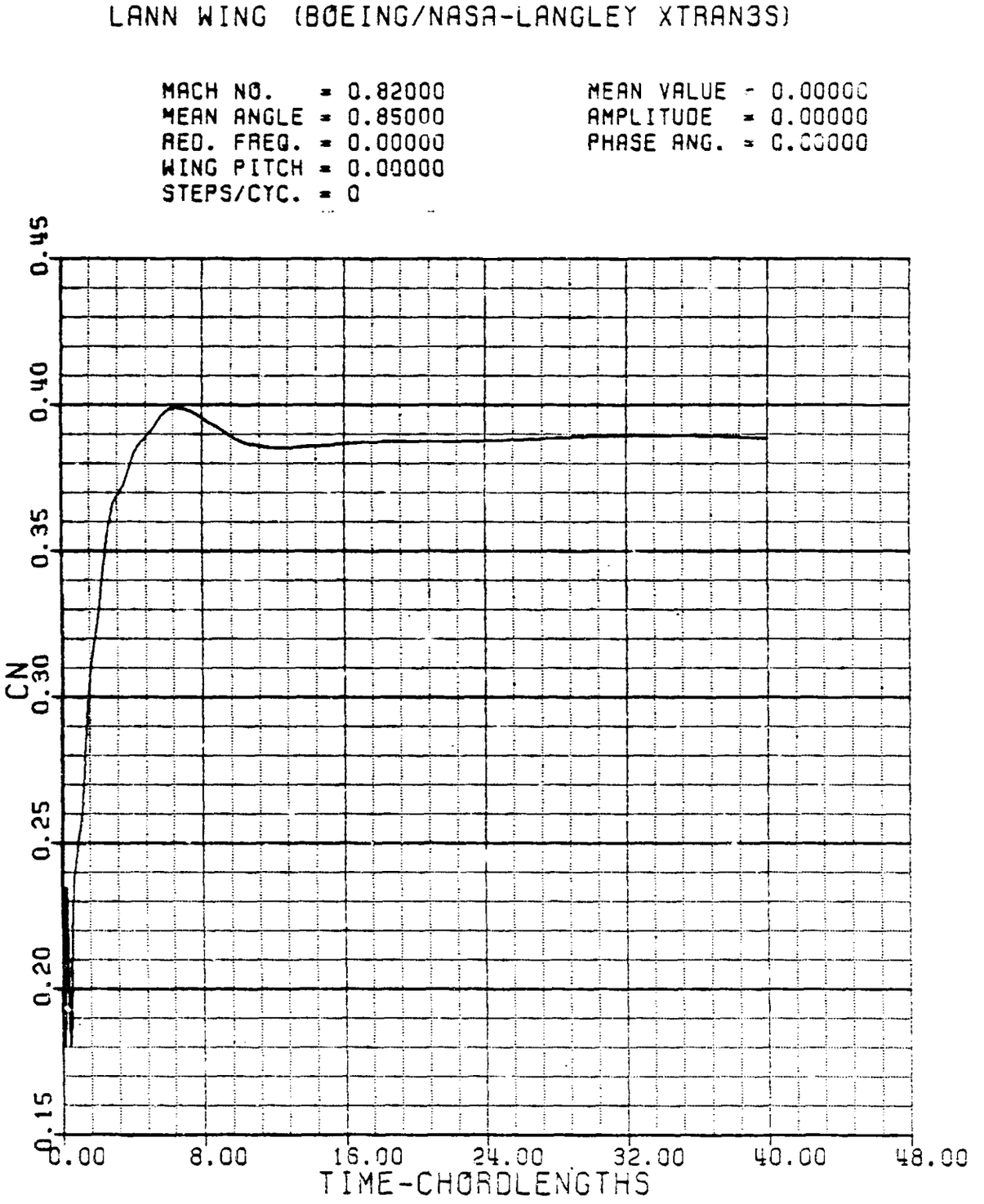

(c) MACH NUMBER = 0.82 AND MEAN ANGLE OF ATTACK = 0.85

Figure 16. Time History of Steady Flow Calculations with XTRAN3S Code (Sheet 3 of 4)

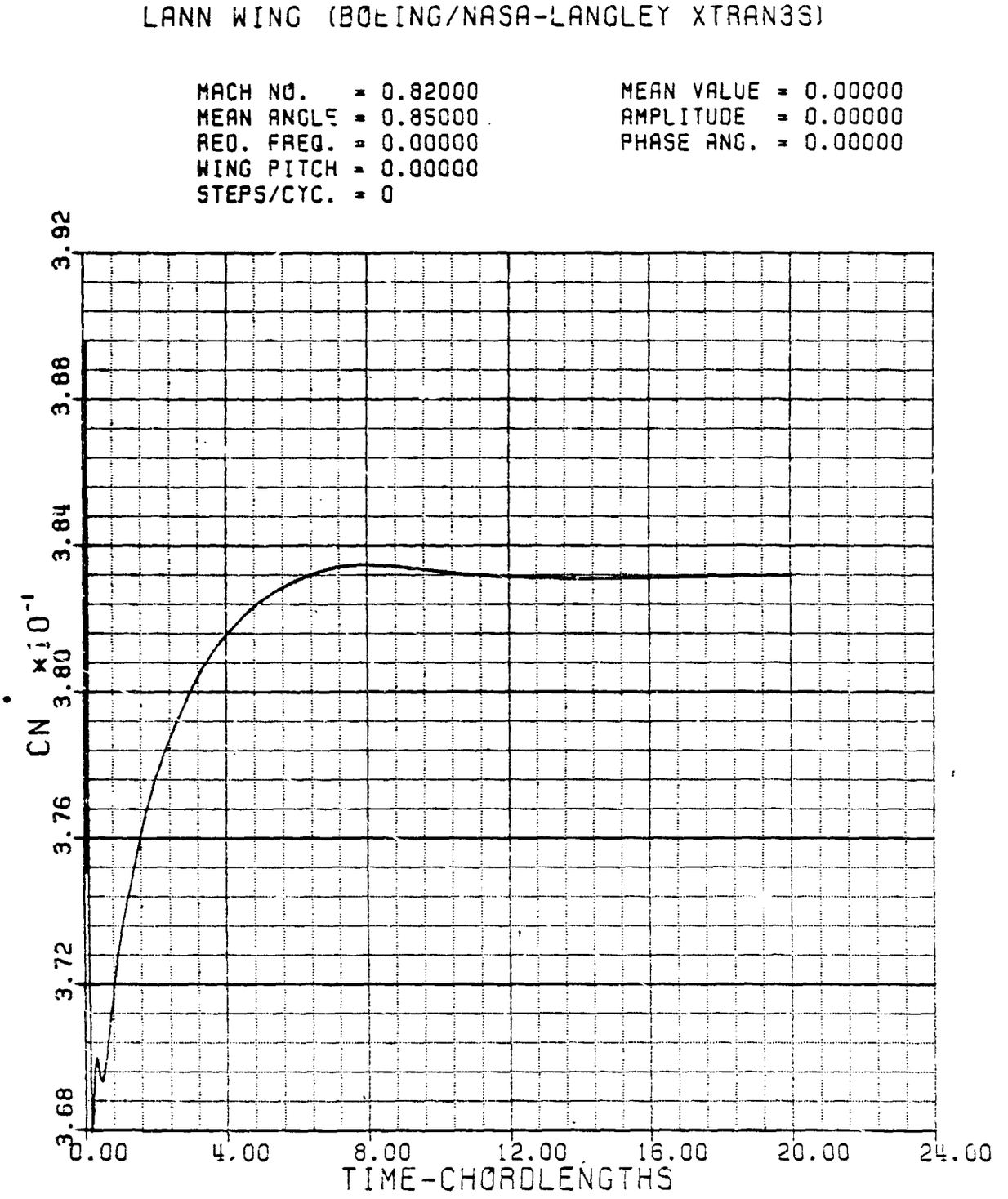

(d) MACH NUMBER = 0.82 AND MEAN ANGLE OF ATTACK = 0.85 (RESTARTED FROM A CONVERGED NON-UNIFORM FLOW FIELD)

Figure 16. Time History of Steady Flow Calculations with XTRAN3S Code (Sheet 4 of 4)

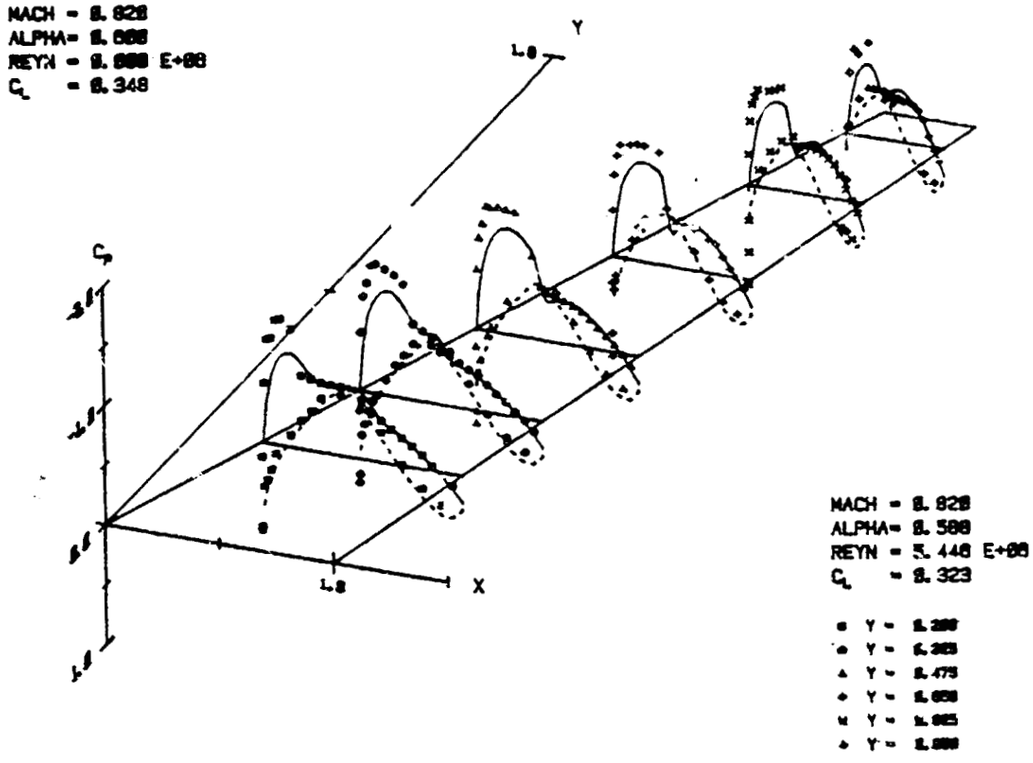

Figure 17. Comparison of Pressure Distribution on Wing Computed with XTRAN3S Code

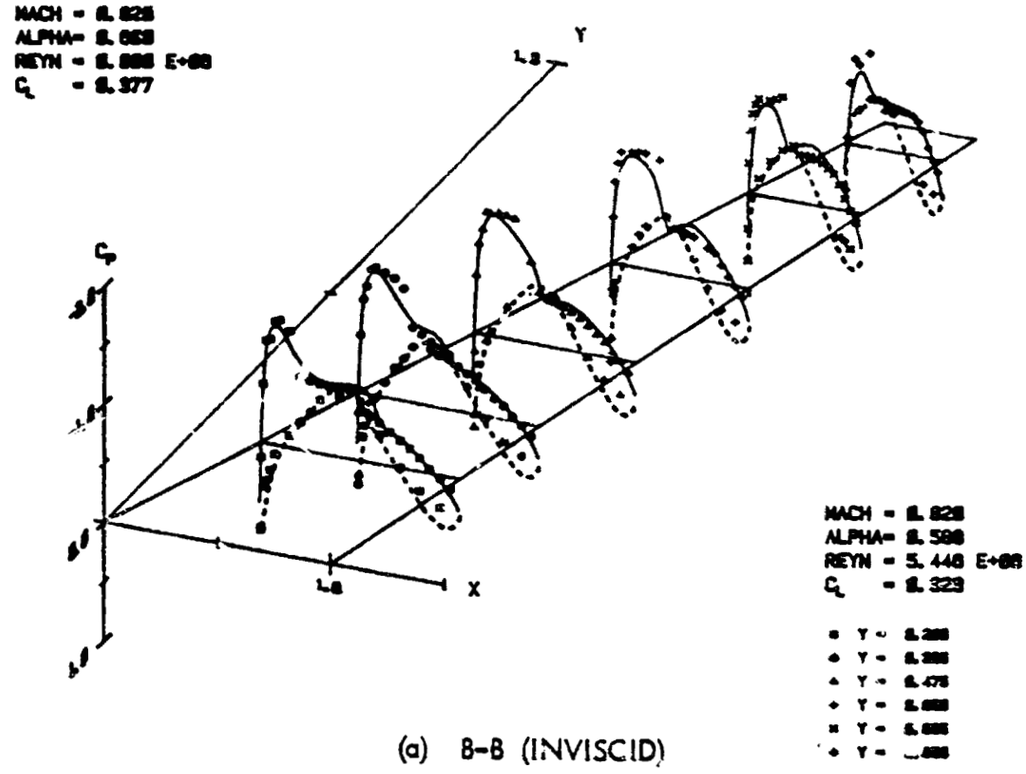

(a) B-B (INVISCID)

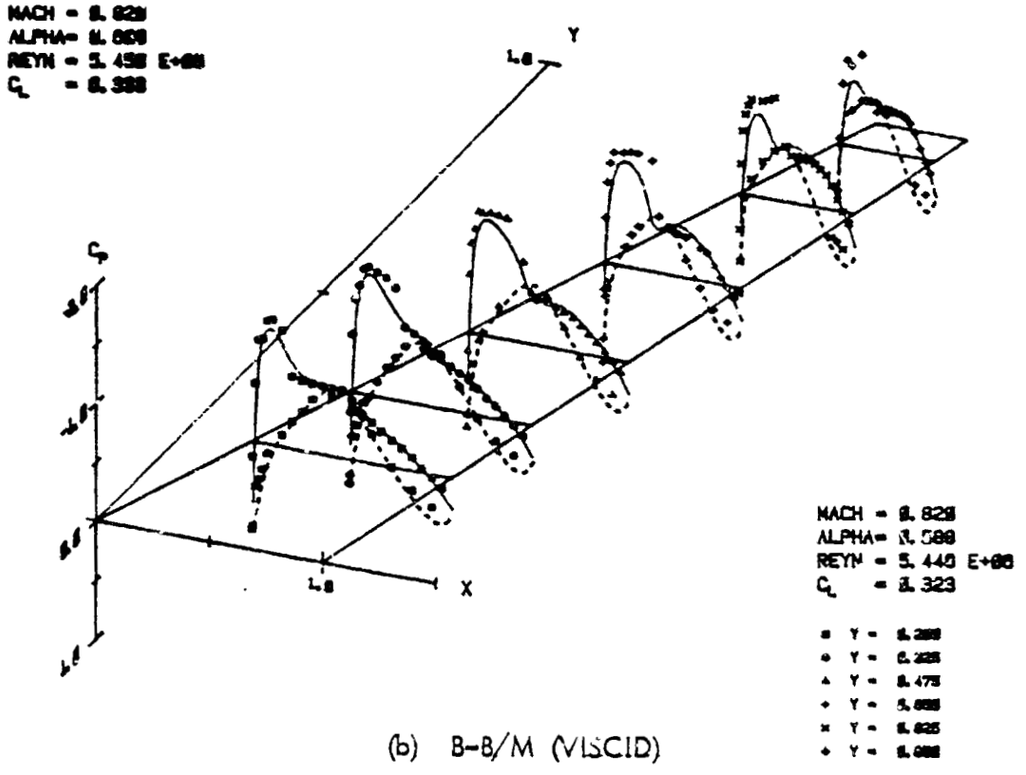

(b) B-B/M (VISCID)

Figure 18. Comparison of Pressure Distribution on Wing Computed with B-B/M Code

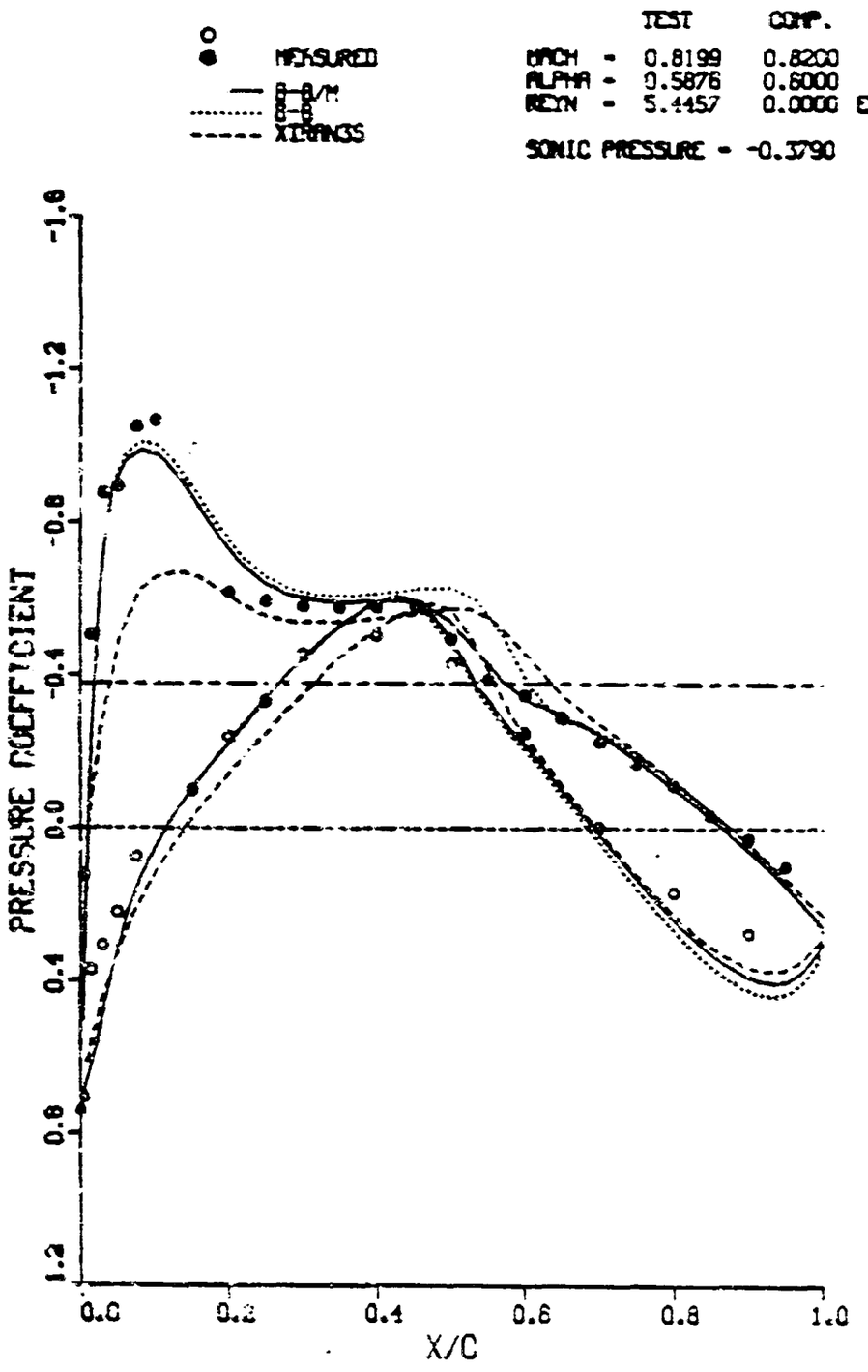

(a) SPAN-STATION = 0.200

Figure 19. Comparison of Computed and Measured Pressure Distributions (Sheet 1 of 6)

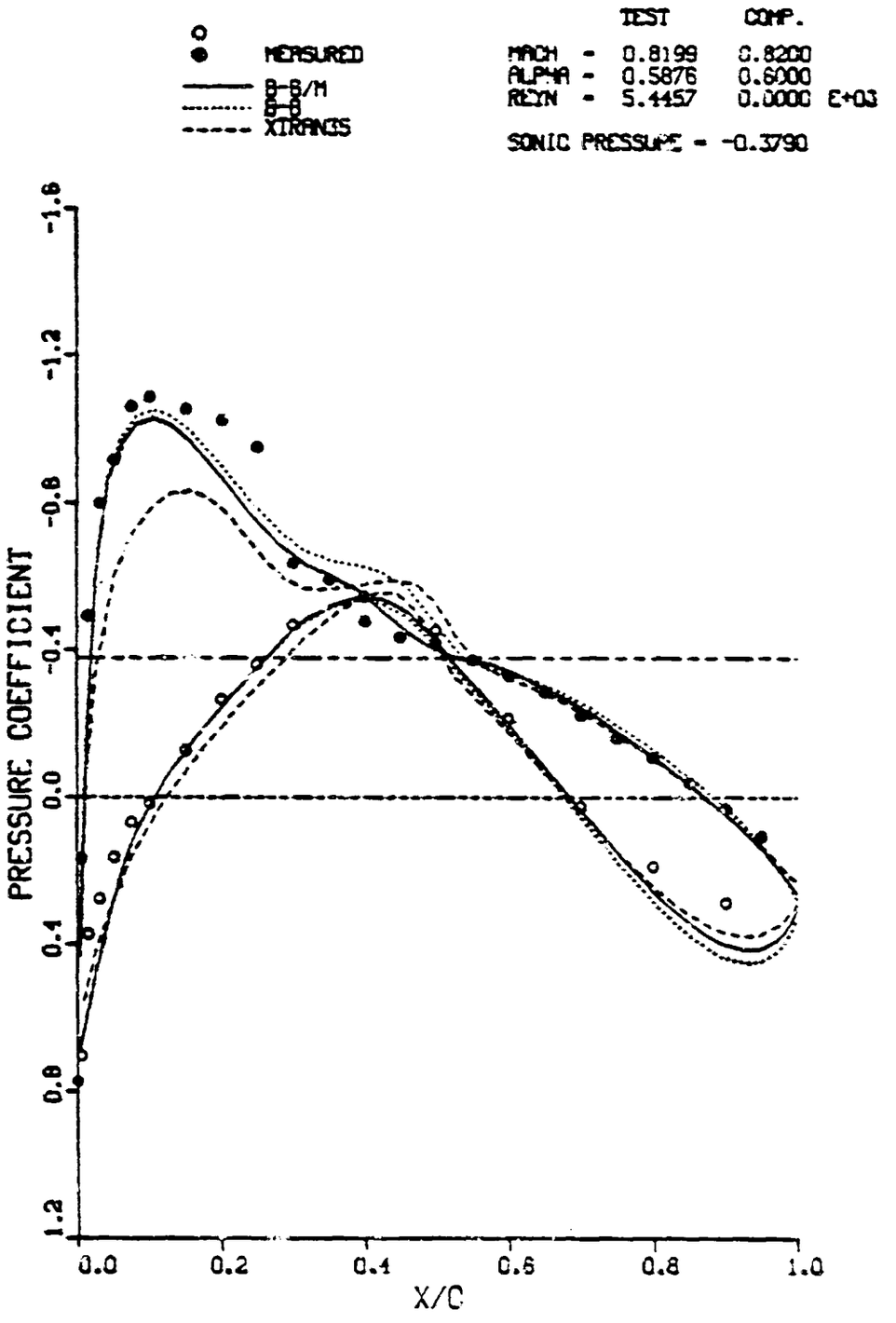

(b) SPAN STATION = 0.325

Figure 19. Comparison of Computed and Measured Pressure Distributions (Sheet 2 of 6)

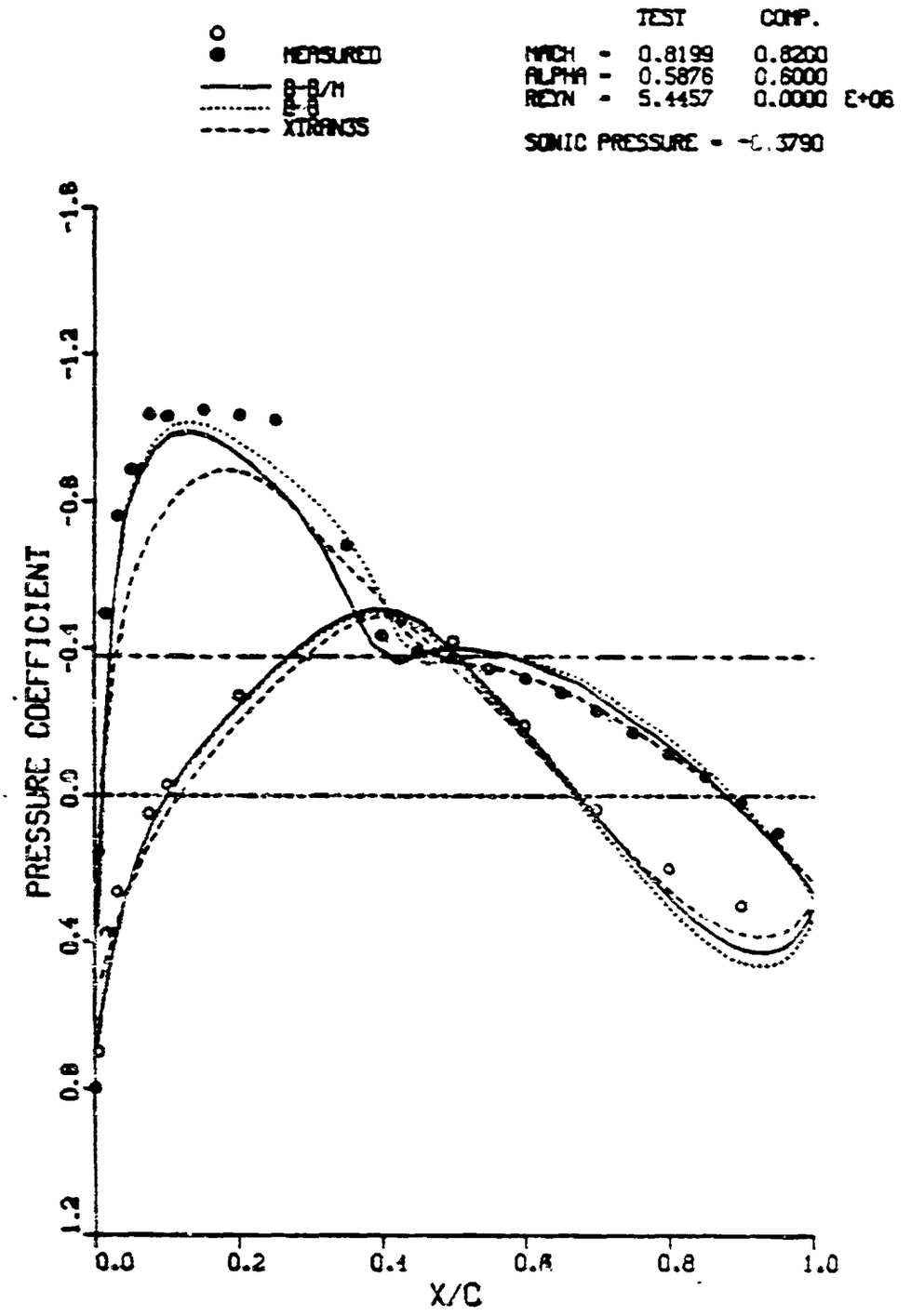

(c) SPAN-STATION = 0.475

Figure 19. Comparison of Computed and Measured Pressure Distributions (Sheet 3 of 6)

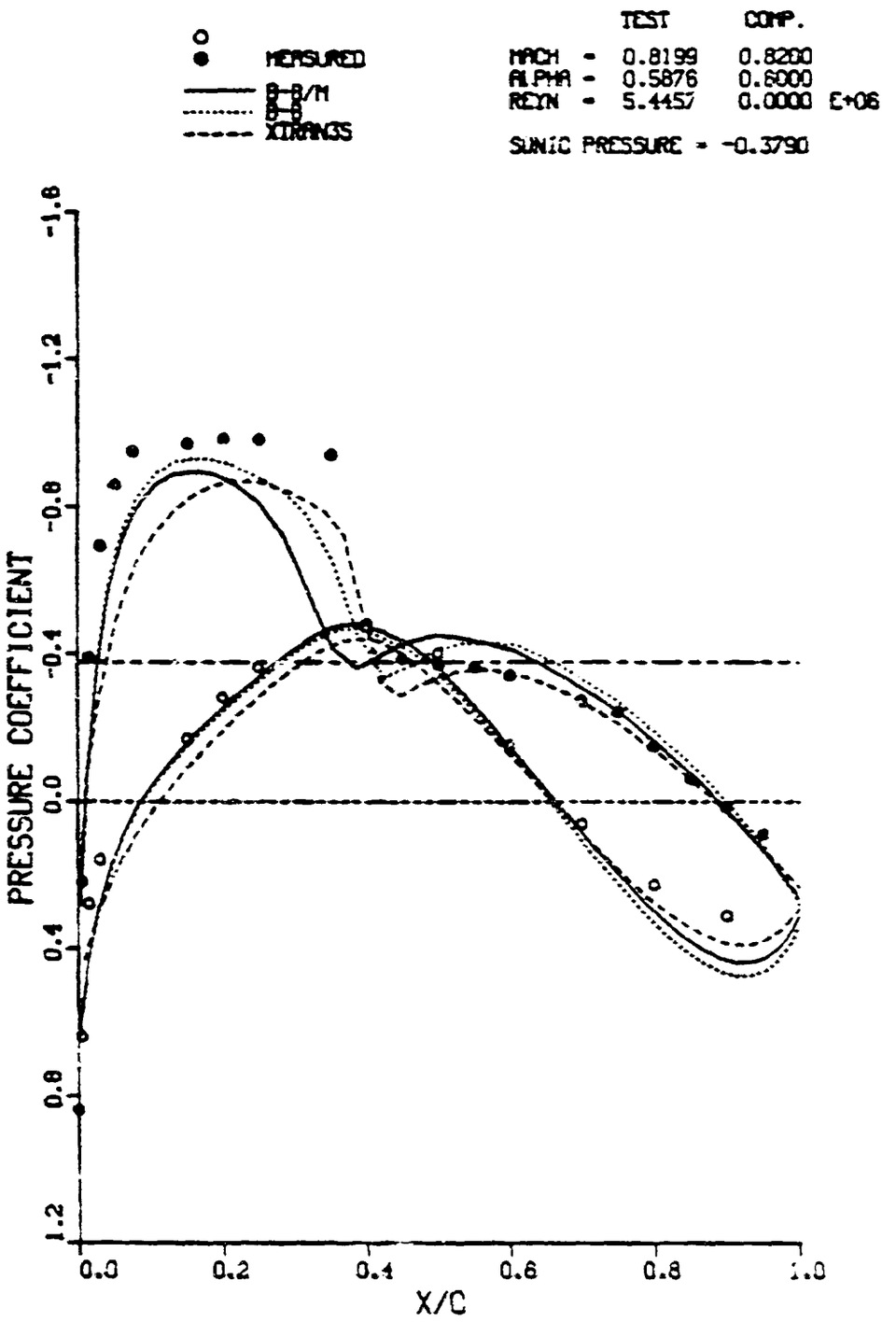

(d) SPAN-STATION = 0.650

Figure 19. Comparison of Computed and Measured Pressure Distributions (Sheet 4 of 6)

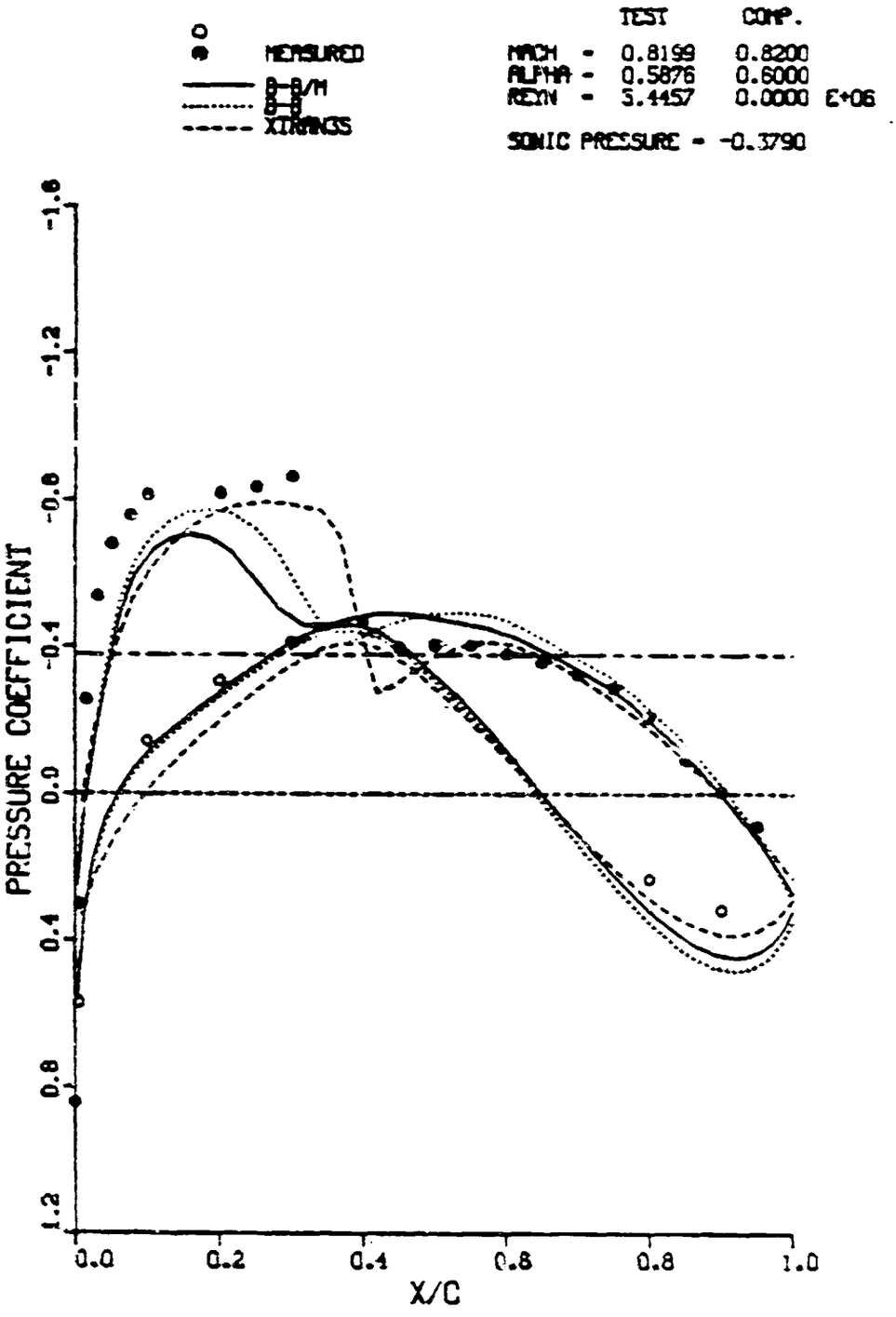

(e) SPAN-STATION = 0.825

Figure 19. Comparison of Computed and Measured Pressure Distributions (Sheet 5 of 6)

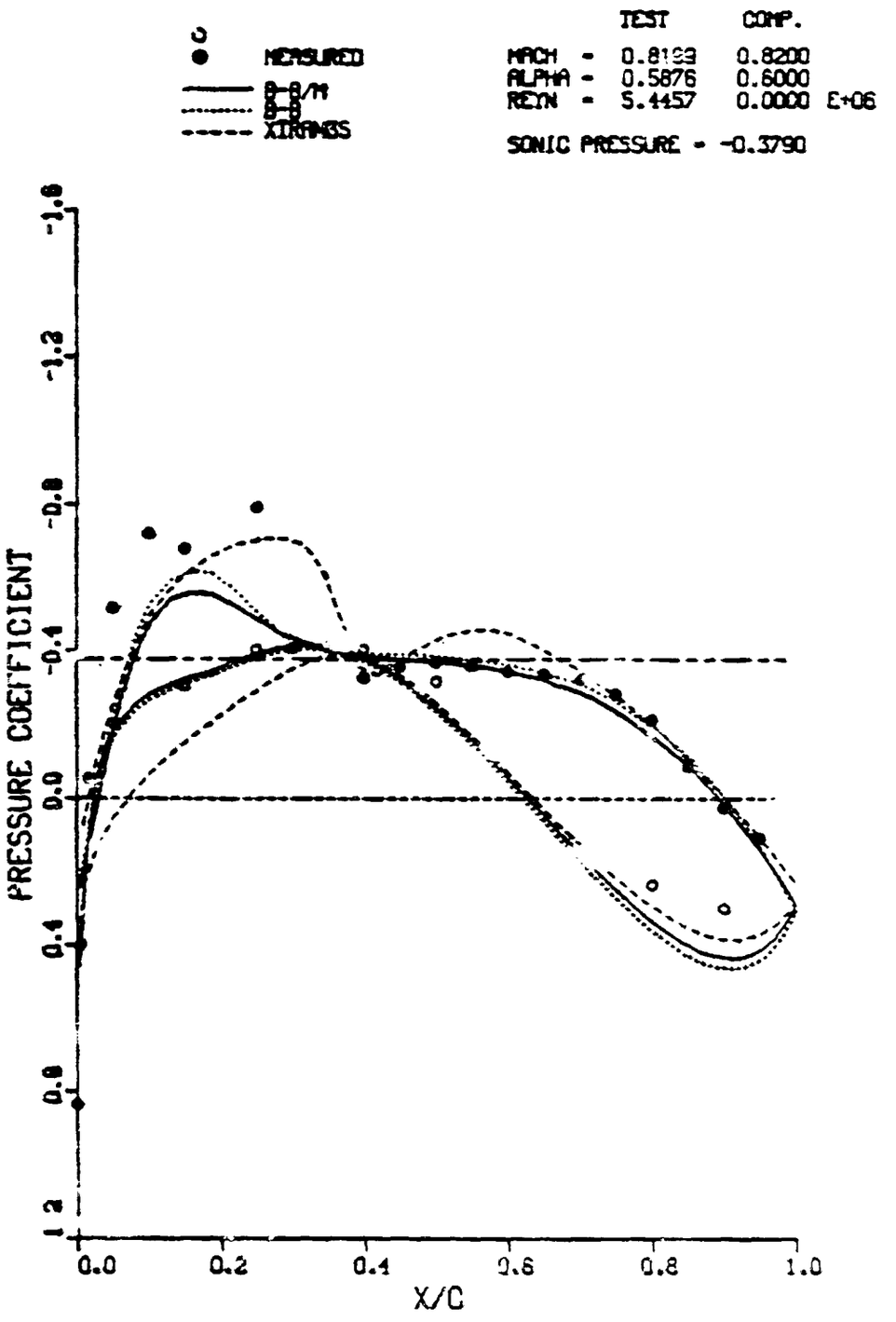

(f) SPAN-STATION = 0.950

Figure 19. Comparison of Computed and Measured Pressure Distributions (Sheet 6 of 6)

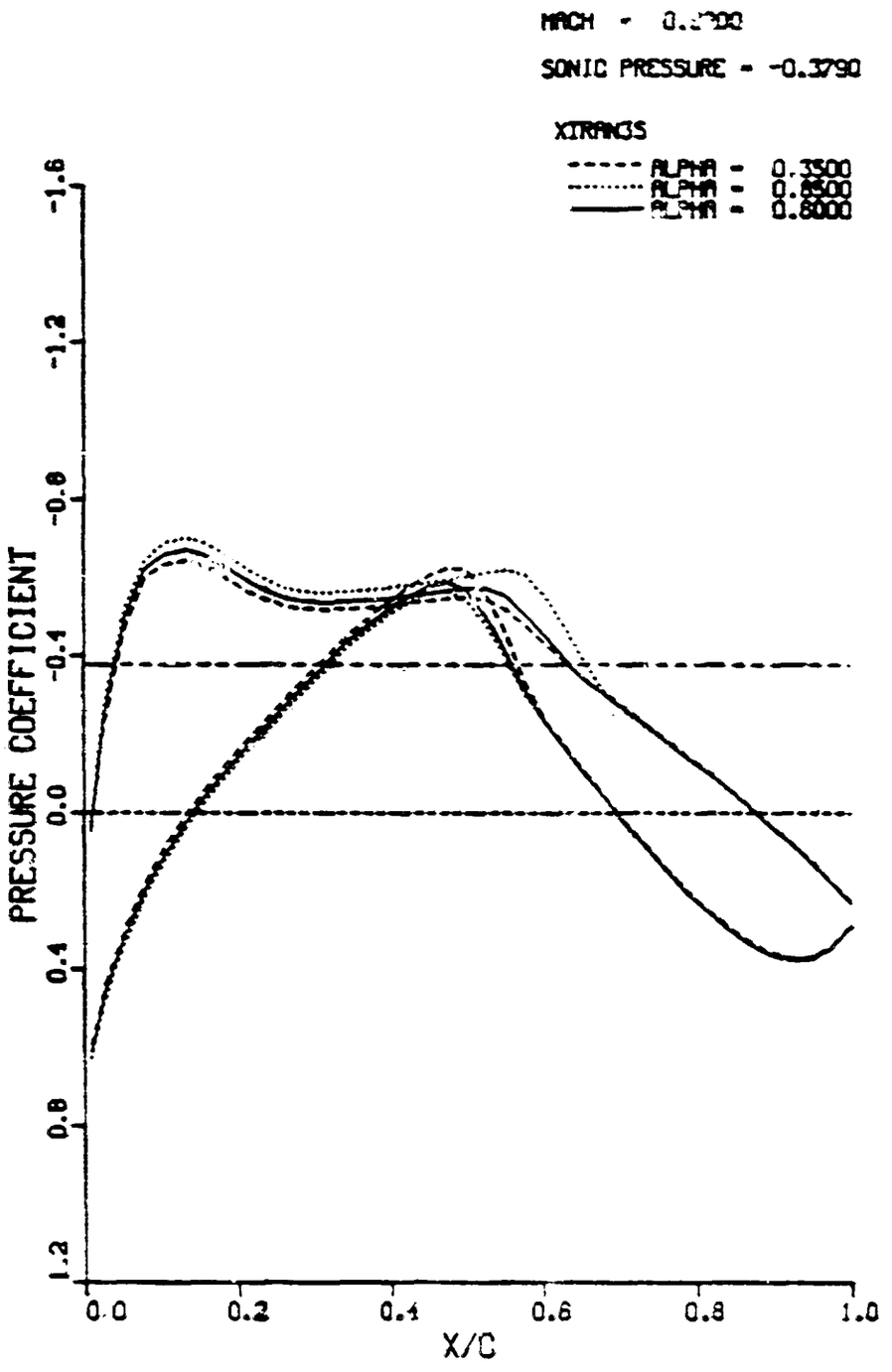

(a) SPAN-STATION = 0.200

Figure 20. Effect of Change in Mean Angle of Attack on Pressure Distributions - XTRAN3S (Sheet 1 of 6)

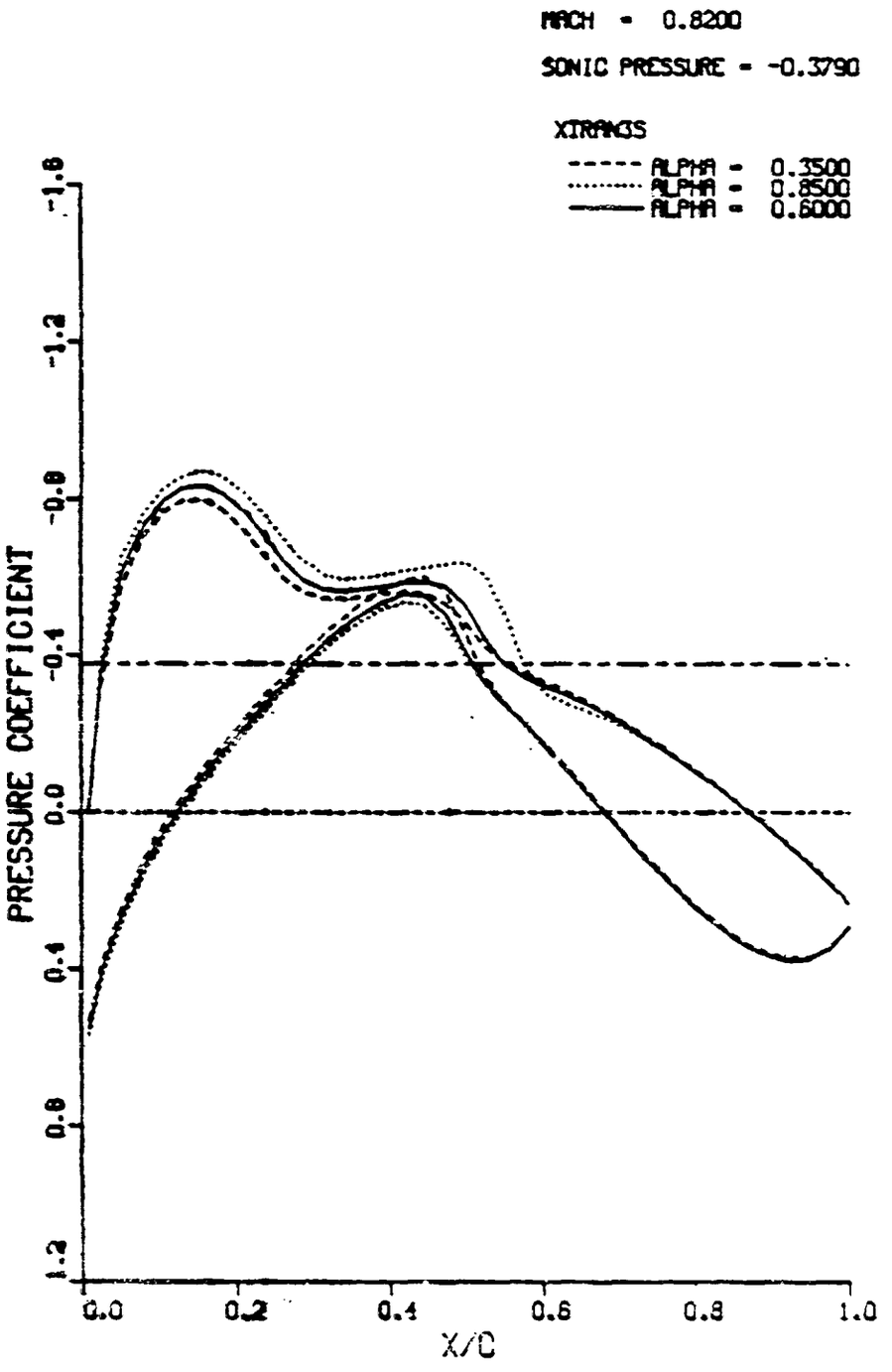

(b) SPAN-STATION = 0.325

Figure 20. Effect of Change in Mean Angle of Attack on Pressure Distributions - XTRAN3S (Sheet 2 of 6)

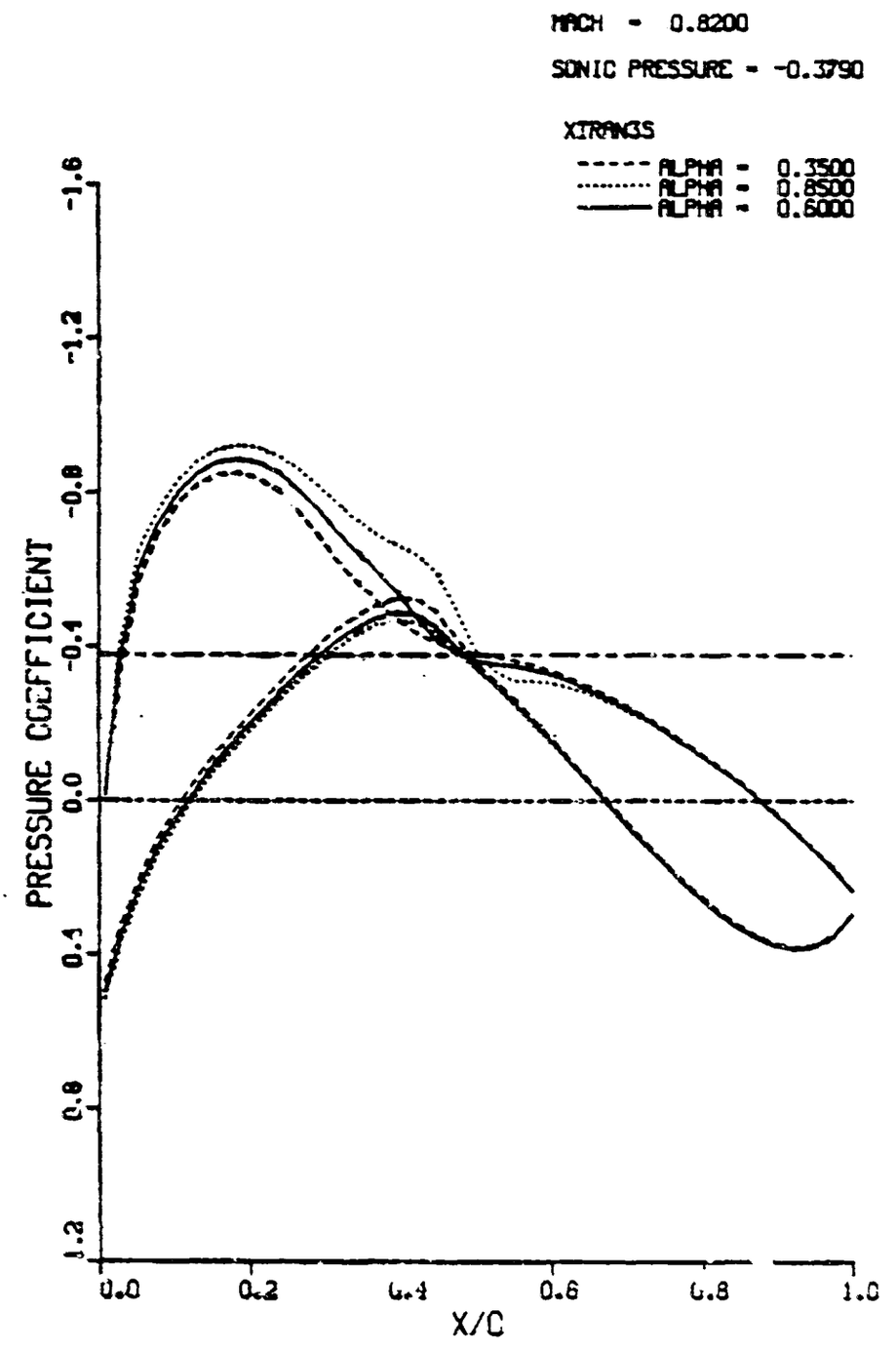

(c) SPAN-STATION = 0.475

Figure 20. Effect of Change in Mean Angle of Attack on Pressure Distributions - XTRAN3S (Sheet 3 of 6)

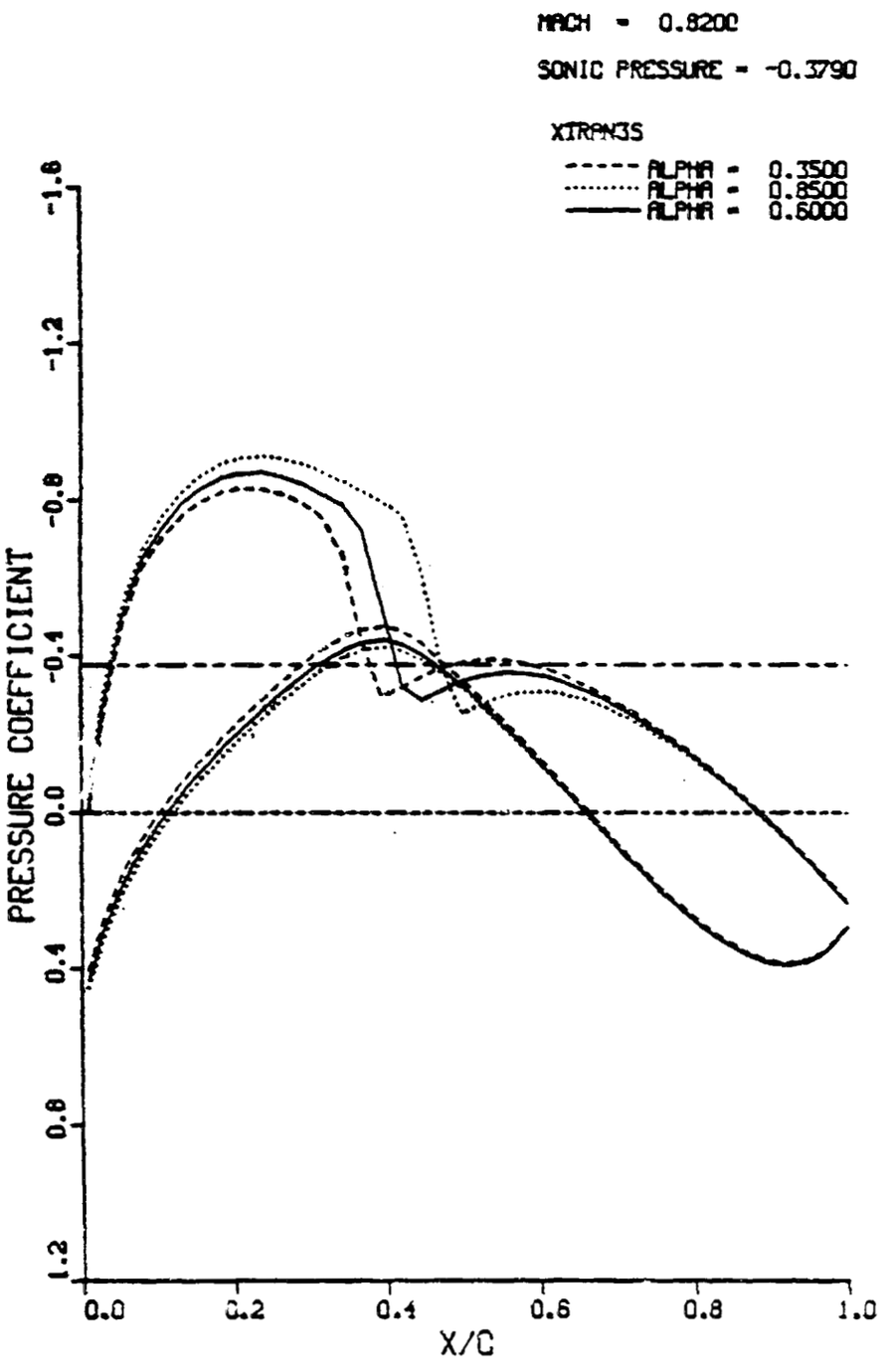

(d) SPAN-STATION = 0.650

Figure 20. Effect of Change in Mean Angle of Attack on Pressure Distributions - XTRAN3S (Sheet 4 of 6)

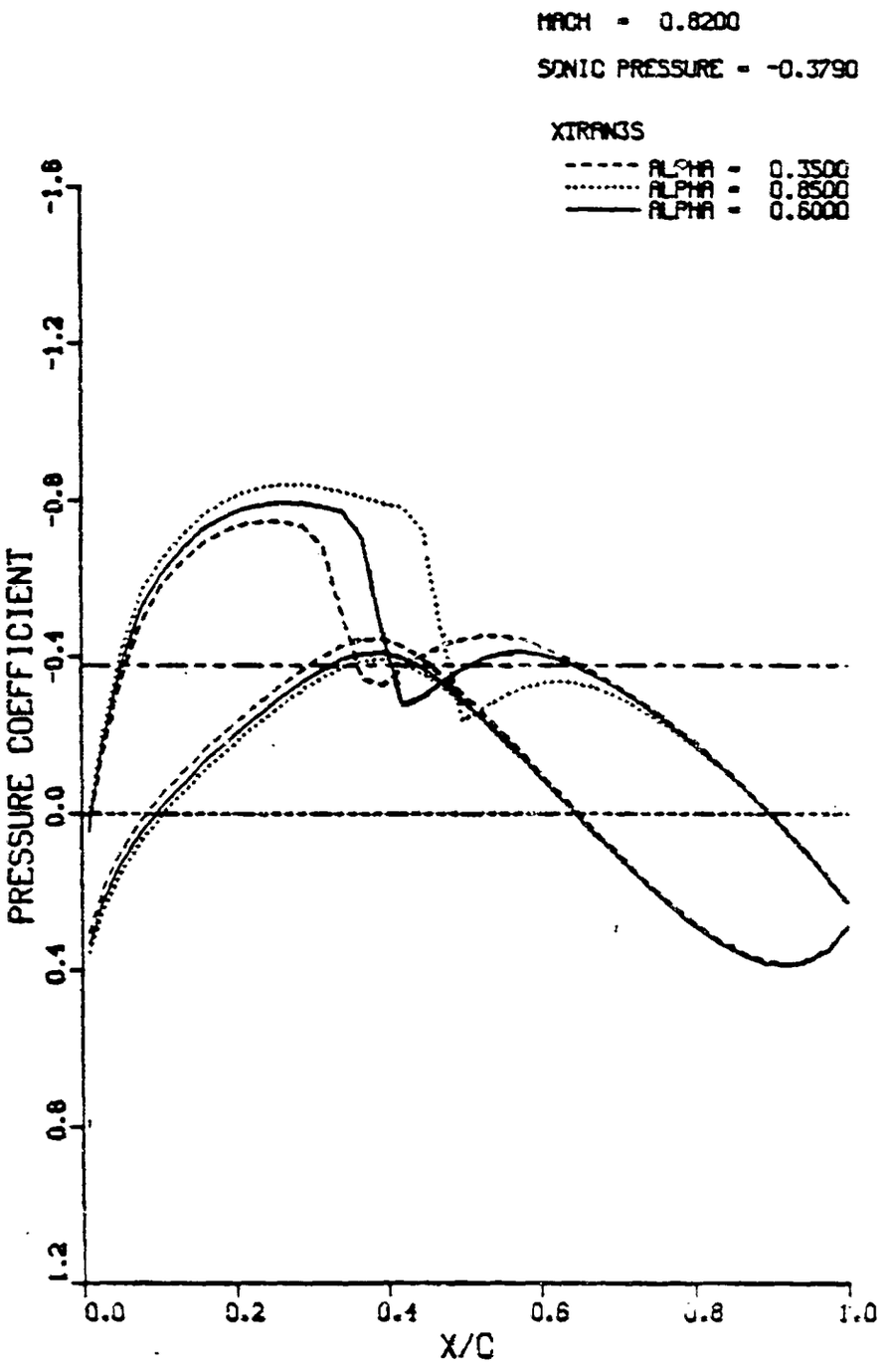

(e) SPAN-STATION = 0.925

Figure 20. Effect of Change in Mean Angle of Attack on Pressure Distributions - XTRAN3S (Sheet 5 of 6)

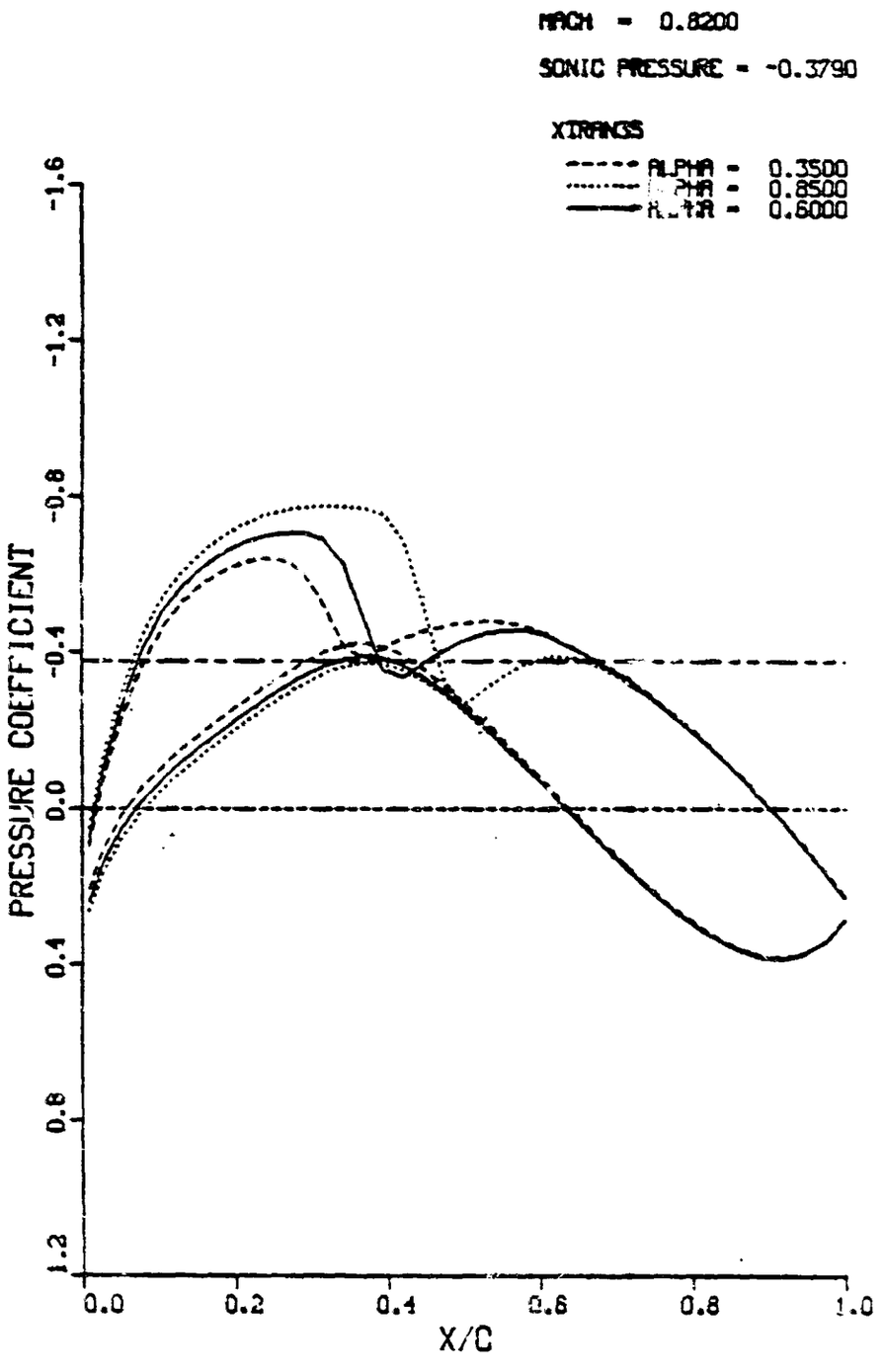

(f) SPAN-STATION = 0.950

Figure 20. Effect of Change in Mean Angle of Attack on Pressure Distributions - XTRAN3S (Sheet 6 of 6)

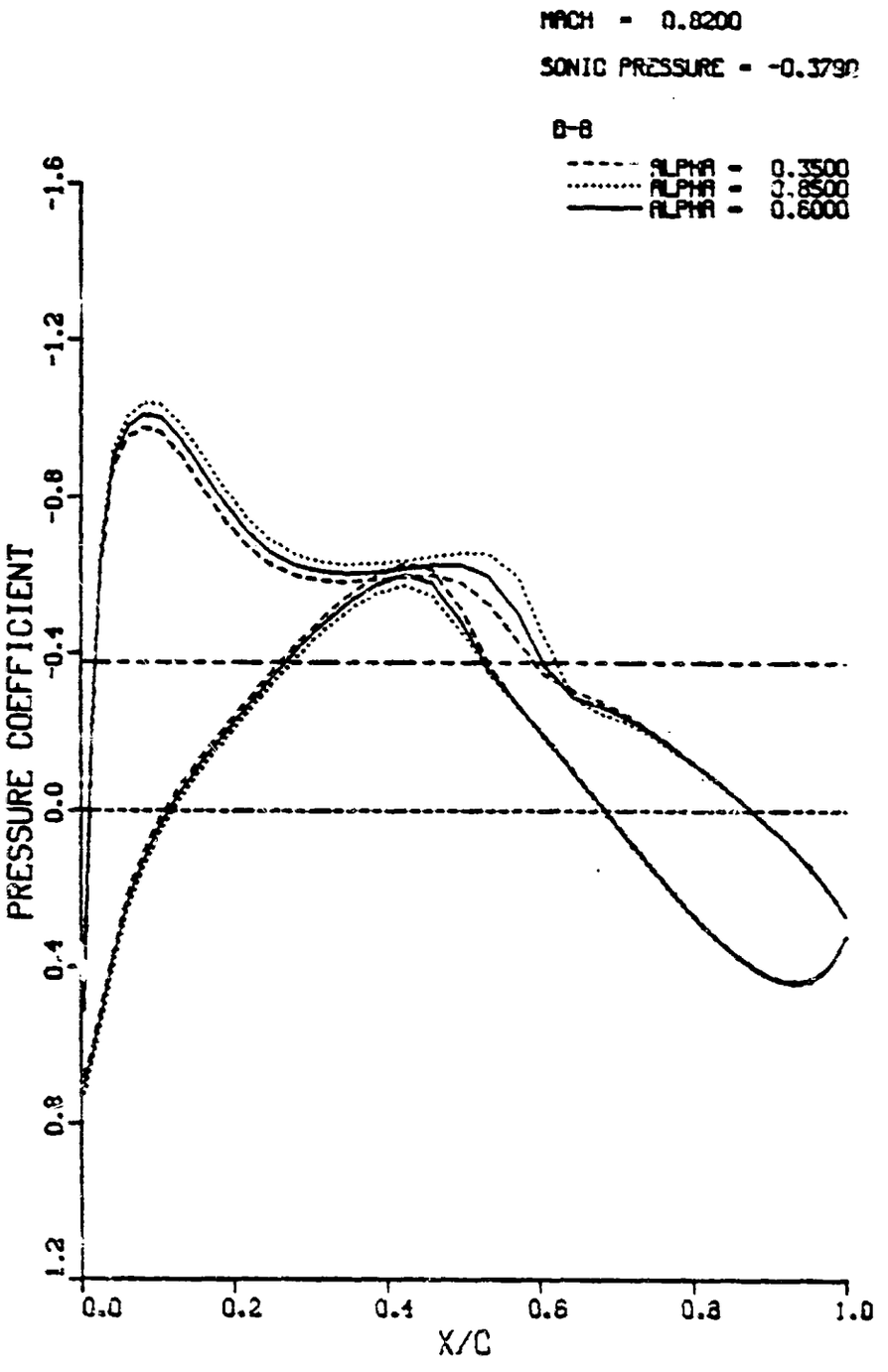

(a) SPAN-STATION = 0.200

Figure 21. Effect of Change in Mean Angle of Attack on Pressure Distributions - B-B Code (Sheet 1 of 6)

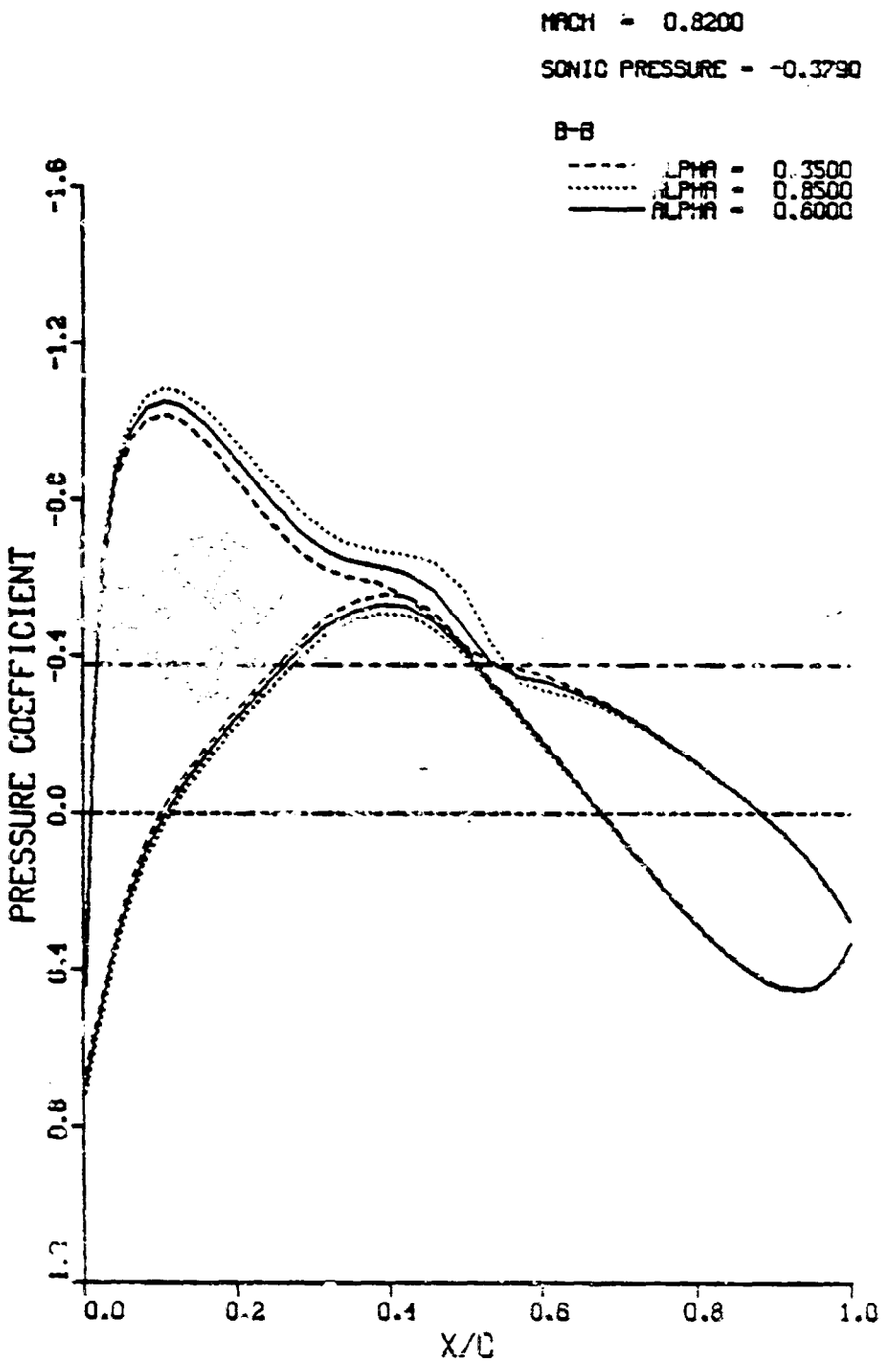

(b) SPAN-STATION = 0.325

Figure 21. Effect of Change in Mean Angle of Attack on Pressure Distributions - B-B Code (Sheet 2 of 6)

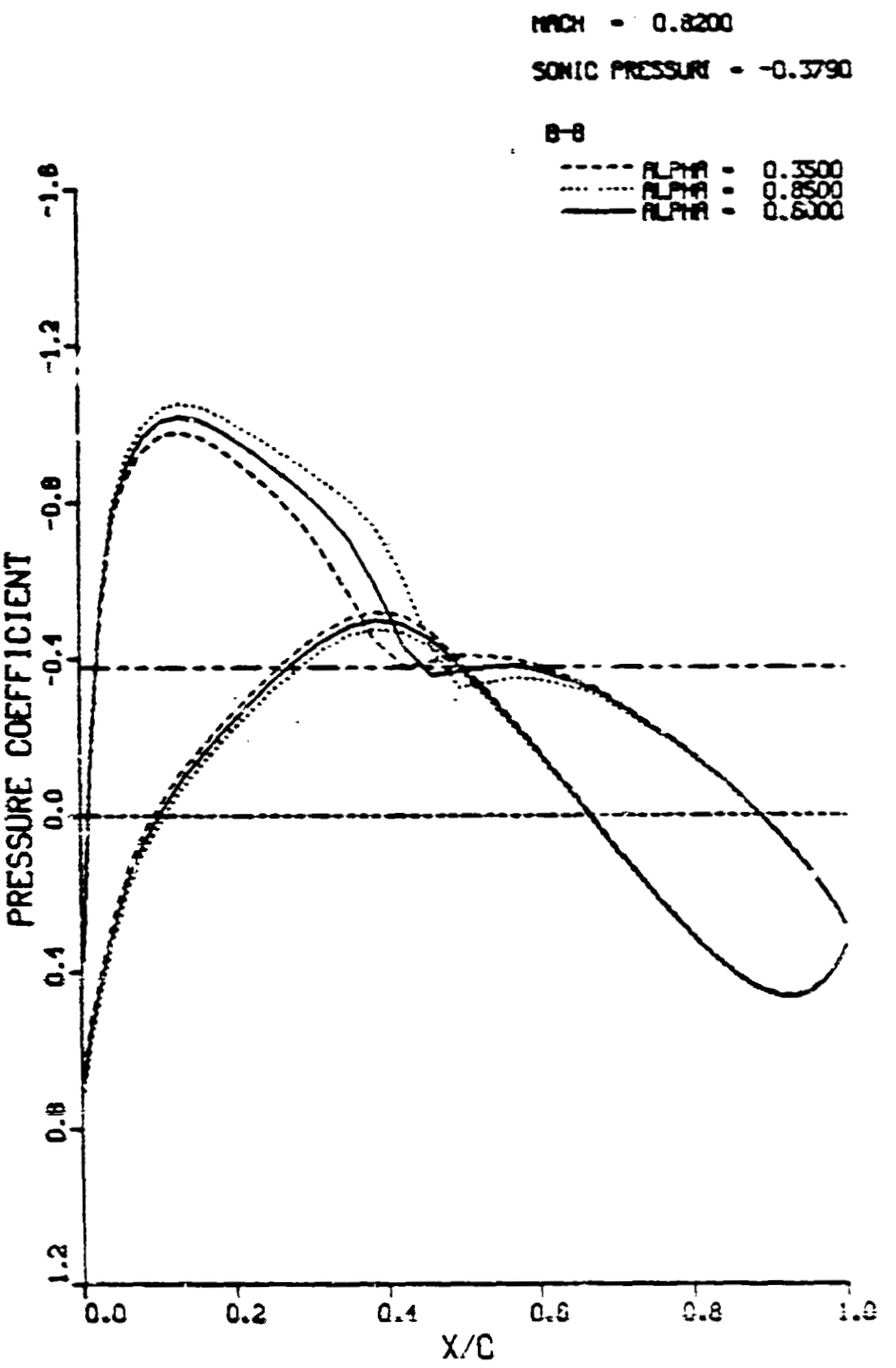

(c) SPAN-STATION = 0.475

Figure 21. Effect of Change in Mean Angle of Attack on Pressure Distributions - B-B Code (Sheet 3 of 6)

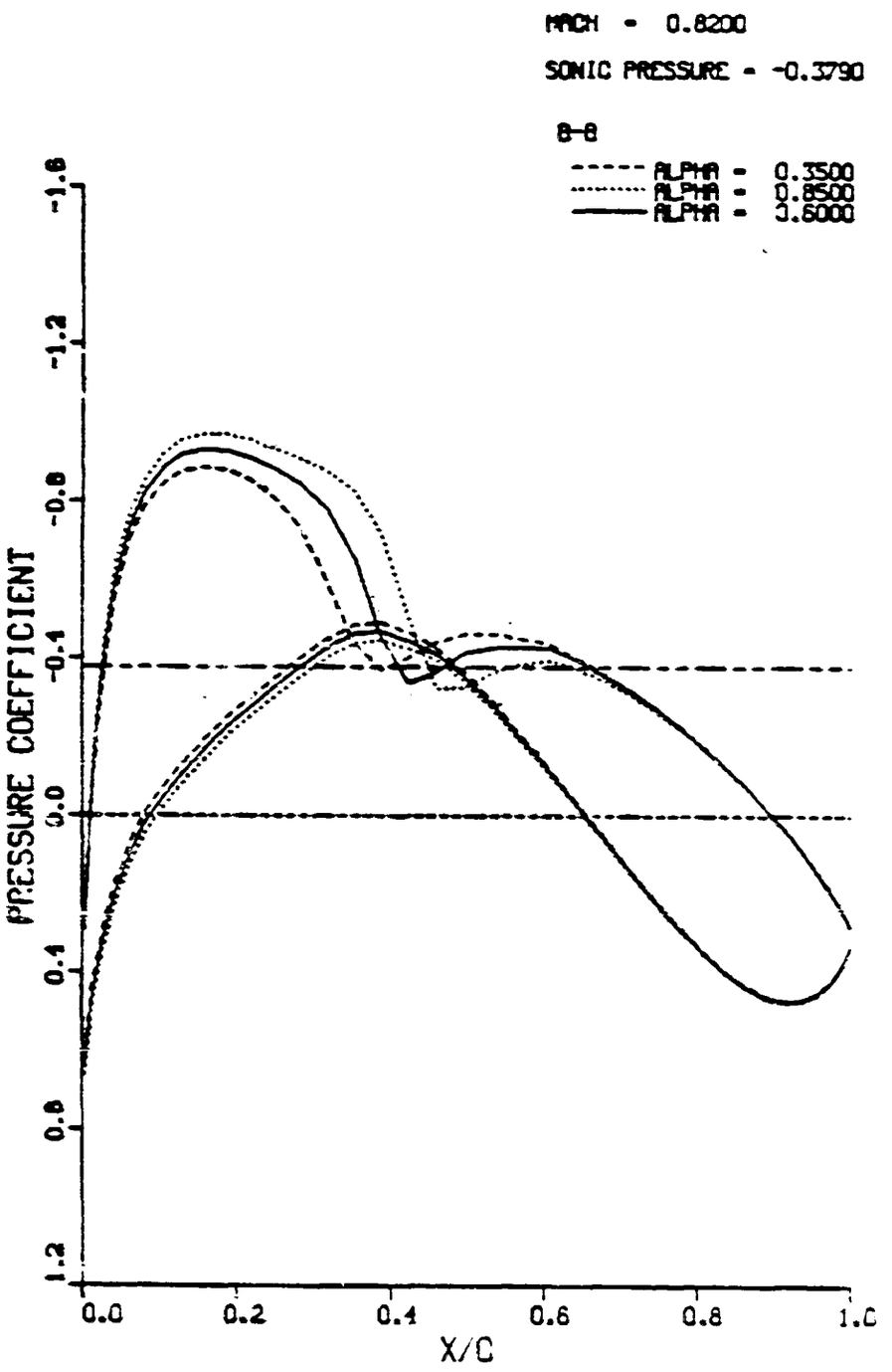

(d) SPAN-STATION = 0.650

Figure 21. Effect of Change in Mean Angle of Attack on Pressure Distributions - B-B Code (Sheet 4 of 6)

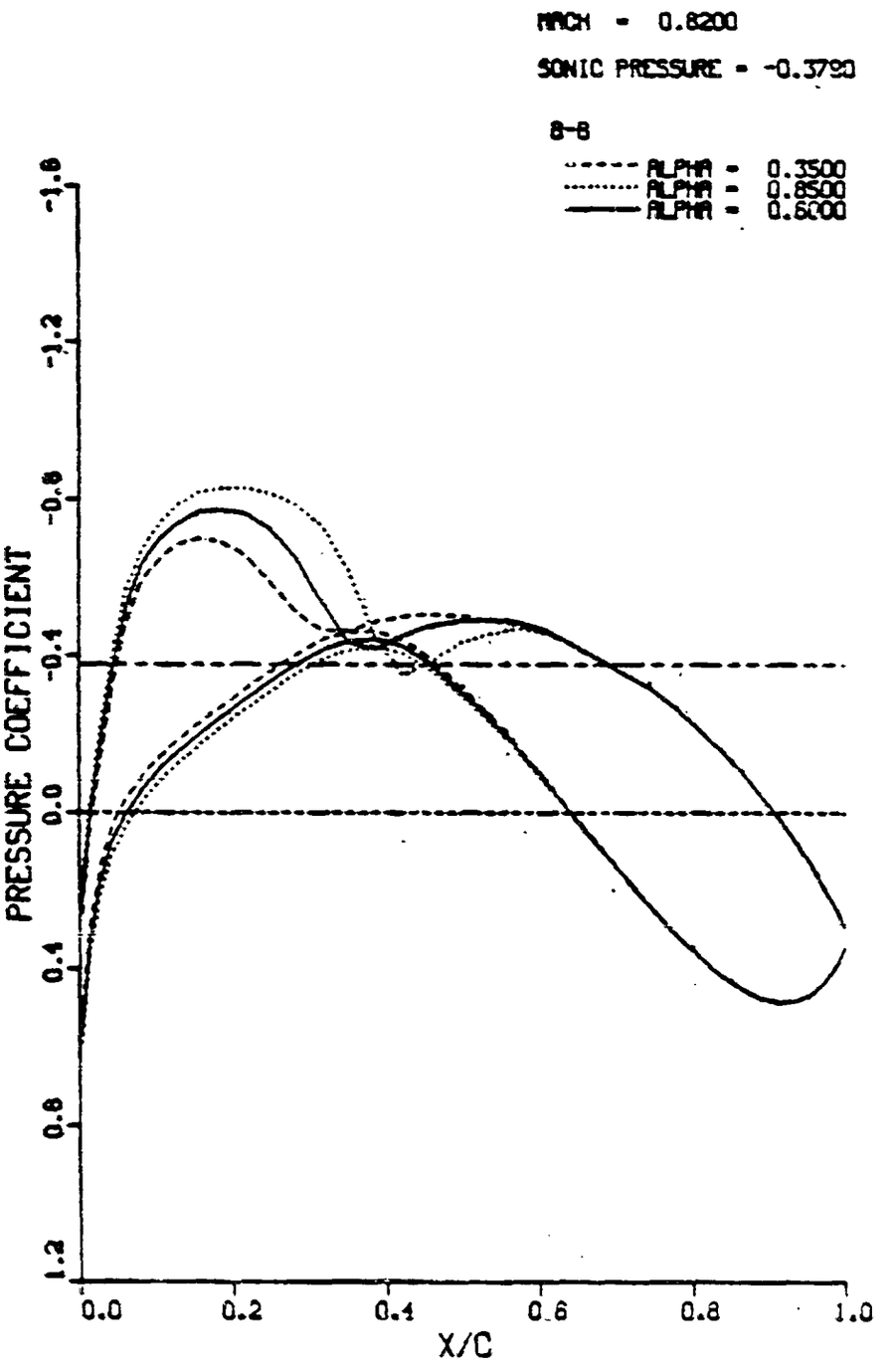

(e) SPAN-STATION = 0.825

Figure 21. Effect of Change in Mean Angle of Attack on Pressure Distributions - B-B Code (Sheet 5 of 6)

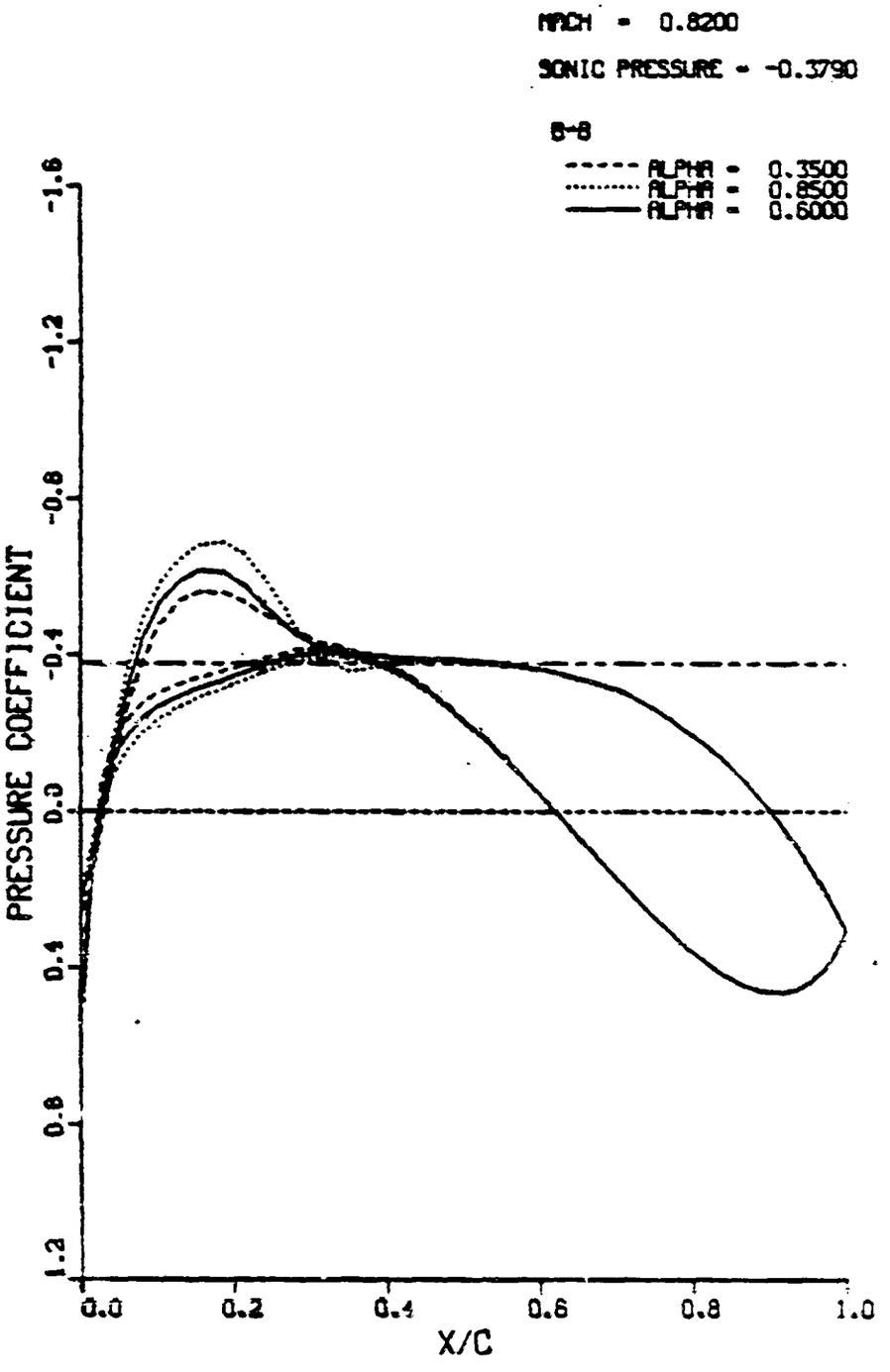

(f) SPAN-STATION = 0.950

Figure 21. Effect of Change in Mean Angle of Attack on Pressure Distributions - B-B Code (Sheet 6 of 6)

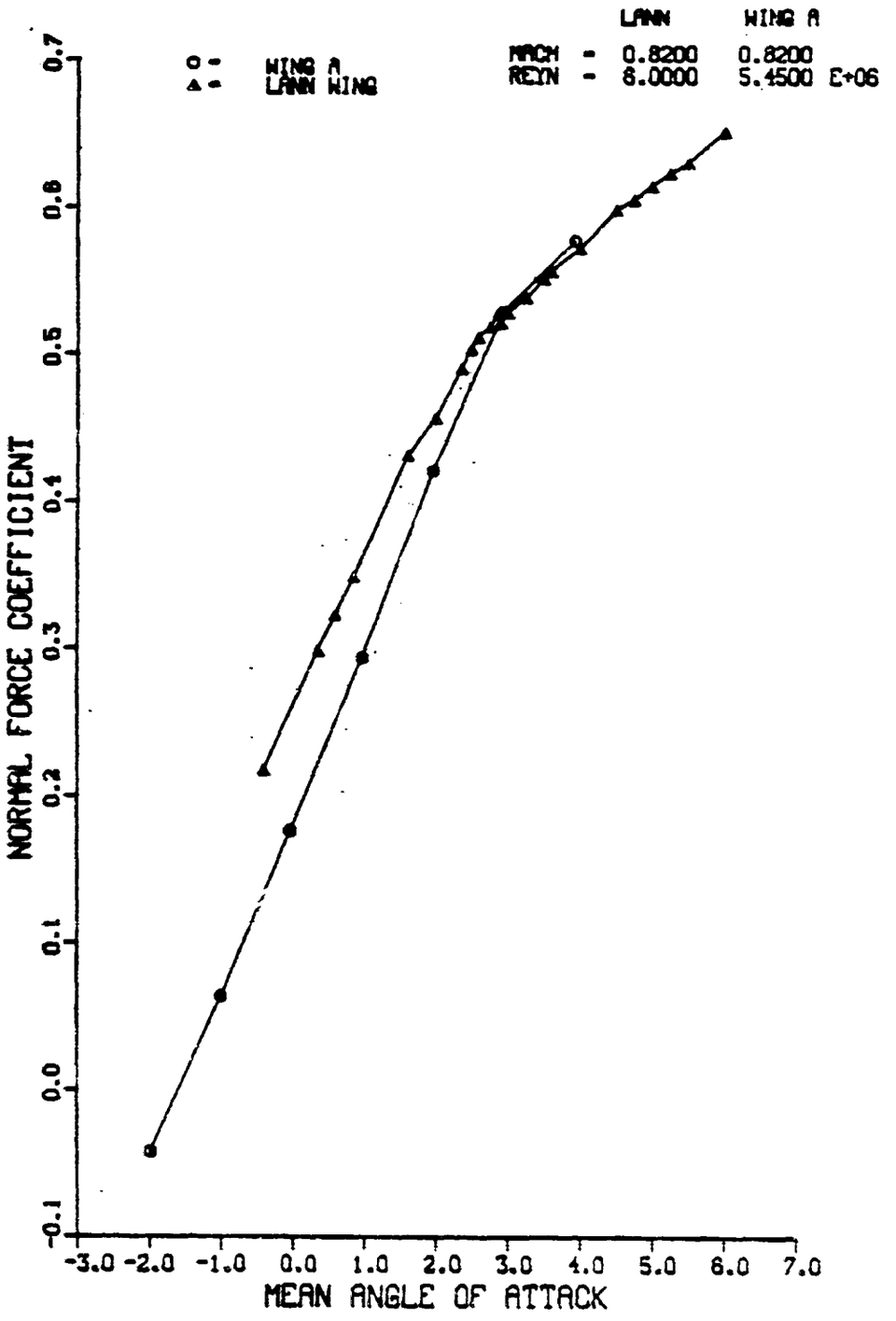

(a) MEASURED NORMAL FORCE OF LANN WING AND WING A

Figure 22. Comparison of Normal Force versus Mean Angle of Attack for Fixed Mach Number (Sheet 1 of 2)

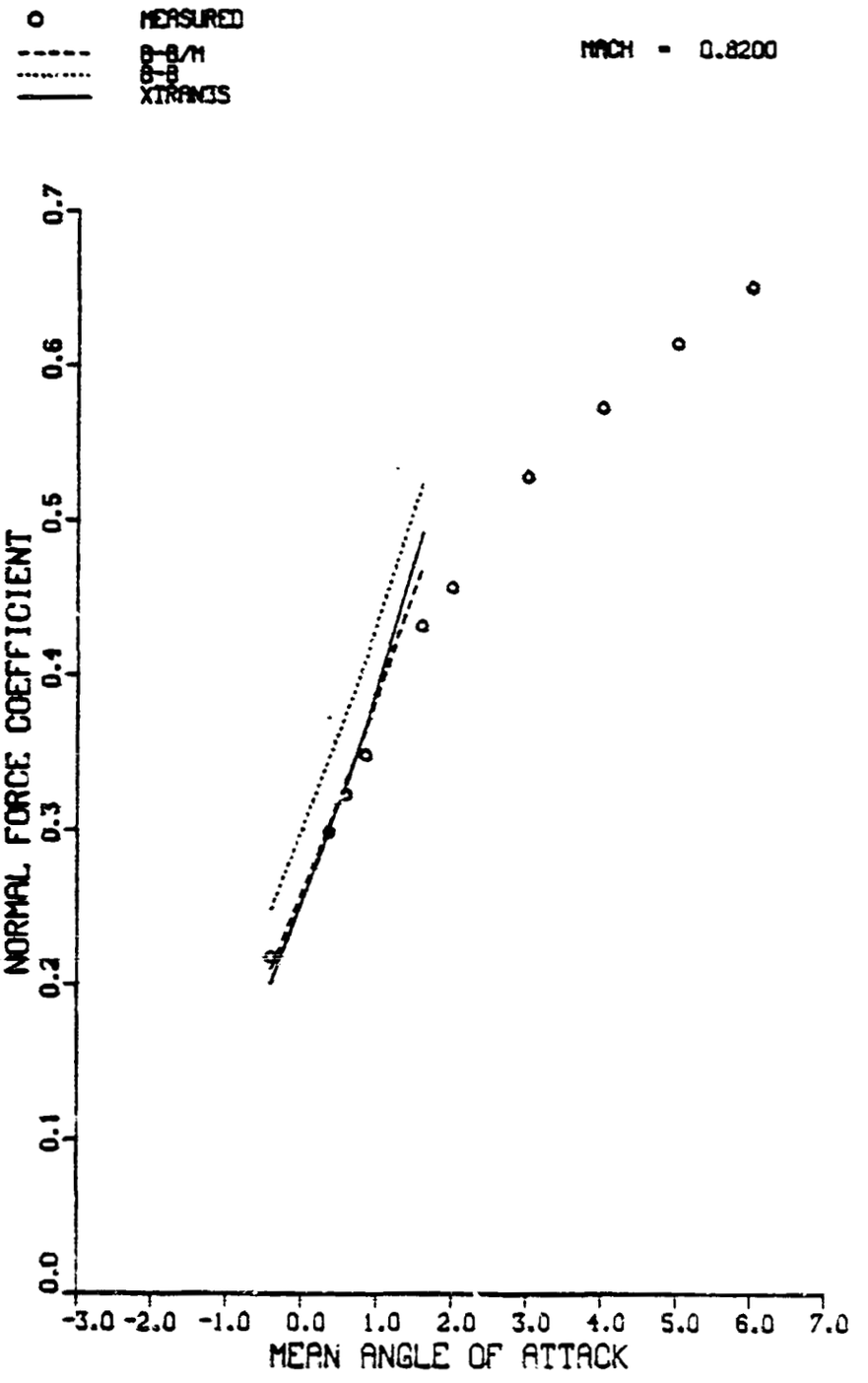

(b) COMPUTED AND MEASURED RESULTS

Figure 22. Comparison of Normal Force versus Mean Angle of Attack for Fixed Mach Number (Sheet 2 of 2)

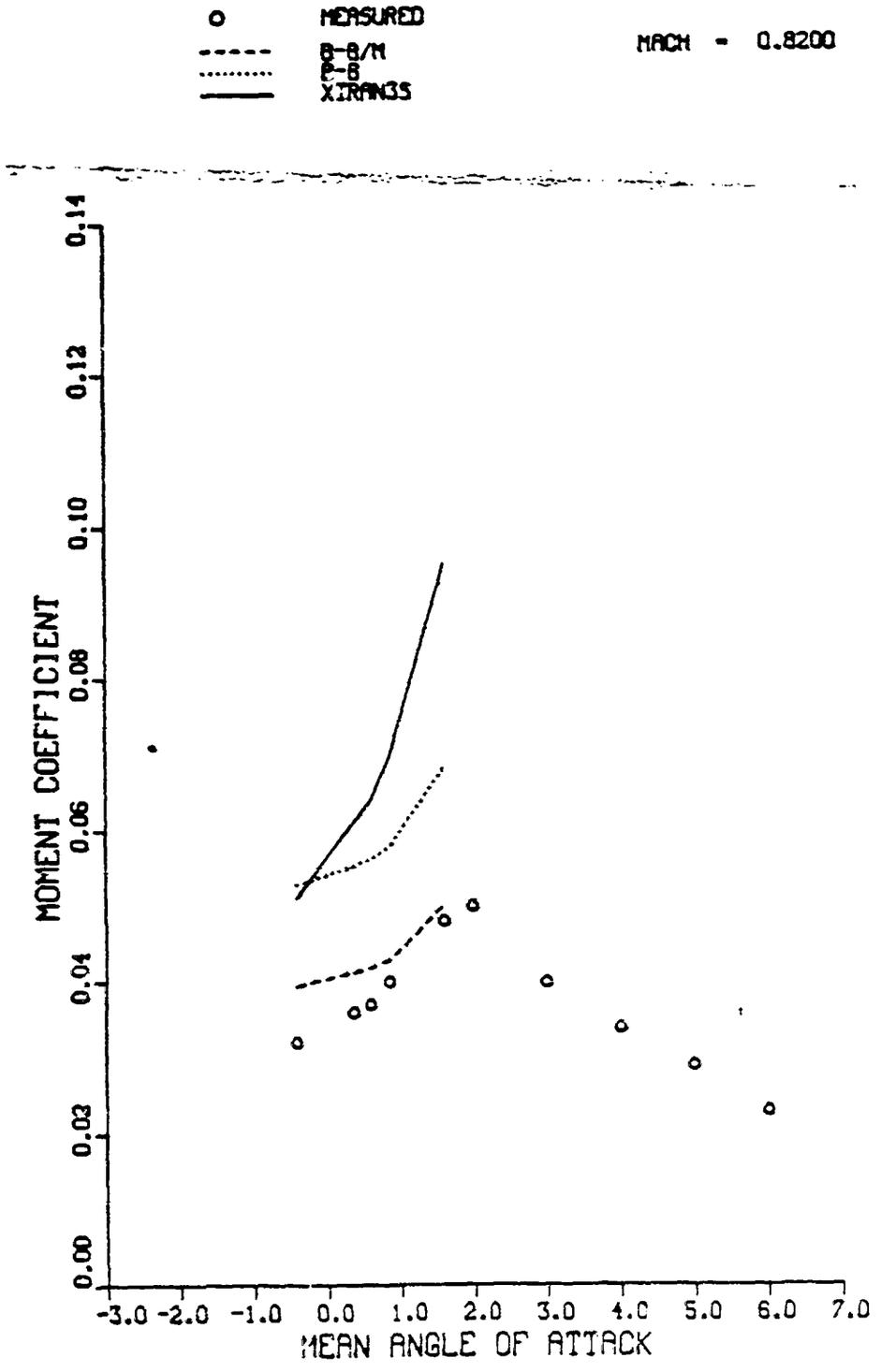

Figure 23. Comparison of Computed and Measured Pitch Moment versus Mean Angle of Attack for Fixed Mach Number

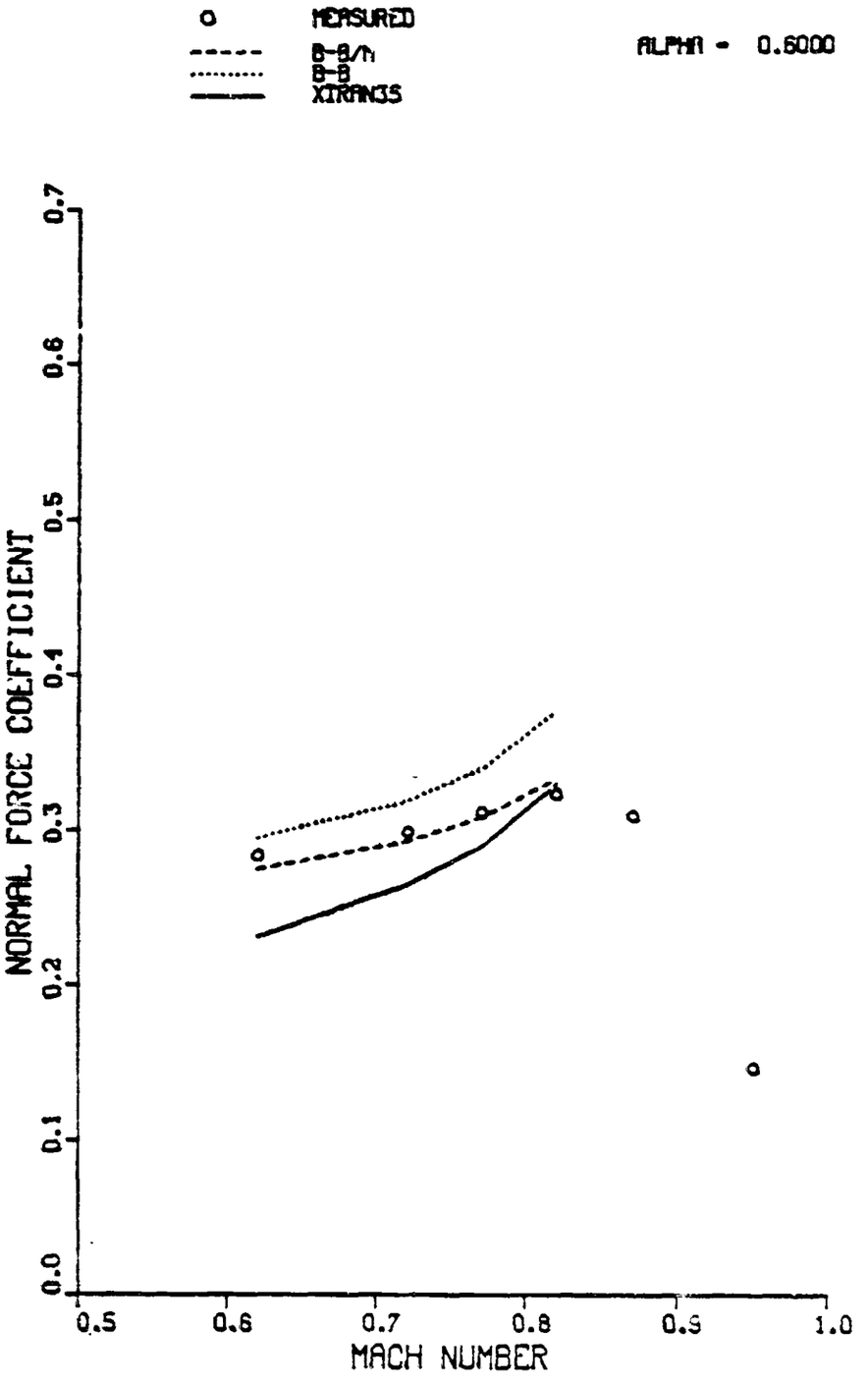

Figure 24. Comparison of Computed and Measured Normal Force versus Mach Number for Fixed Mean Angle of Attack

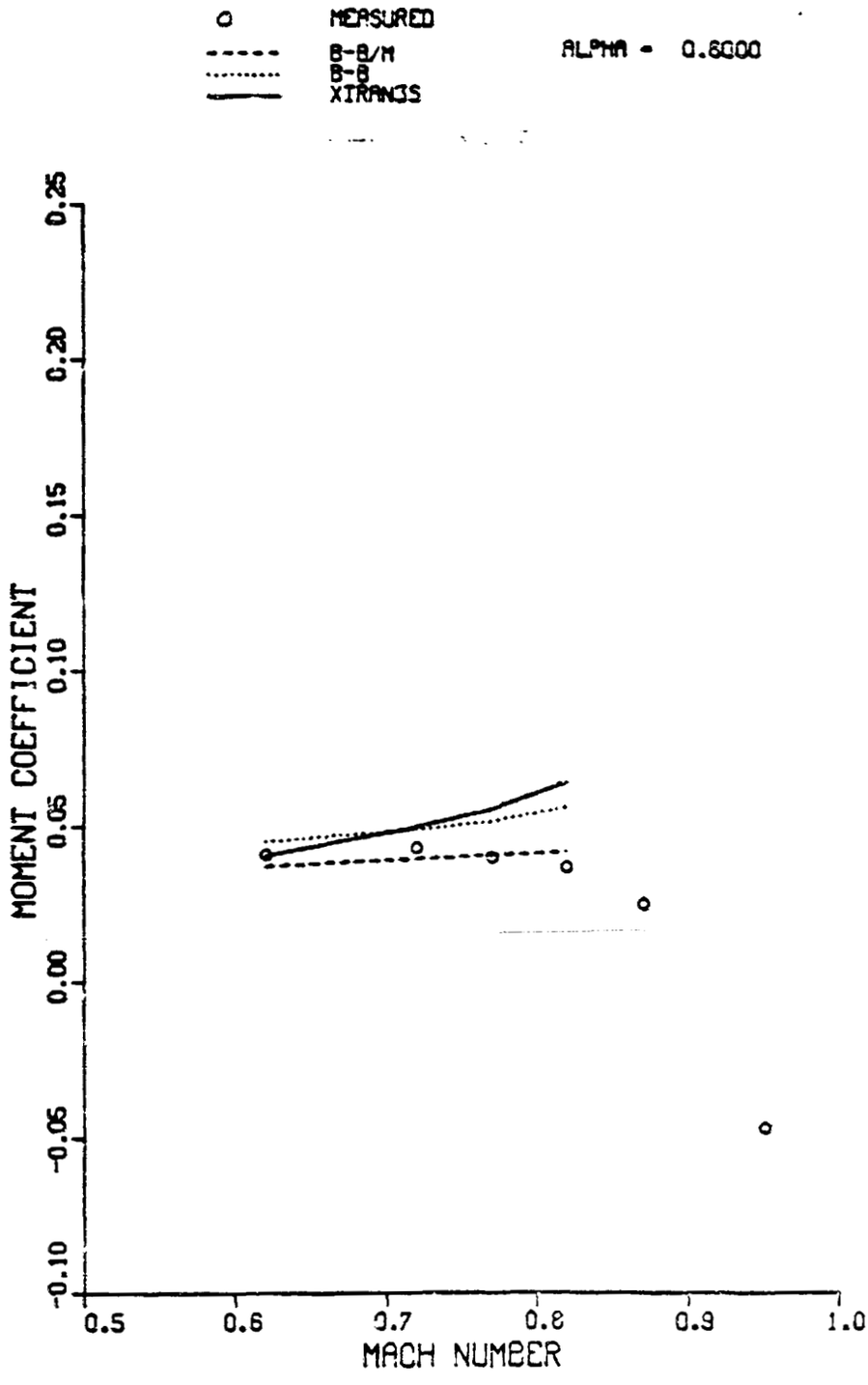

Figure 25. Comparison of Computed and Measured Pitch Moment versus Mach Number for Fixed Mean Angle of Attack

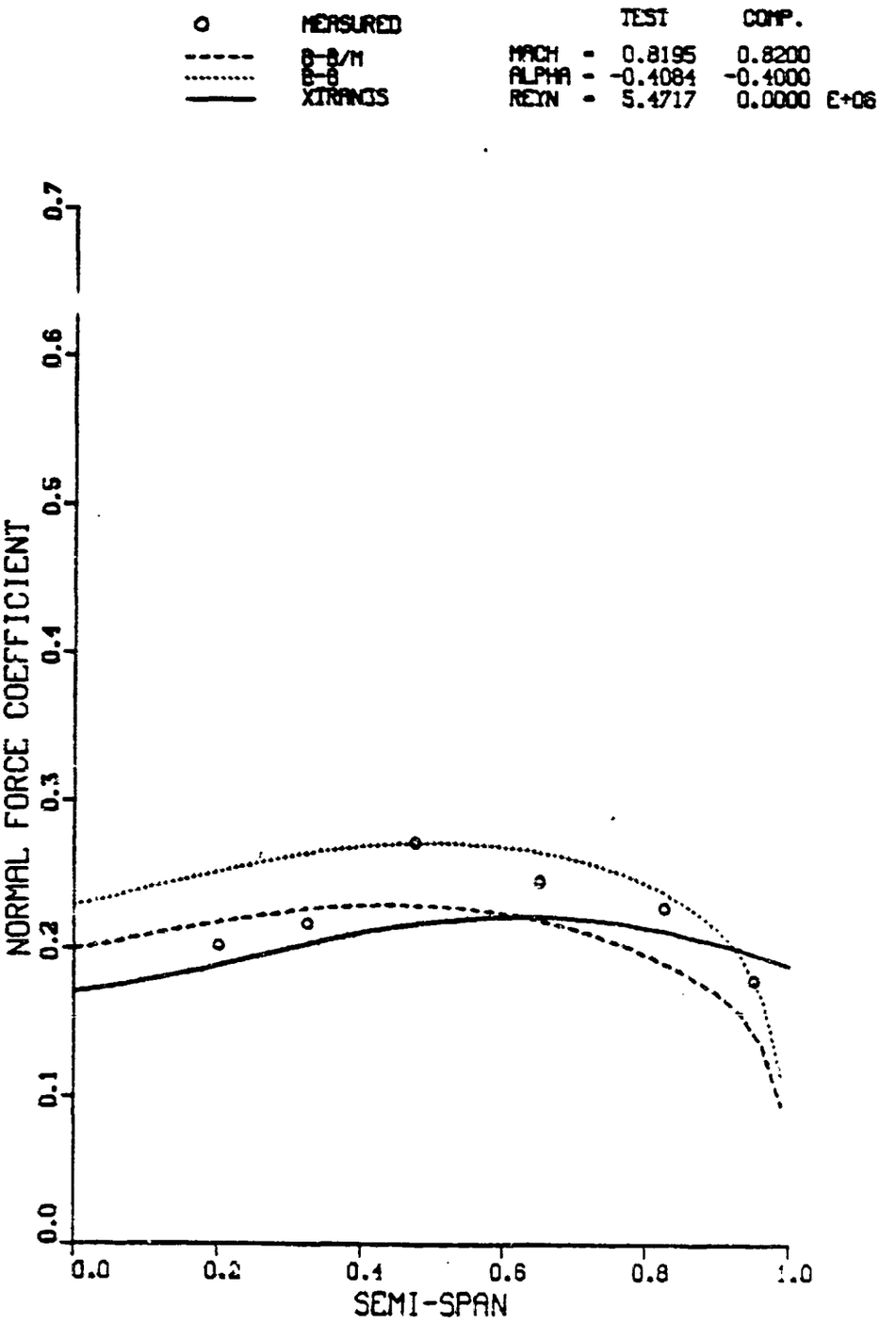

(a) MEAN ANGLE OF ATTACK = -0.40 DEGREE

Figure 26. Comparison of Computed and Measured Span-Loading Distributions at Design Mach Number (Sheet 1 of 5)

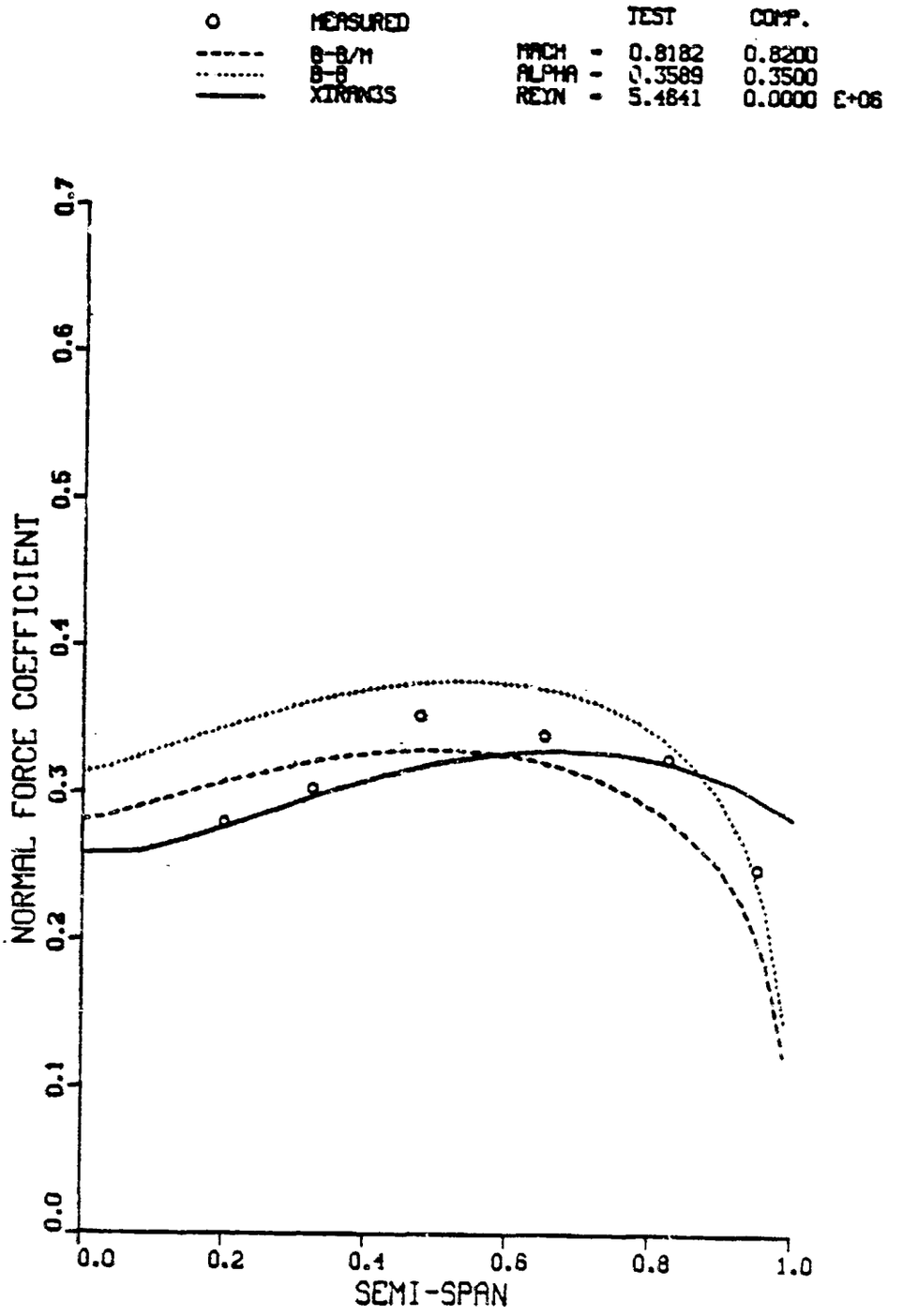

(b) MEAN ANGLE OF ATTACK = 0.35 DEGREE

Figure 26. Comparison of Computed and Measured Span-Loading Distributions at Design Mach Number (Sheet 2 of 5)

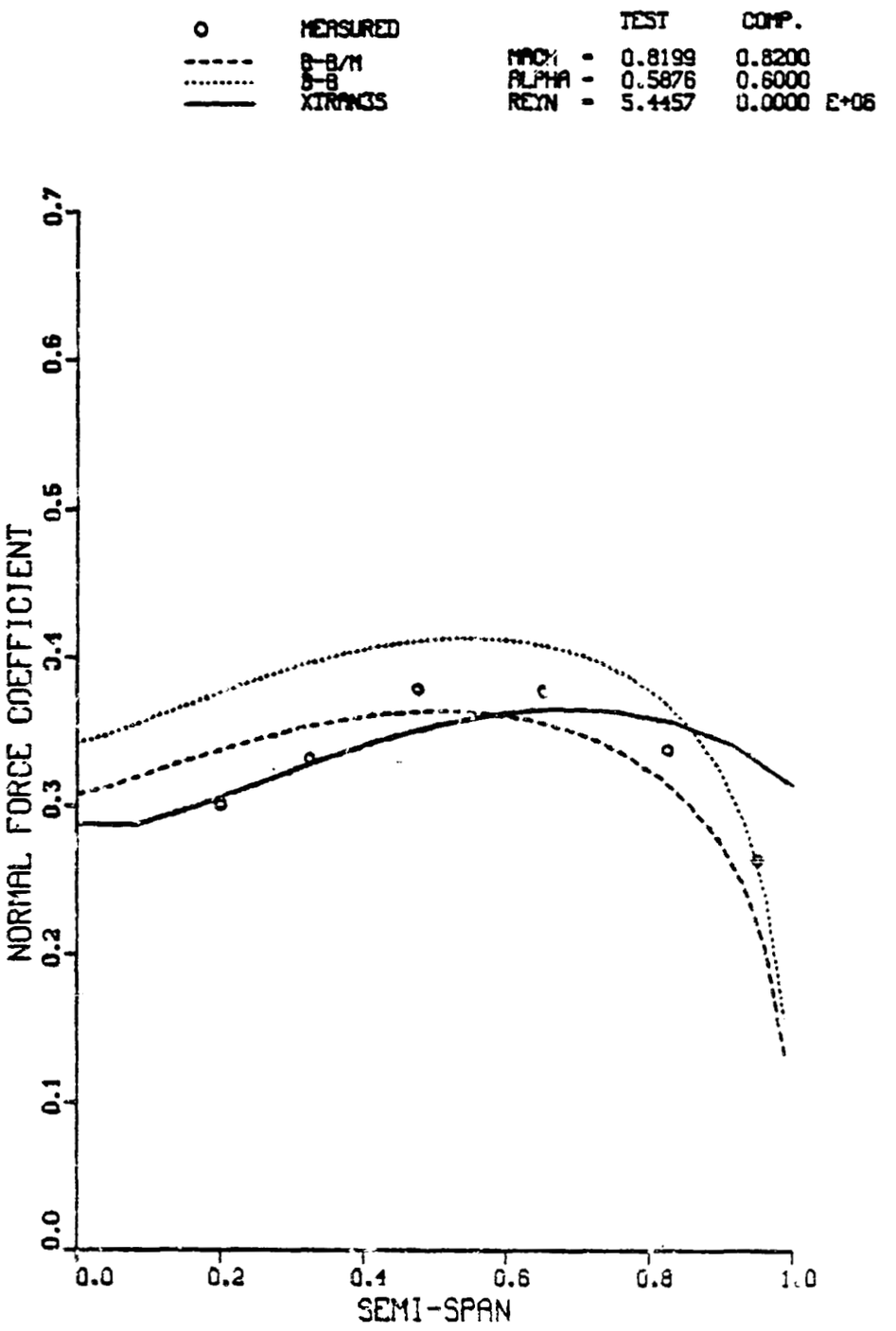

(c) MEAN ANGLE OF ATTACK = 0.60 DEGREE

Figure 26. Comparison of Computed and Measured Span-Loading Distributions at Design Mach Number (Sheet 3 of 5)

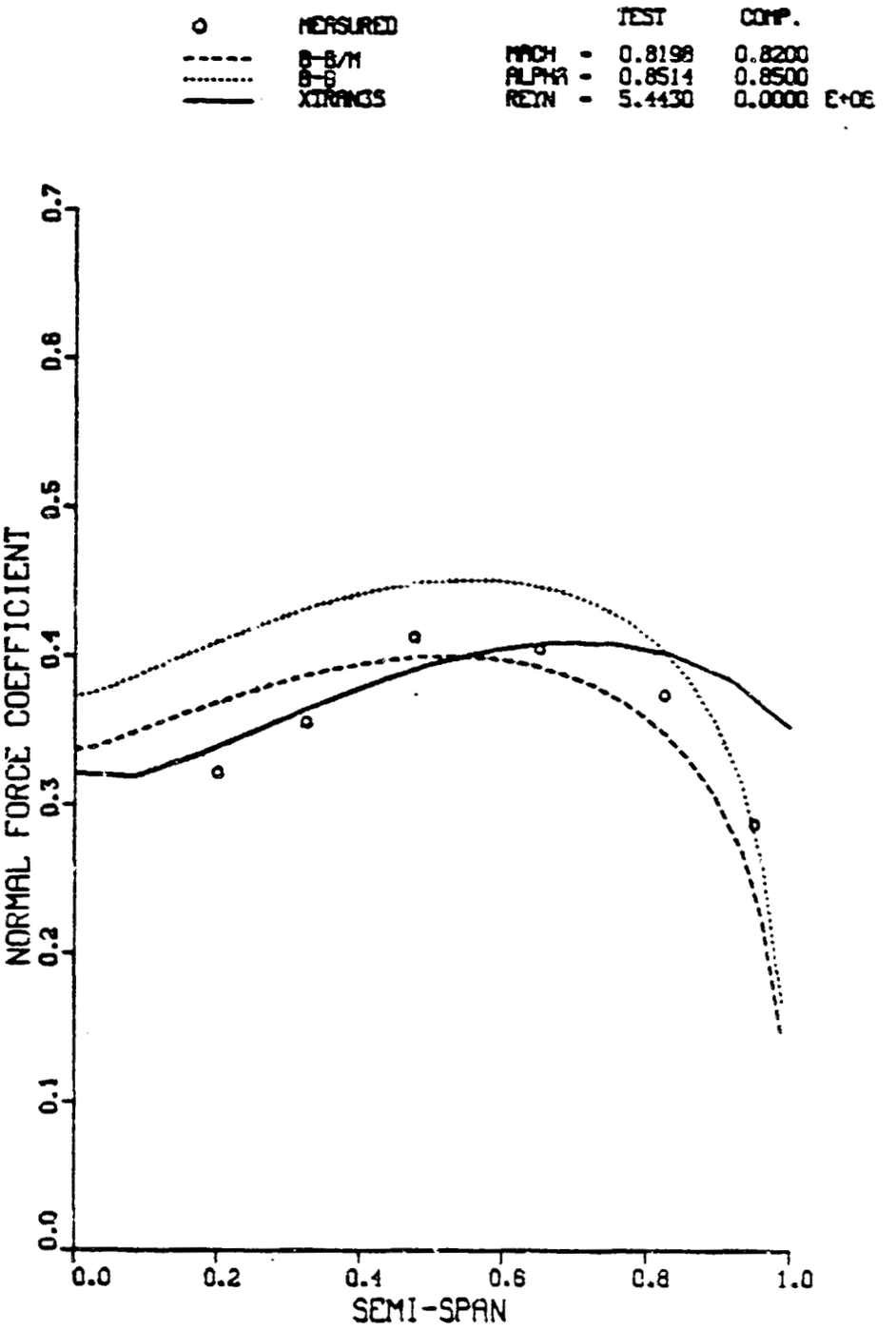

(d) MEAN ANGLE OF ATTACK = 0.85 DEGREE

Figure 26. Comparison of Computed and Measured Span-Loading Distributions at Design Mach Number (Sheet 4 of 5)

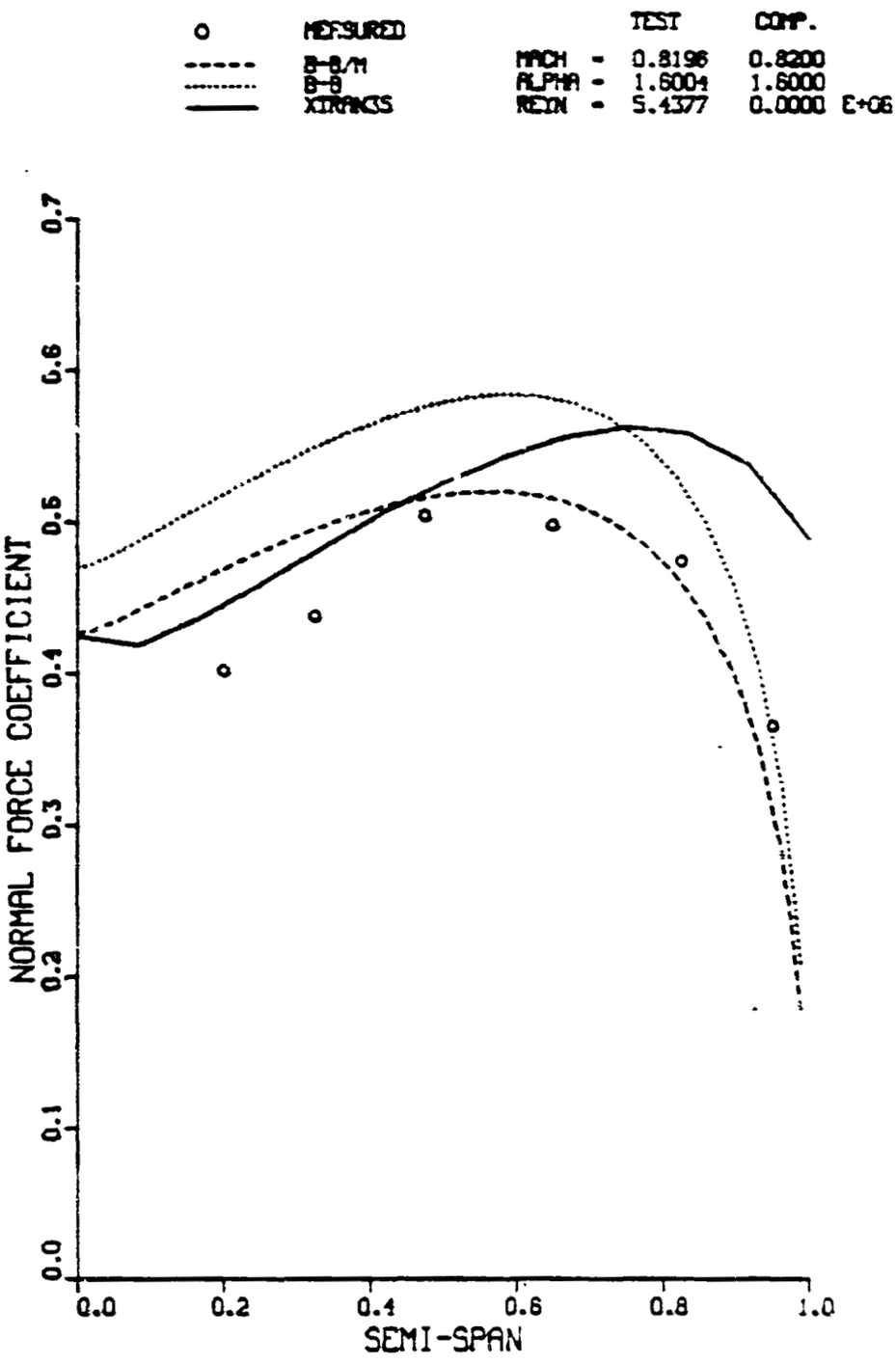

(e) MEAN ANGLE OF ATTACK = 1.6 DEGREE

Figure 26. Comparison of Computed and Measured Span-Loading Distributions at Design Mach Number (Sheet 5 of 5)

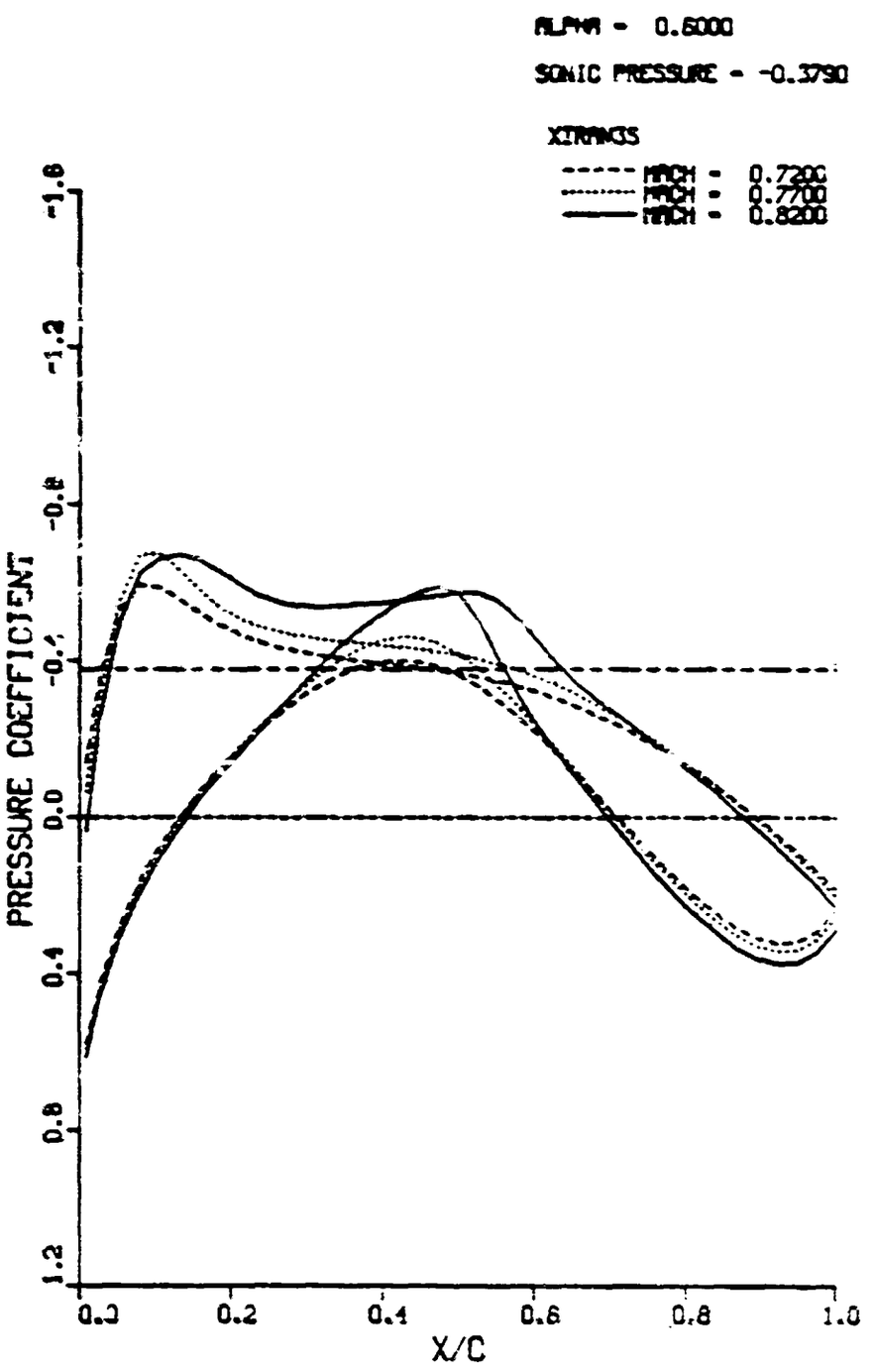

(a) SPAN-STATION = 0.200

Figure 27. Effect of Mach Number Variation on Pressure Distributions for Fixed Mean Angle of Attack (Sheet 1 of 6)

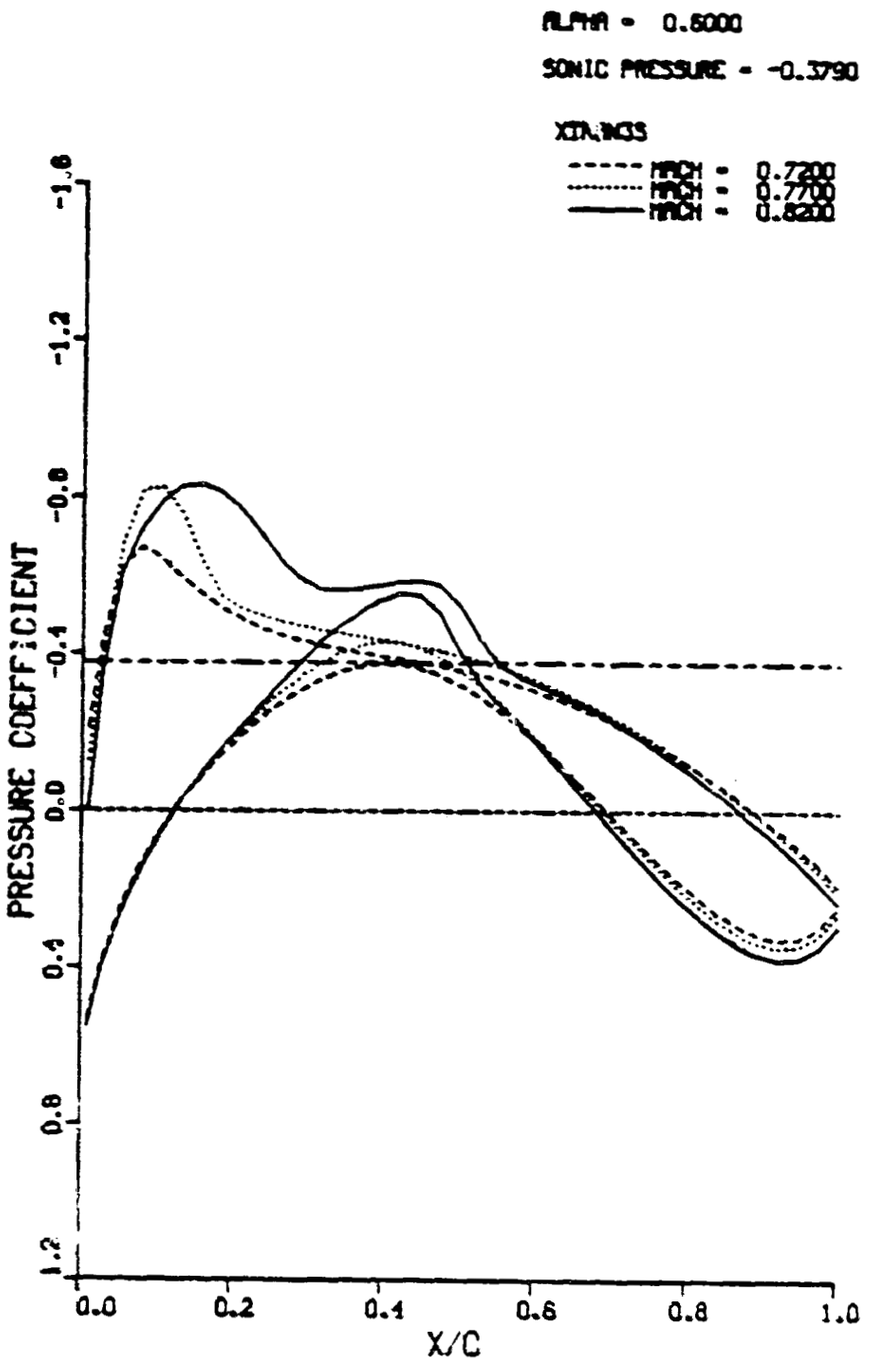

(b) SPAN-STATION = 0.325

Figure 27. Effect of Mach Number Variation on Pressure Distributions for Fixed Mean Angle of Attack (Sheet 2 of 6)

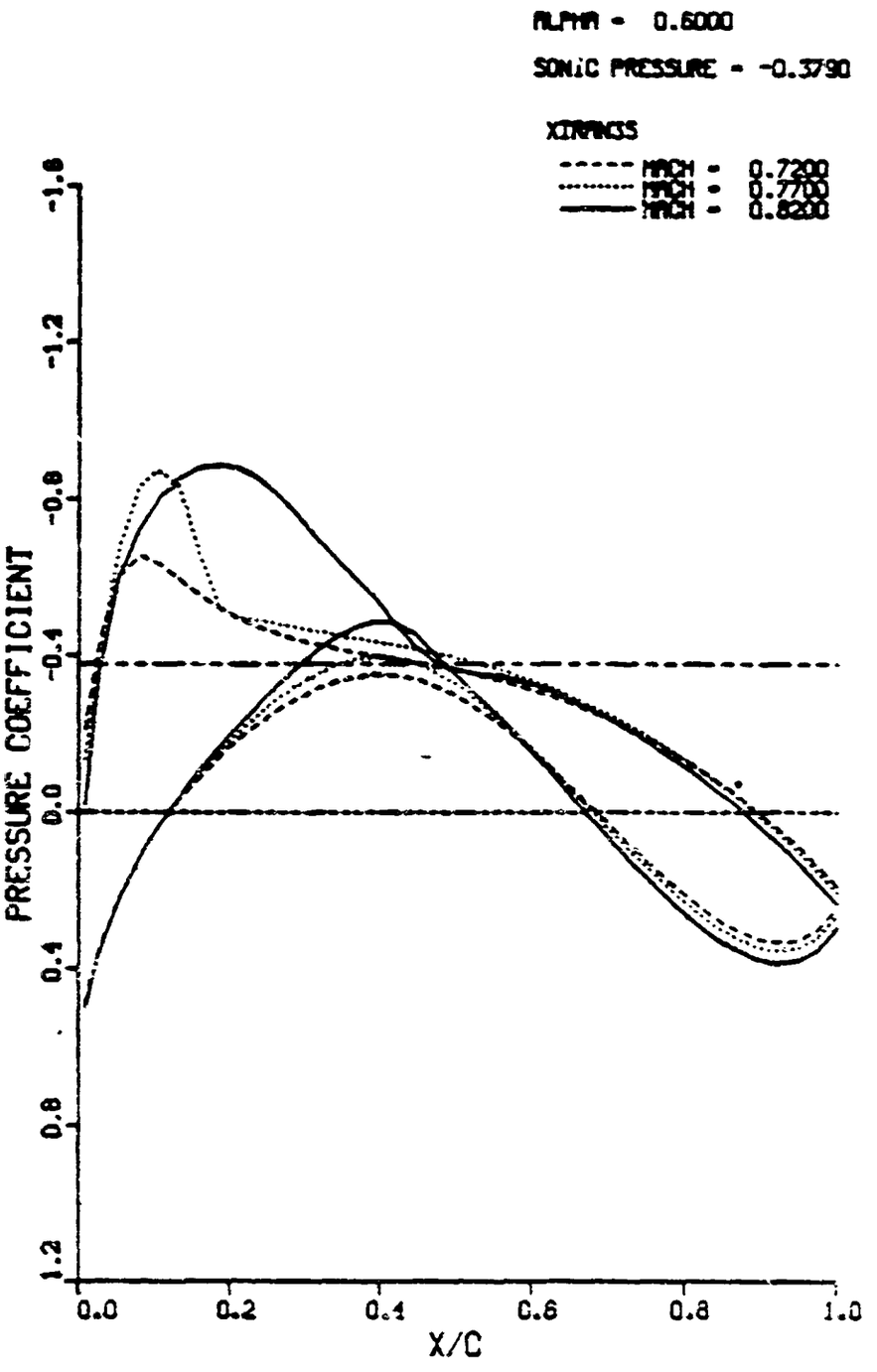

(c) SPAN-STATION = 0.475

Figure 27. Effect of Mach Number Variation on Pressure Distributions for Fixed Mean Angle of Attack (Sheet 3 of 6)

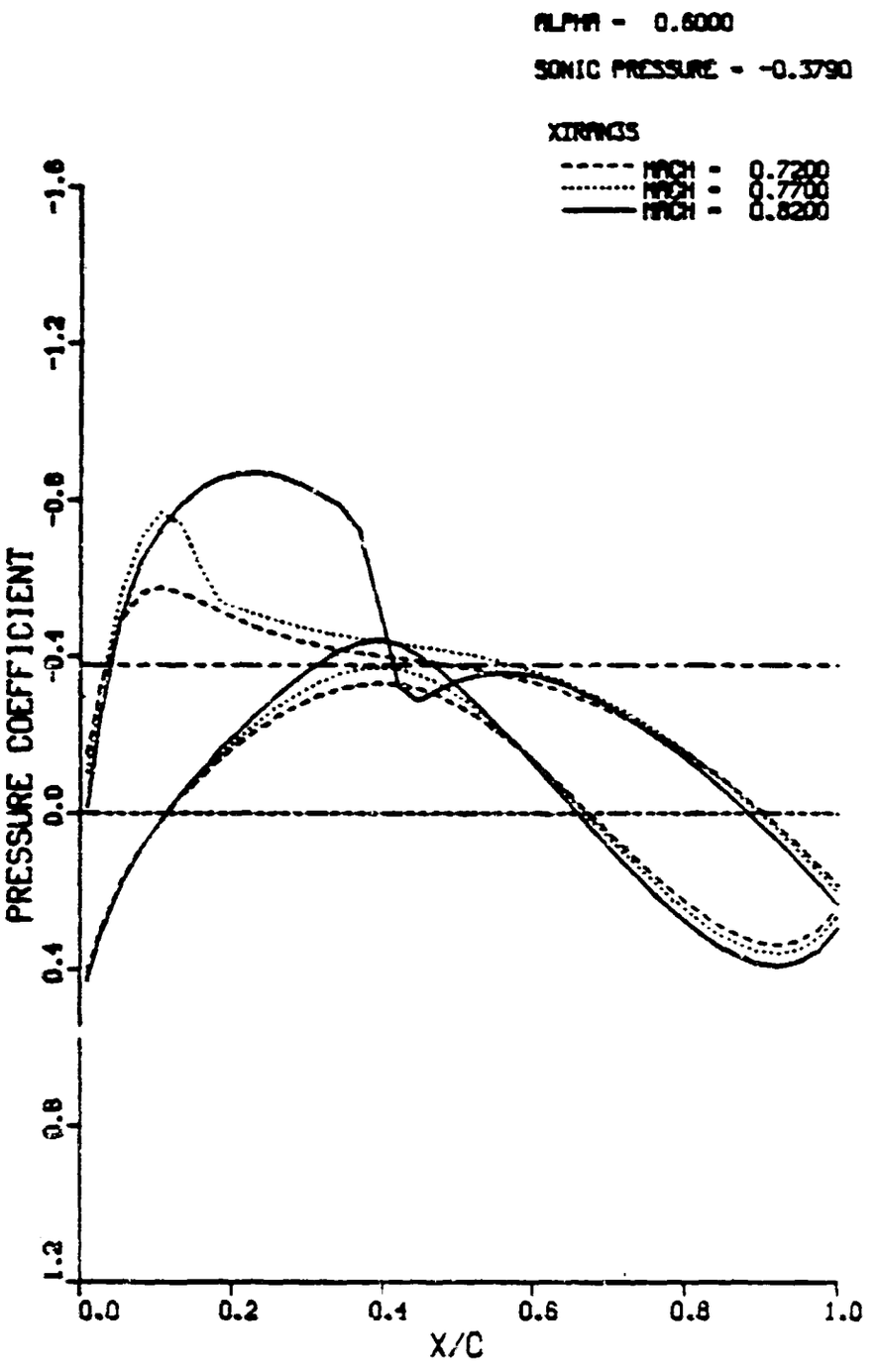

(d) SPAN-STATION = 0.650

Figure 27. Effect of Mach Number Variation on Pressure Distributions for Fixed Mean Angle of Attack (Sheet 4 of 6)

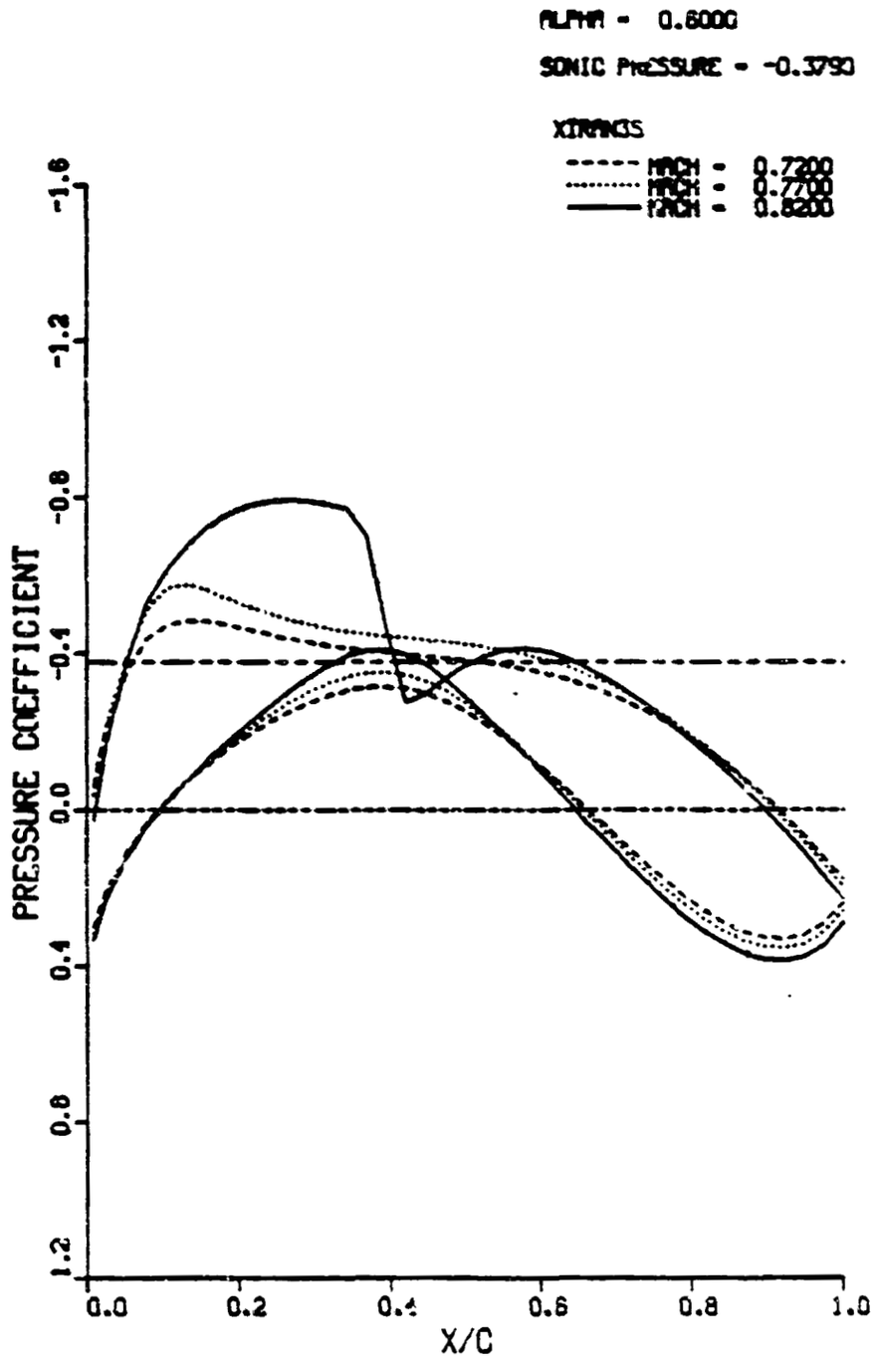

(e) SPAN-STATION = 0.825

Figure 27. Effect of Mach Number Variation on Pressure Distributions for Fixed Mean Angle of Attack (Sheet 5 of 6)

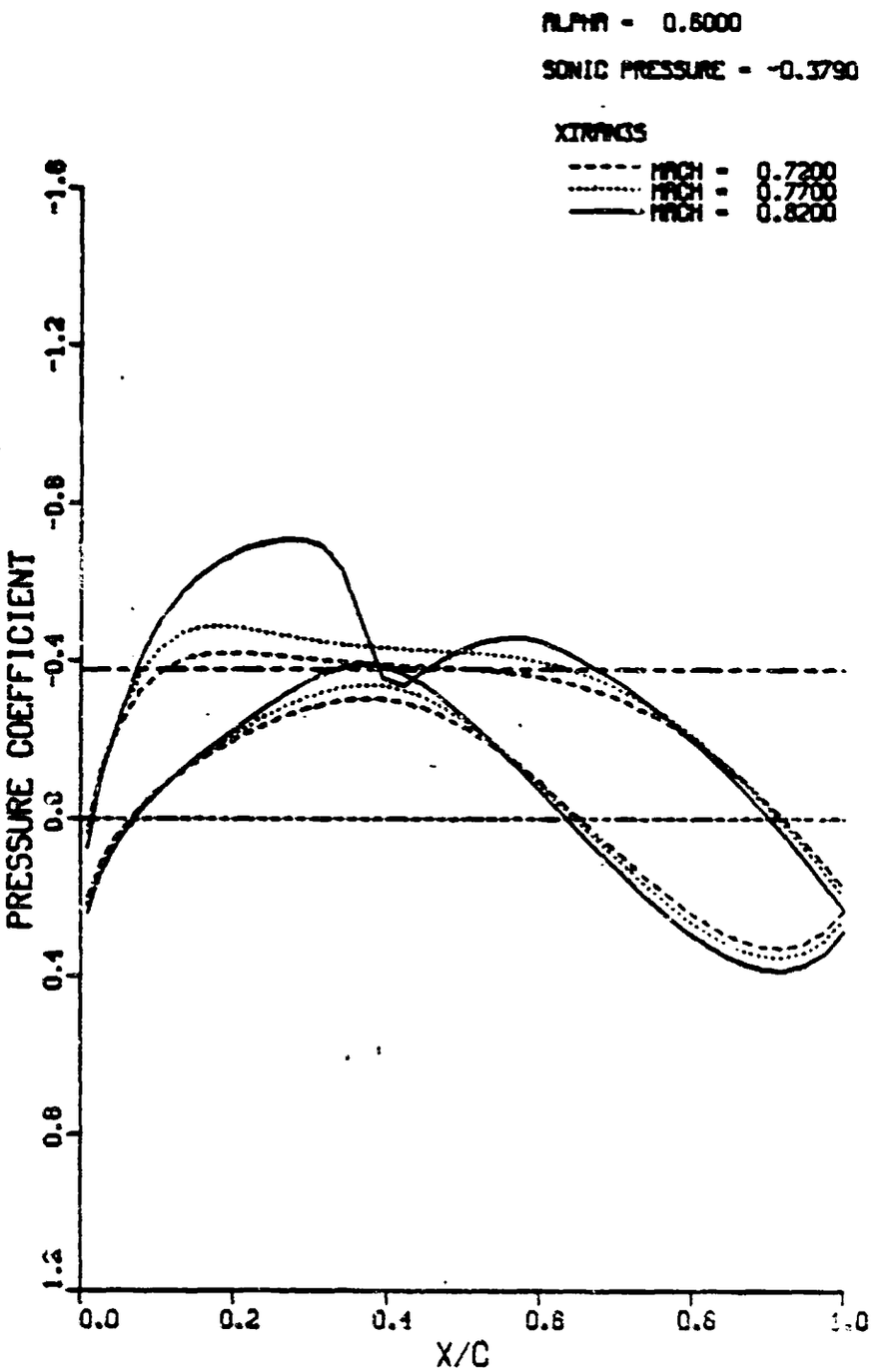

(f) SPAN-STATION = 0.950

Figure 27. Effect of Mach Number Variation on Pressure Distributions for Fixed Mean Angle of Attack (Sheet 6 of 6)

LANN WING

MACH NO. = 0.82000
MEAN ANGLE = 0.60000
RED. FREQ. = 0.20463
WING PITCH = 0.62080
STEPS/CYC. = 720

MEAN VALUE = 0.35029
AMPLITUDE = 0.02964
PHASE ANG. = 9.59324

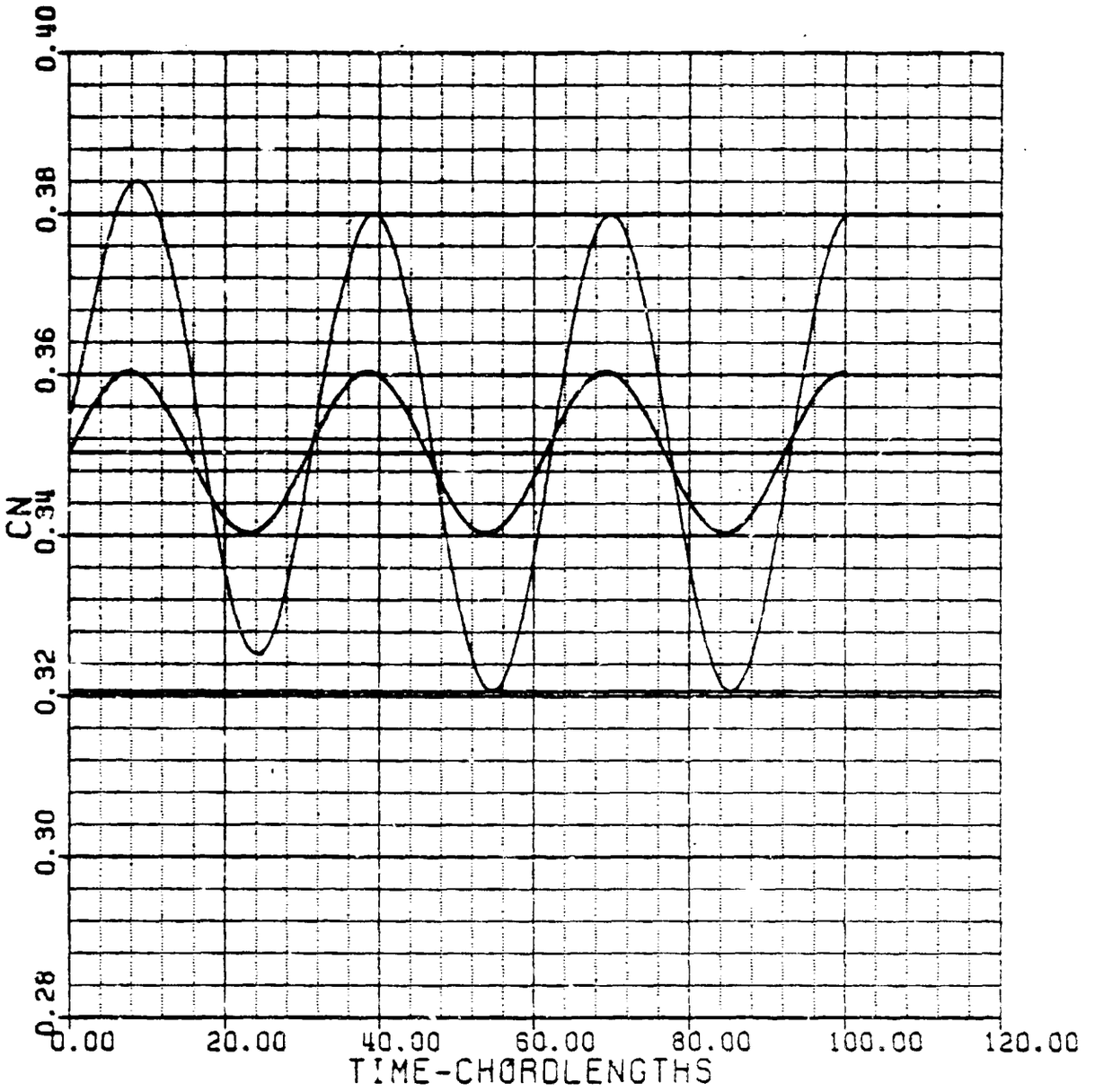

(a) TIME-HISTORY OF XTRAN3S CODE CALCULATION FOR RUN 73 (24 Hz)

Figure 28. Unsteady Normal Force Due to Pitch Oscillation at Design Conditions (Sheet 1 of 4)

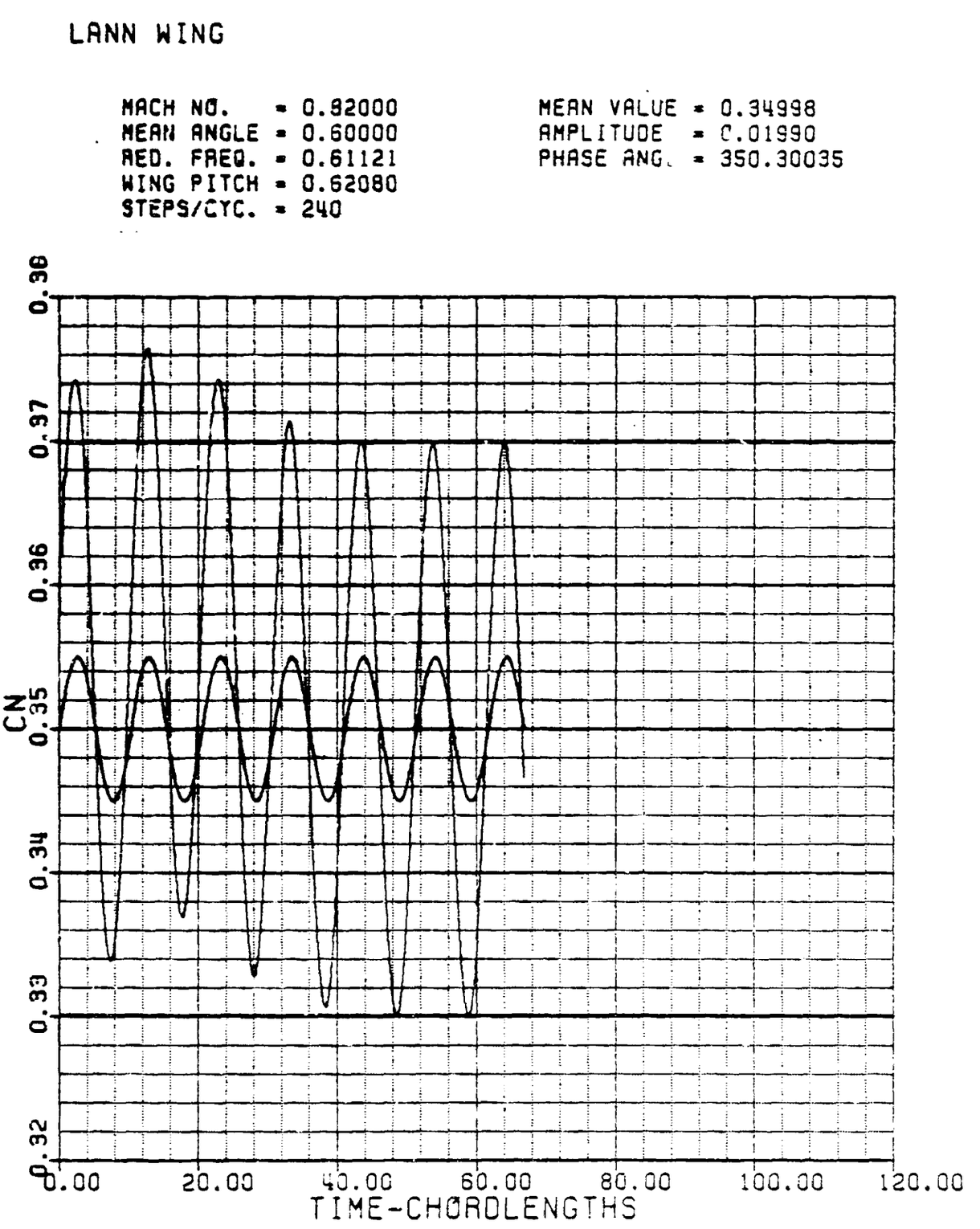

(b) TIME-HISTORY OF XTRAN3S CODE CALCULATION FOR RUN 85 (48 Hz)

Figure 28. Unsteady Normal Force Due to Pitch Oscillation at Design Conditions (Sheet 2 of 4)

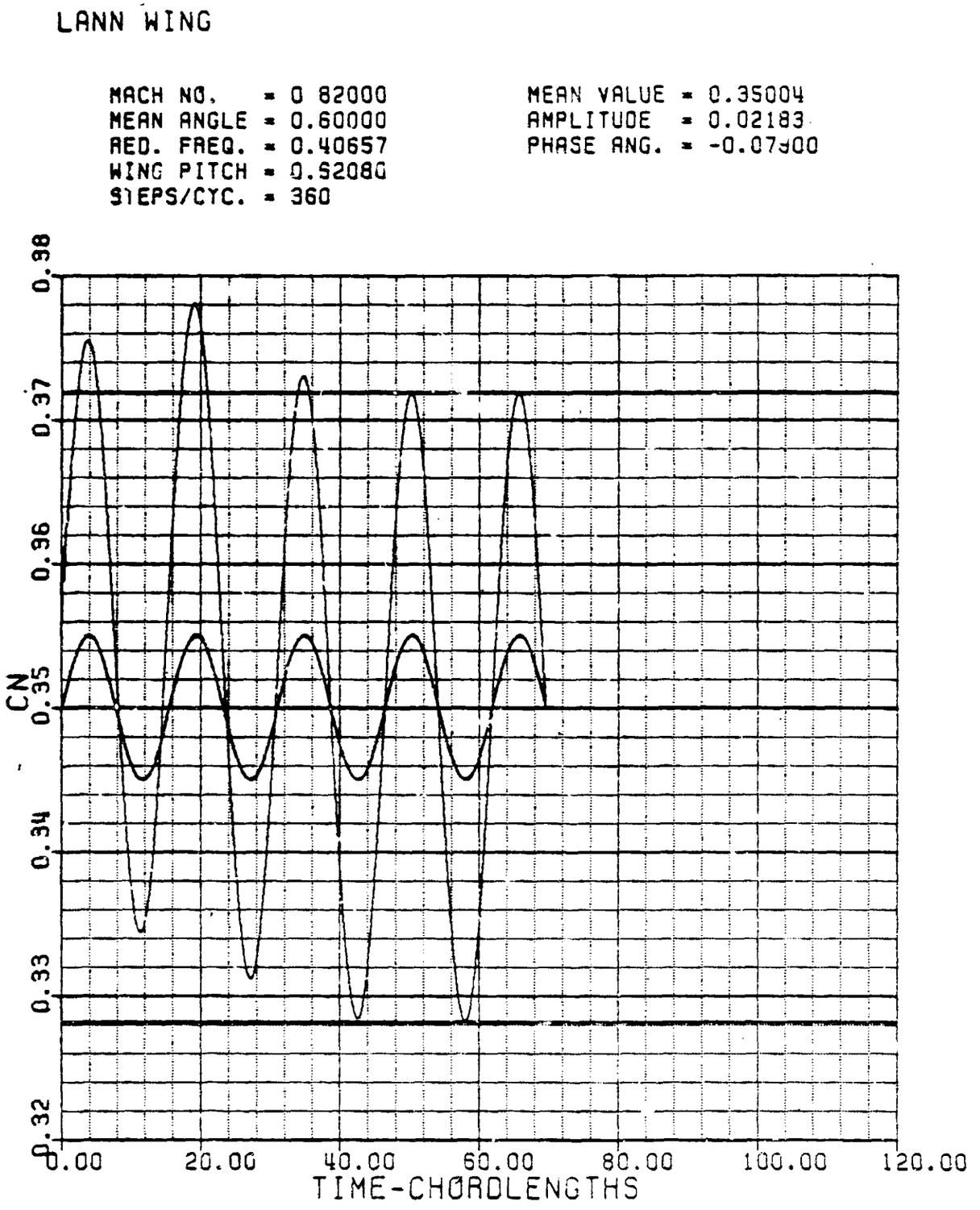

(c) TIME-HISTORY OF XTRAN3S CODE CALCULATION FOR RUN 87 (72 Hz)

Figure 28. Unsteady Normal Force Due to Pitch Oscillation at Design Conditions (Sheet 3 of 4)

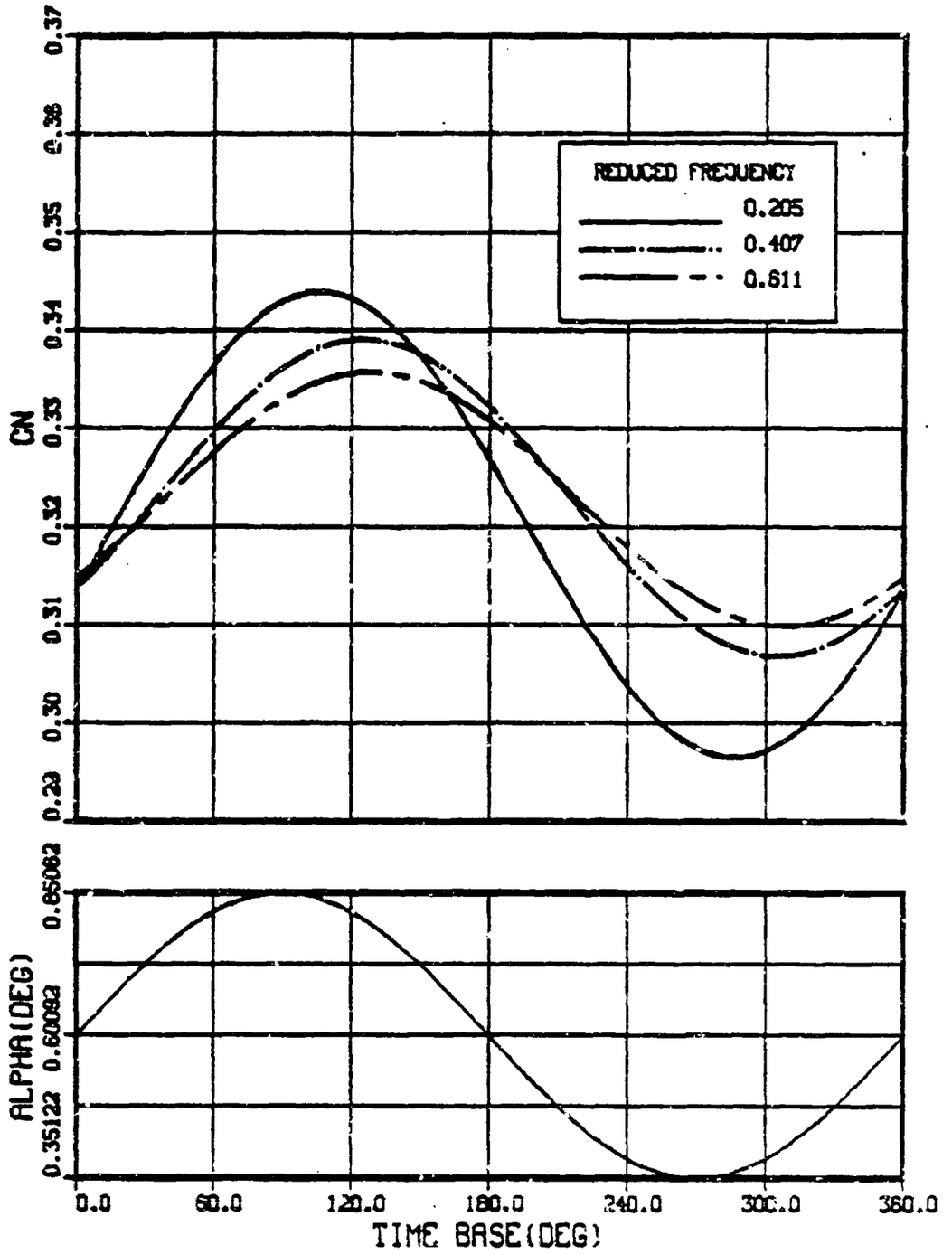

MACH NUMBER = 0.8205 MEAN ALPHA = 0.6009 PITCH AMP(DEG) = 0.2497

(d) MEASURED DATA FOR 24 Hz, 48 Hz AND 72 Hz

Figure 28. Unsteady Normal Force Due to Pitch Oscillation at Design Conditions (Sheet 4 of 4)

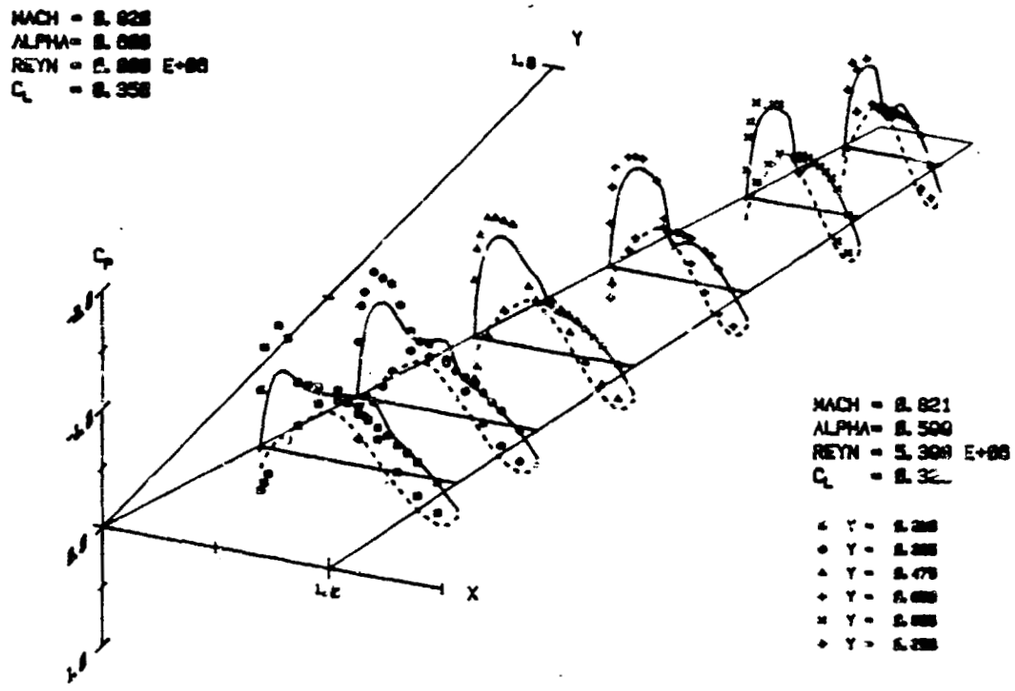

(a) ANGULAR POSITION = 0.0 DEGREE

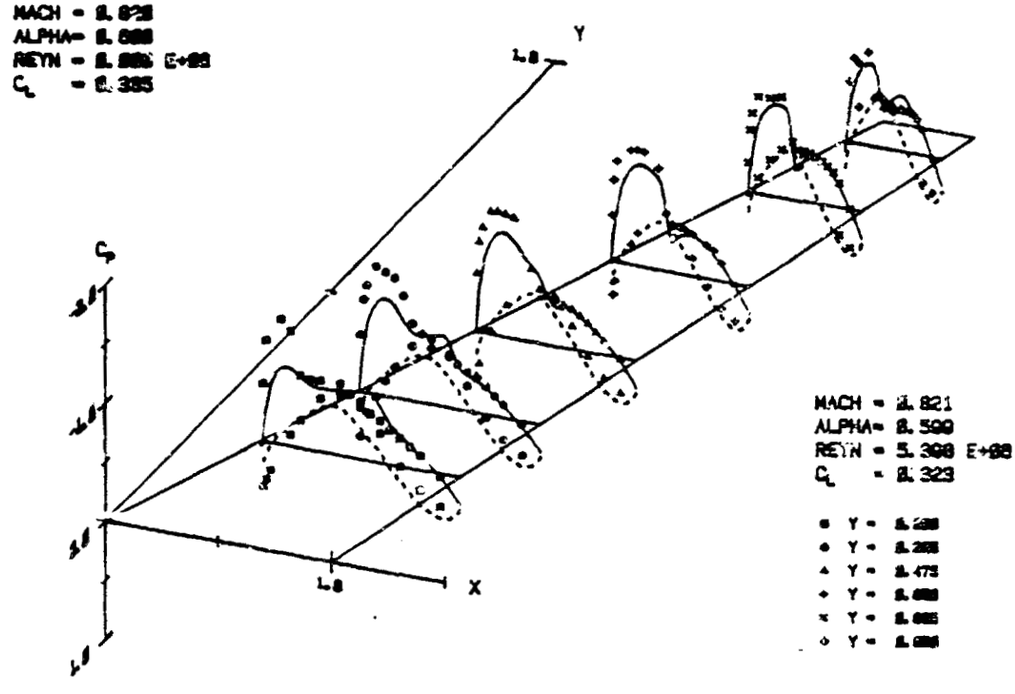

(b) ANGULAR POSITION = 45.0 DEGREES

Figure 29. Comparison of Computed and Measured Pressure Distributions on Wing at Several Pitch Angular Positions for Run 85 (48 Hz) (Sheet 1 of 4)

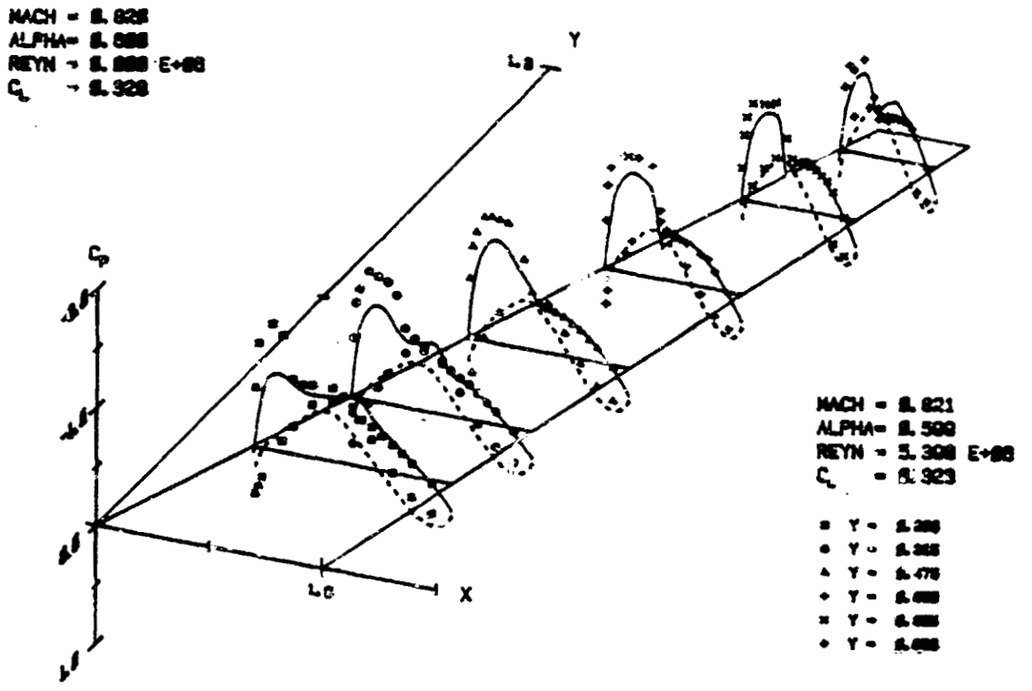

(c) ANGULAR POSITION = 90.0 DEGREES

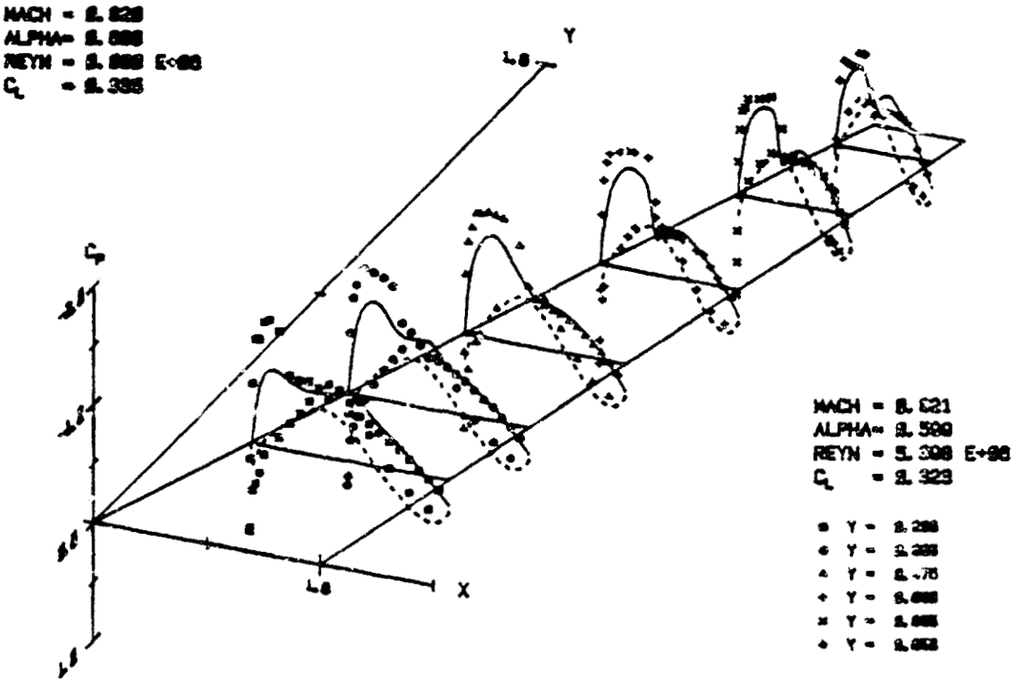

(d) ANGULAR POSITION = 135.0 DEGREES

Figure 27. Comparison of Computed and Measured Pressure Distributions on Wing at Several Pitch Angular Positions for Run 85 (48 Hz) (Sheet 2 of 4)

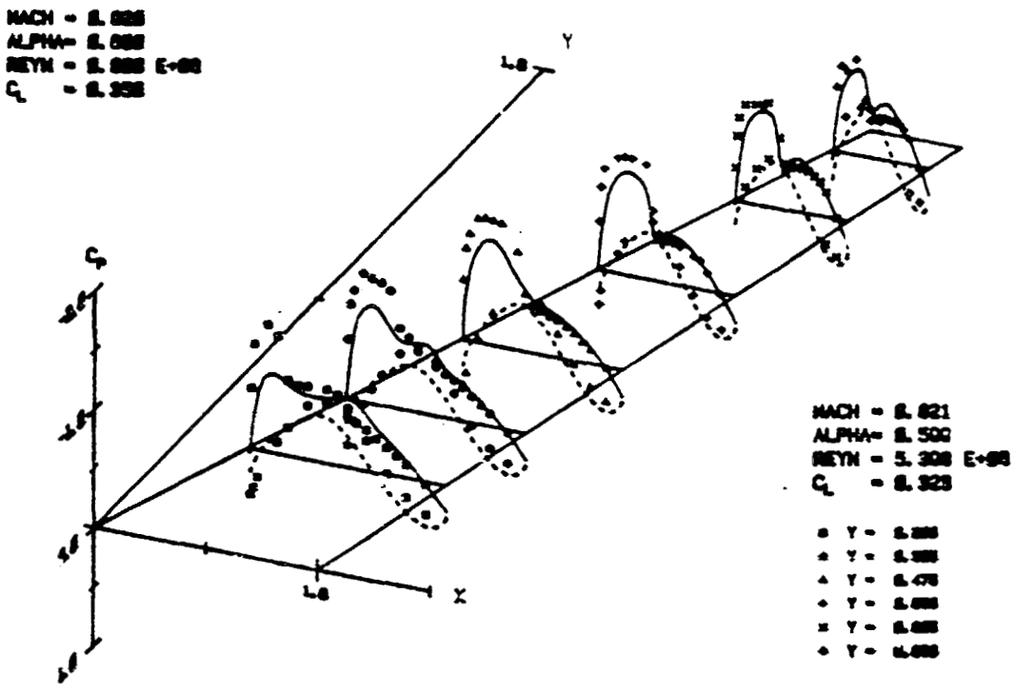

(e) ANGULAR POSITION = 180.0 DEGREES

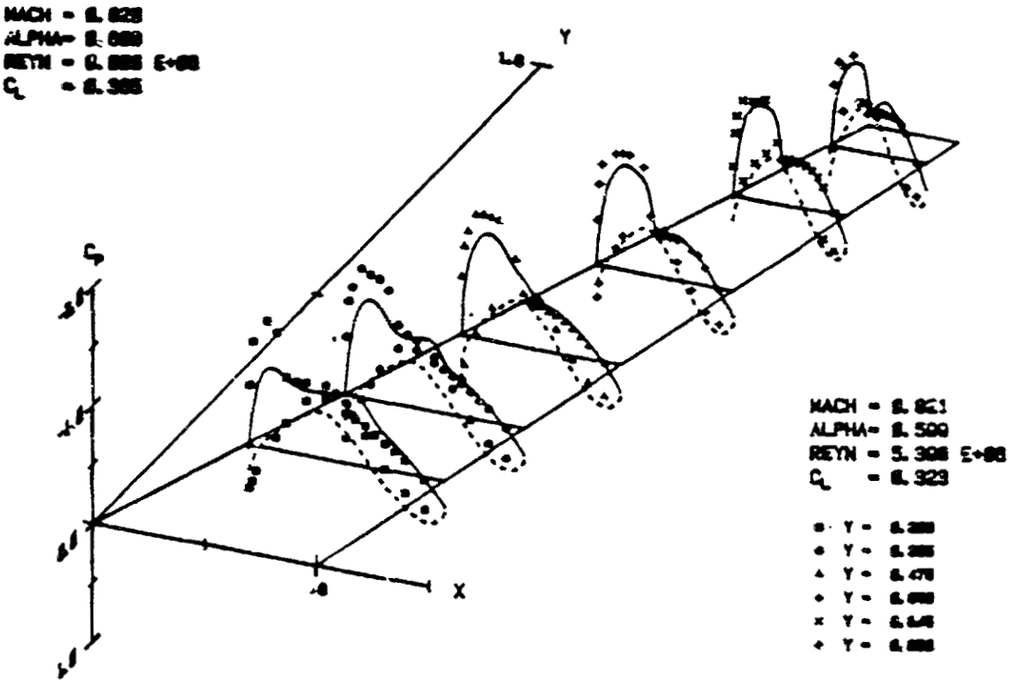

(f) ANGULAR POSITION = 225.0 DEGREES

Figure 29. Comparison of Computed and Measured Pressure Distributions on Wing at Several Pitch Angular Positions for Run 85 (48 Hz) (Sheet 3 of 4)

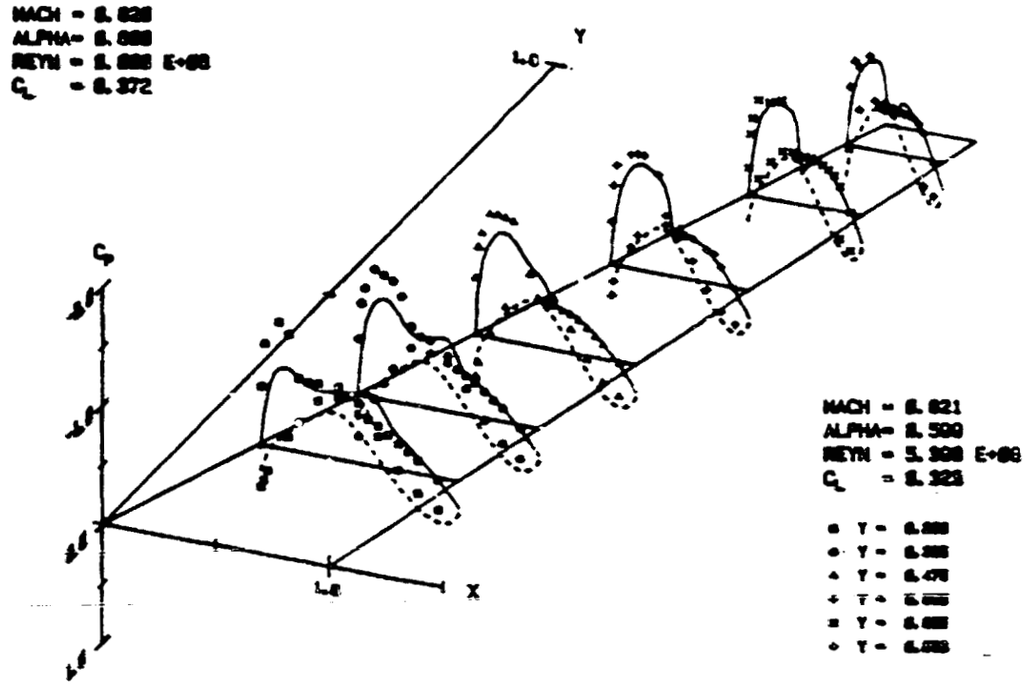

(g) ANGULAR POSITION = 270.0 DEGREES

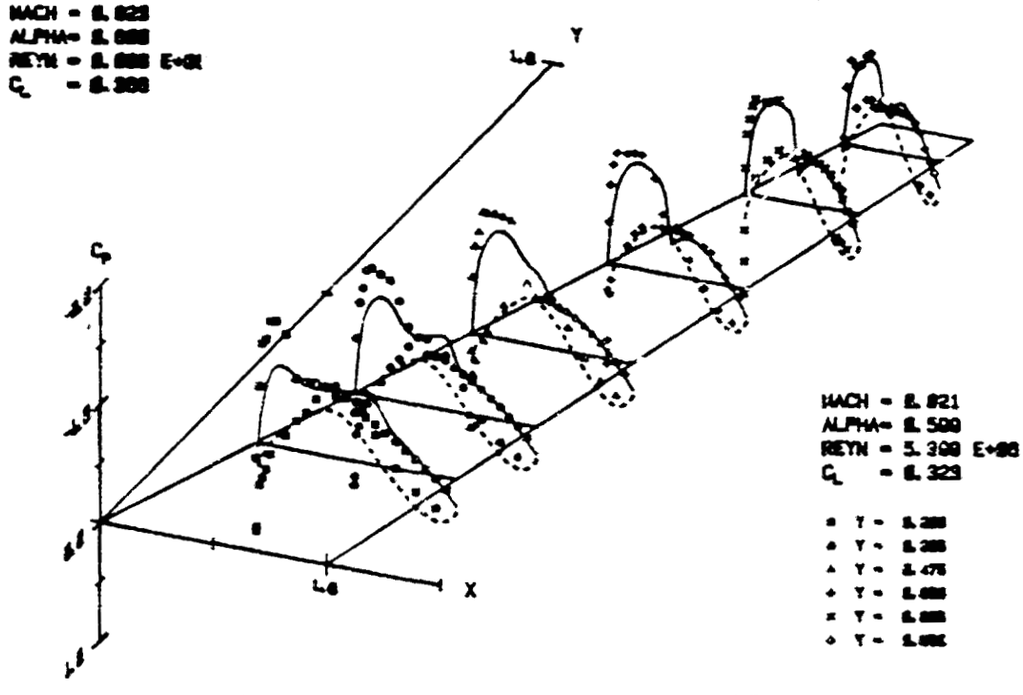

(h) ANGULAR POSITION = 315.0 DEGREES

Figure 29. Comparison of Computed and Measured Pressure Distributions on Wing at Several Pitch Angular Positions for Run 85 (48 Hz) (Sheet 4 of 4)

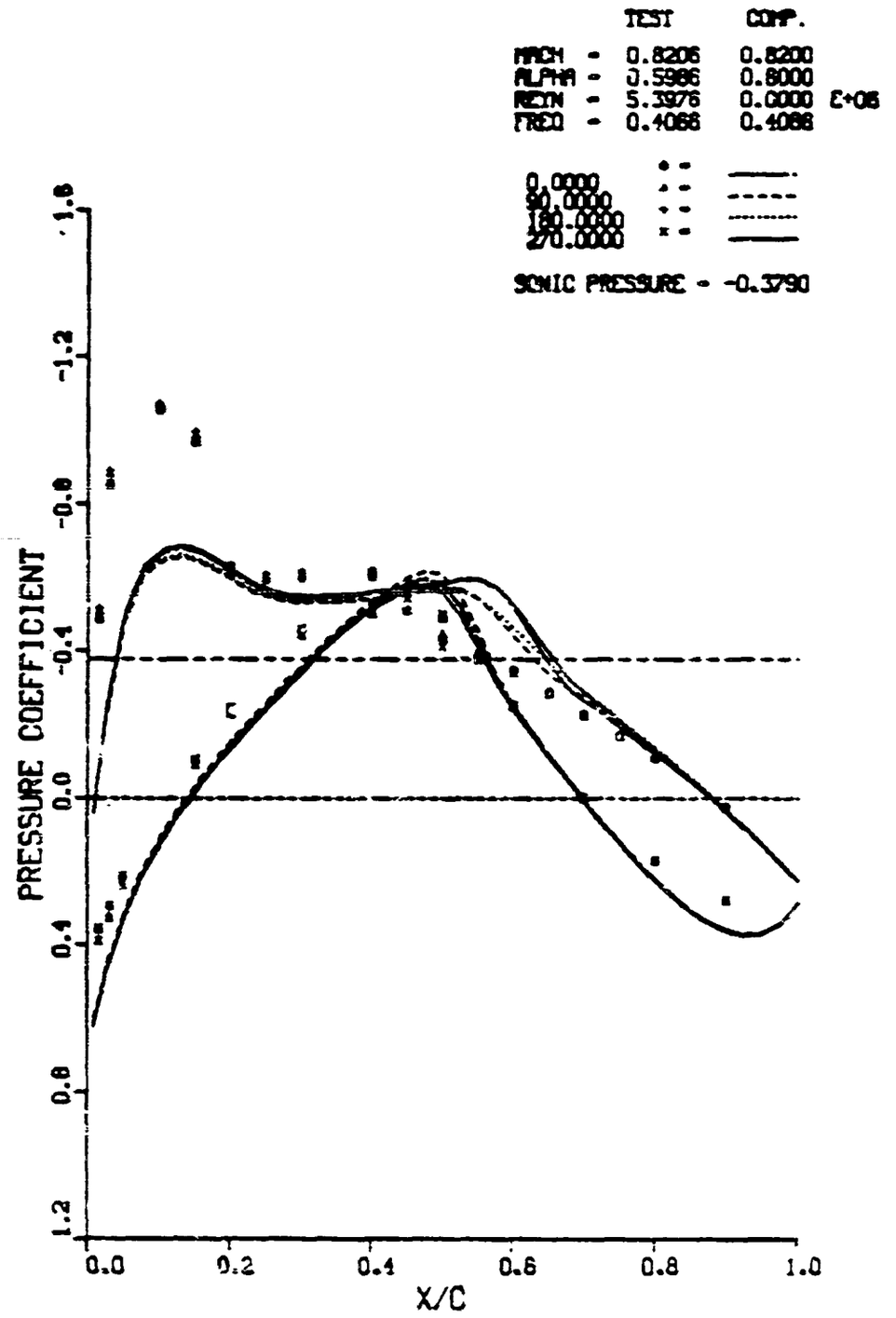

(a) SPAN-STATION 0.200

Figure 30. Comparison of Computed and Measured Chordwise Pressure Distributions at Several Pitch Angular Positions for Run 85 (48 Hz) (Sheet 1 of 6)

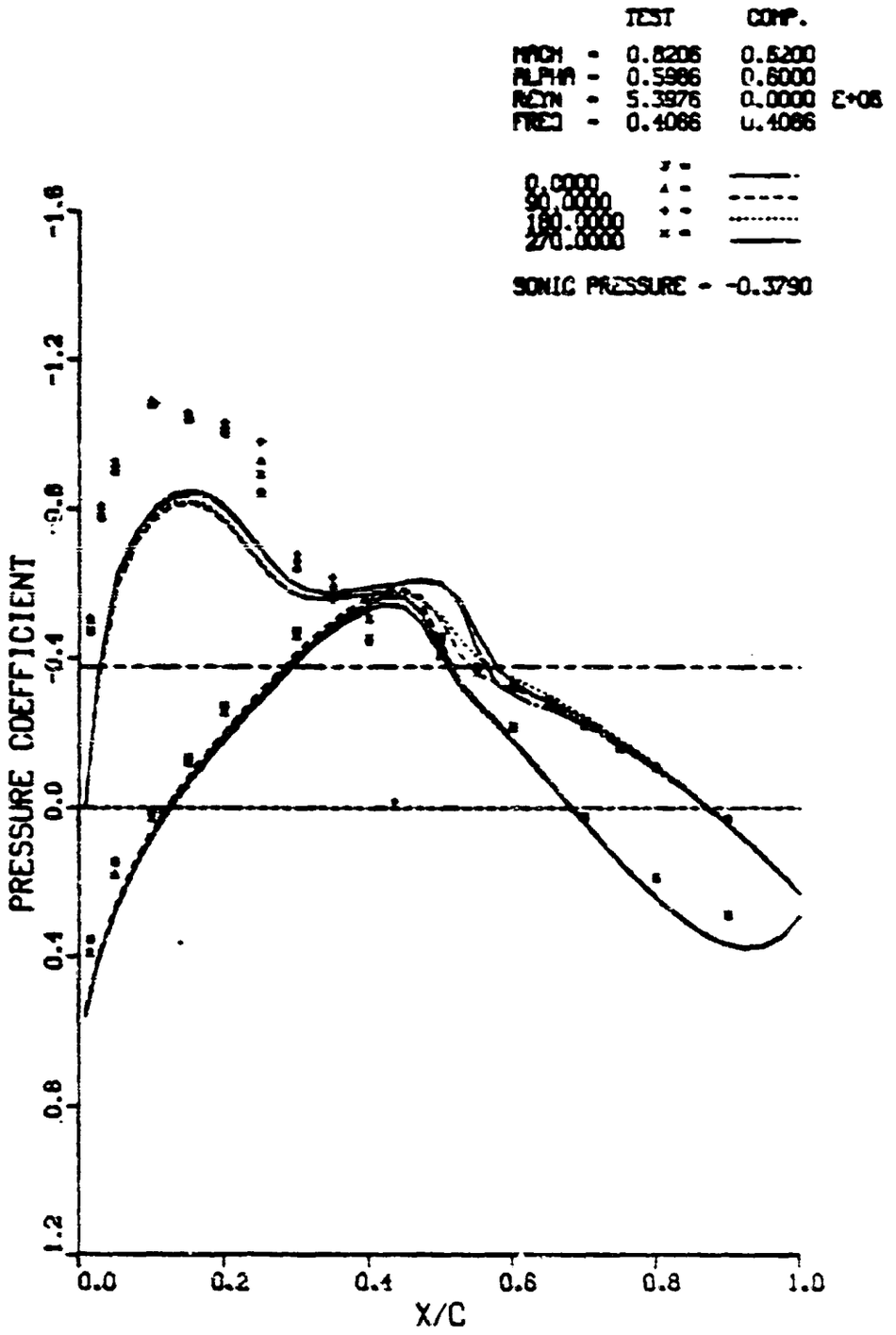

(b) SPAN-STATION = 0.325

Figure 30. Comparison of Computed and Measured Chordwise Pressure Distributions at Several Pitch Angular Positions for Run 85 (48 Hz) (Sheet 2 of 6)

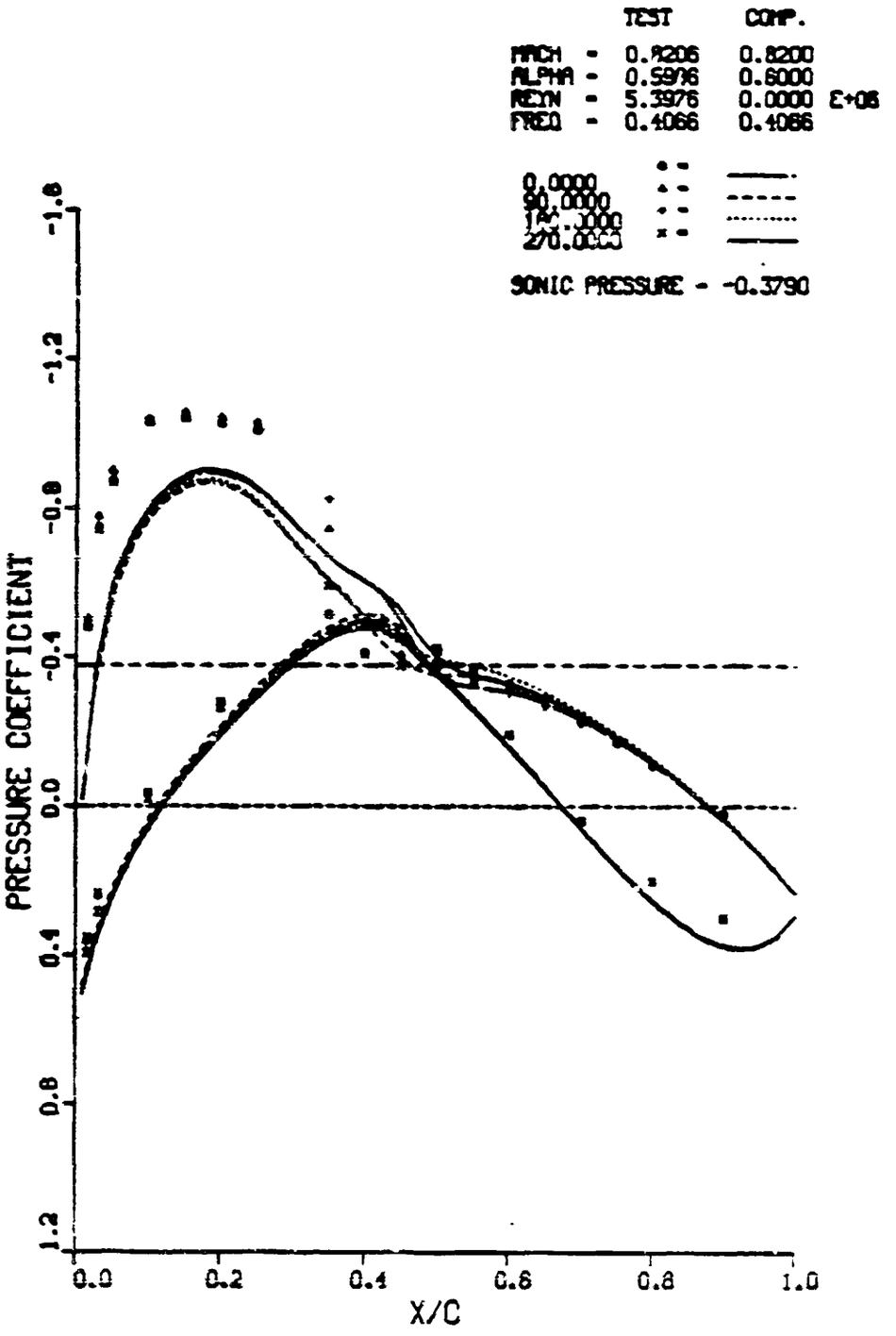

(c) SPAN-STATION = 0.475

Figure 30. Comparison of Computed and Measured Chordwise Pressure Distributions at Several Pitch Angular Positions for Run 85 (48 Hz) (Sheet 3 of 6)

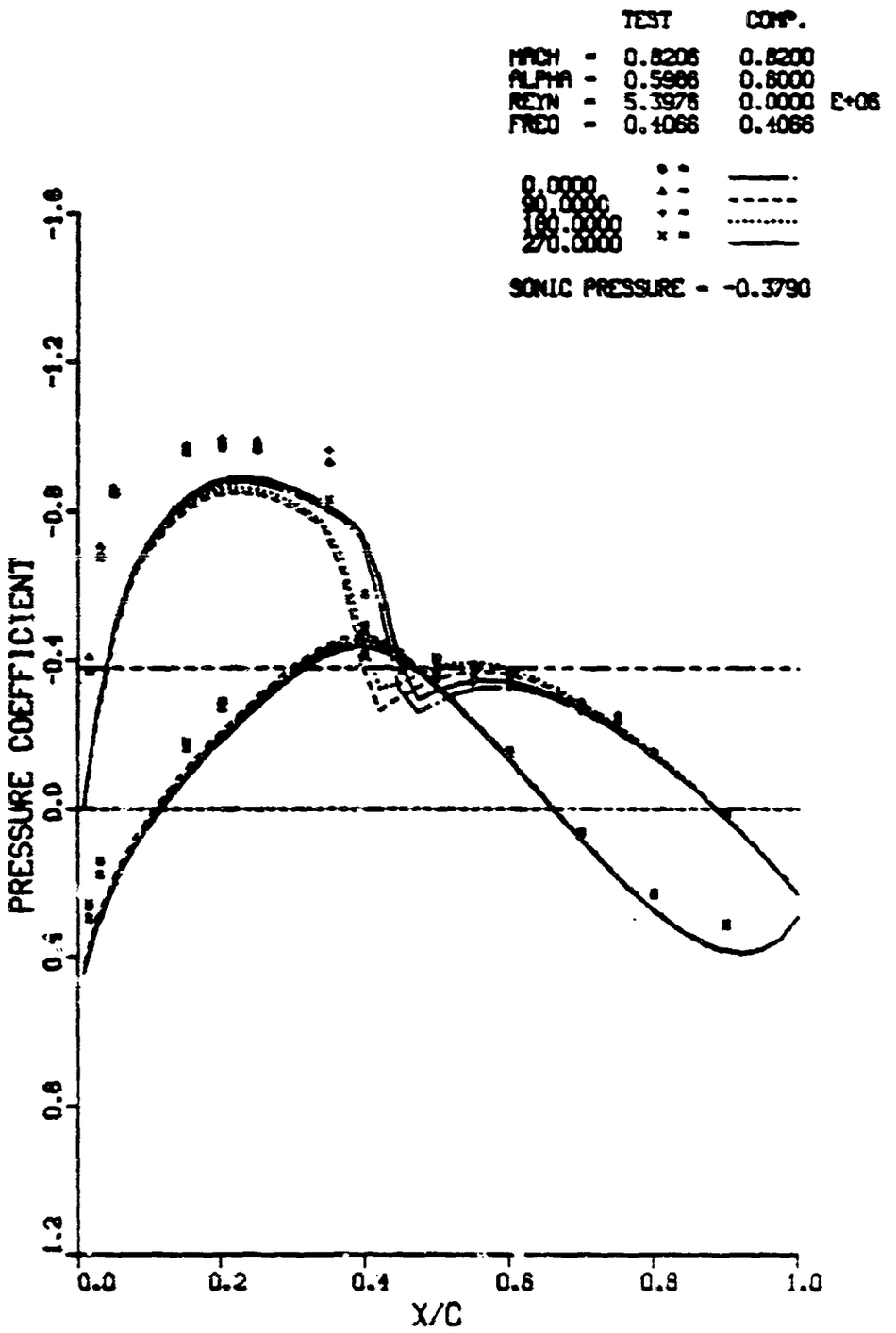

(d) SPAN-STATION = 0.650

Figure 30. Comparison of Computed and Measured Chordwise Pressure Distributions at Several Pitch Angular Positions for Run 85 (48 Hz) (Sheet 4 of 6)

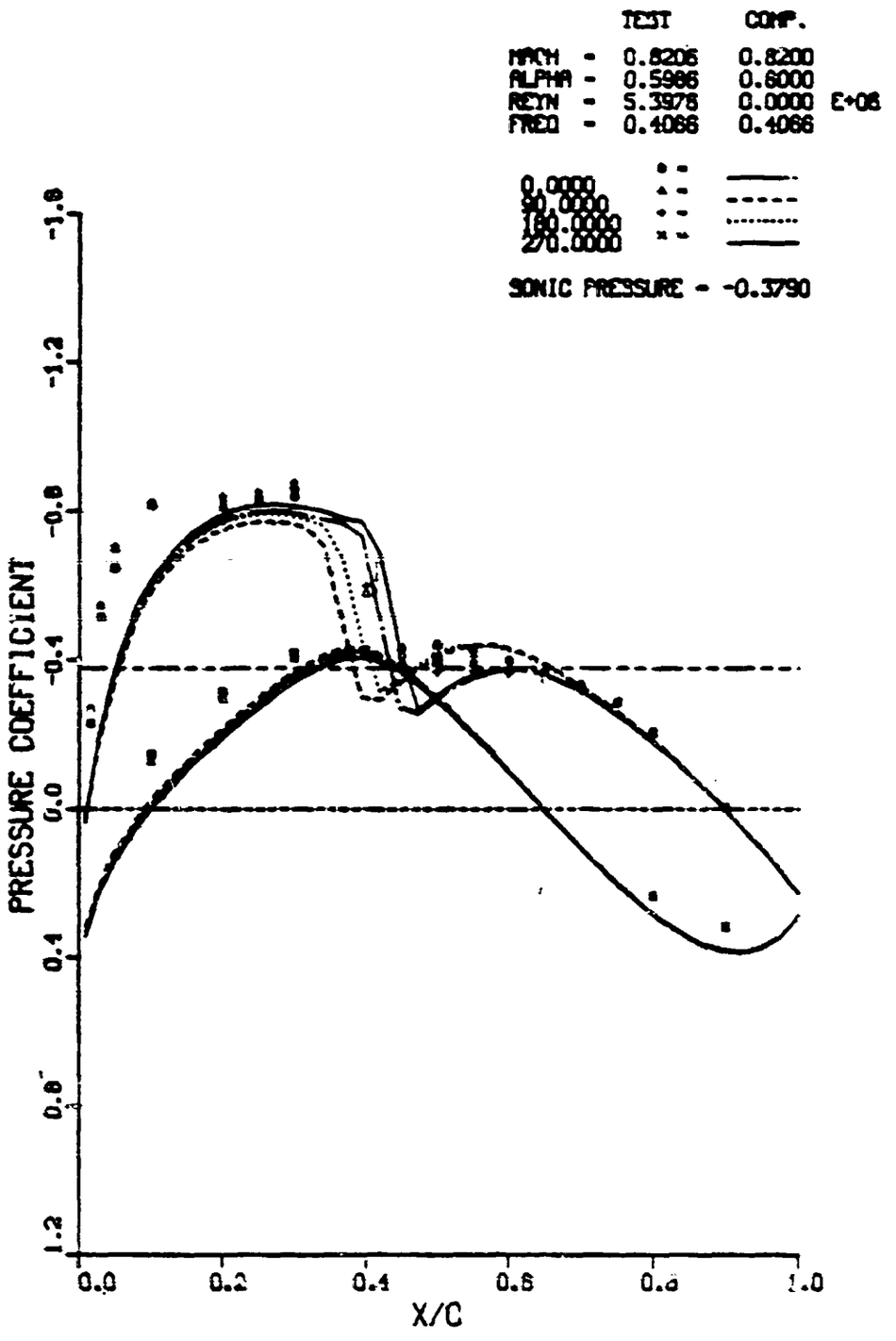

(e) SPAN-STATION = 0.825

Figure 30. Comparison of Computed and Measured Chordwise Pressure Distributions at Several Pitch Angular Positions for Run 85 (+8 Hz) (Sheet 5 of 6)

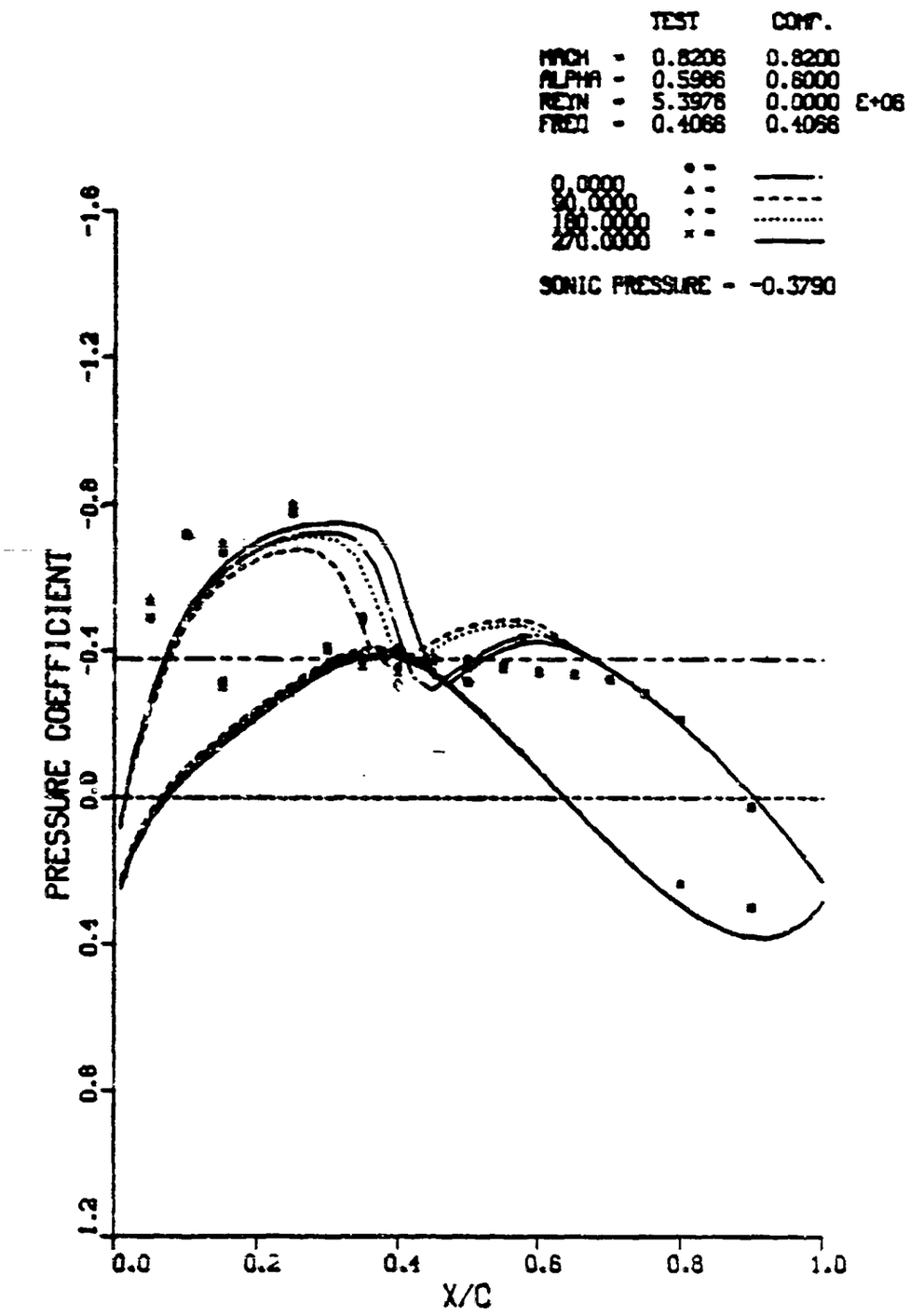

(f) SPAN-STATION = 0.950

Figure 30. Comparison of Computed and Measured Chordwise Pressure Distributions at Several Pitch Angular Positions for Run 85 (48 Hz) (Sheet 6 of 6)

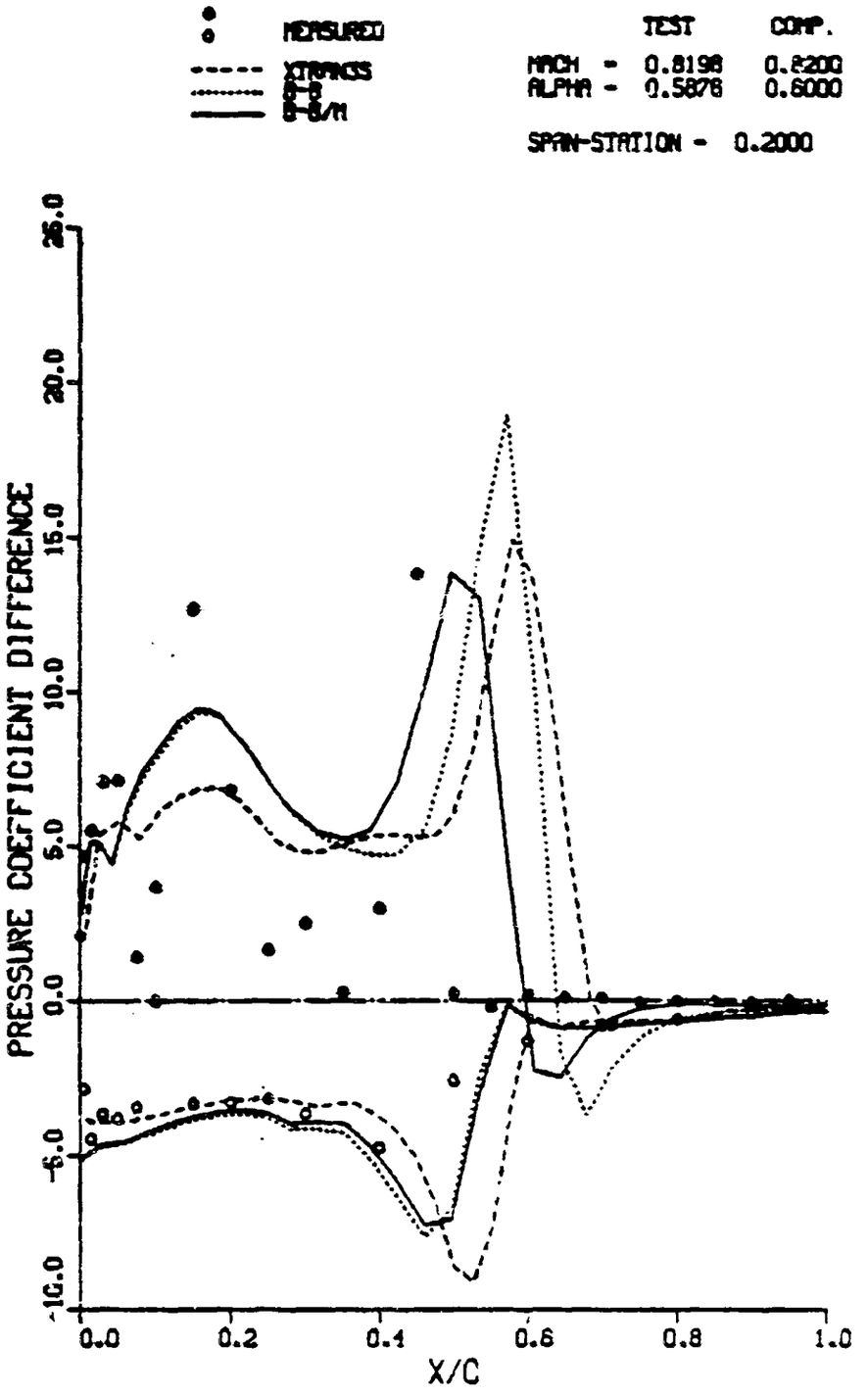

(a) SPAN-STATION = 0.200

Figure 31. Comparison of Computed and Measured Quasi-Steady Pressure Difference at Several Span-Stations (Sheet 1 of 6)

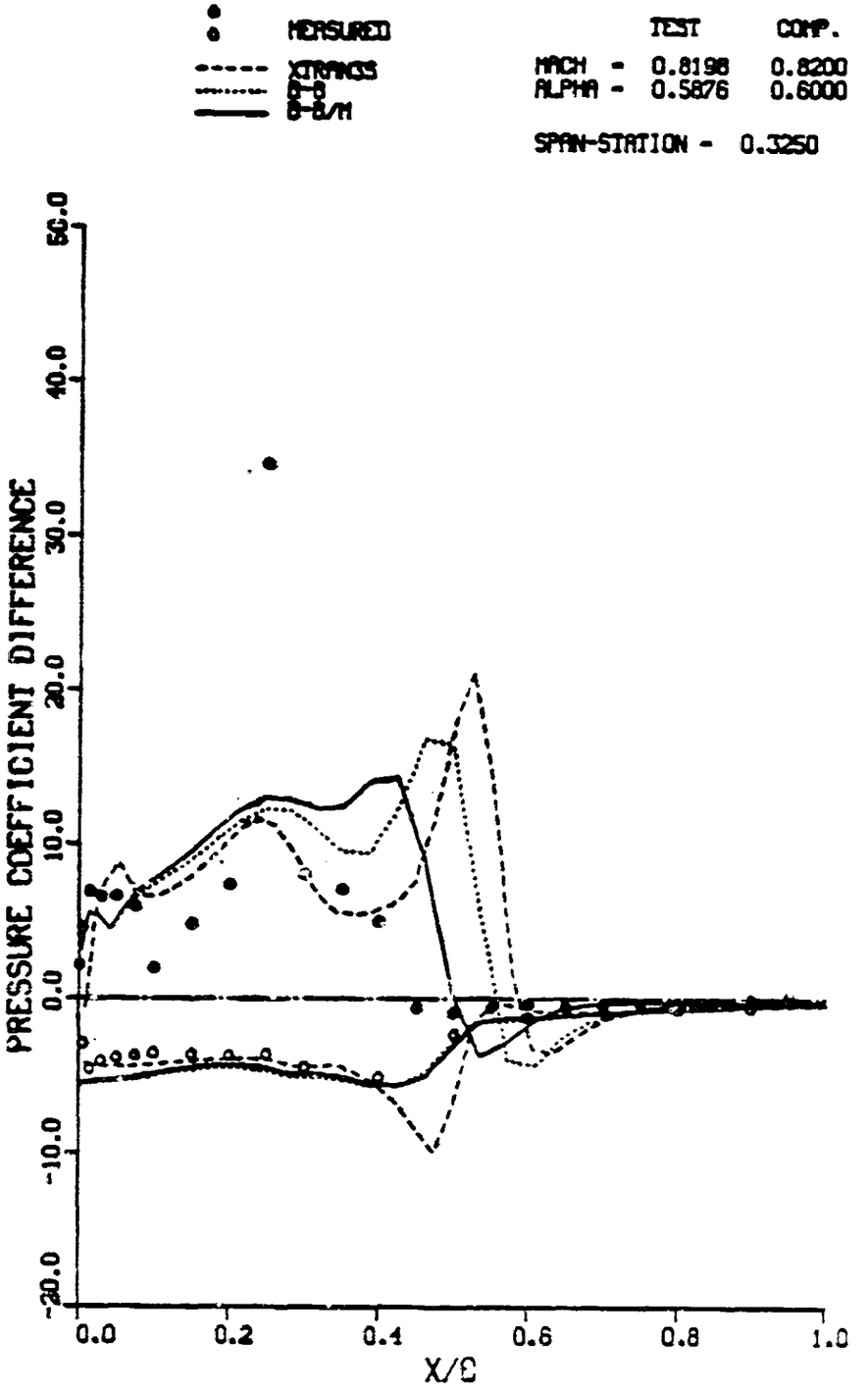

(b) SPAN-STATION = 0.325

Figure 31. Comparison of Computed and Measured Quasi-Steady Pressure Difference at Several Span-Stations (Sheet 2 of 6)

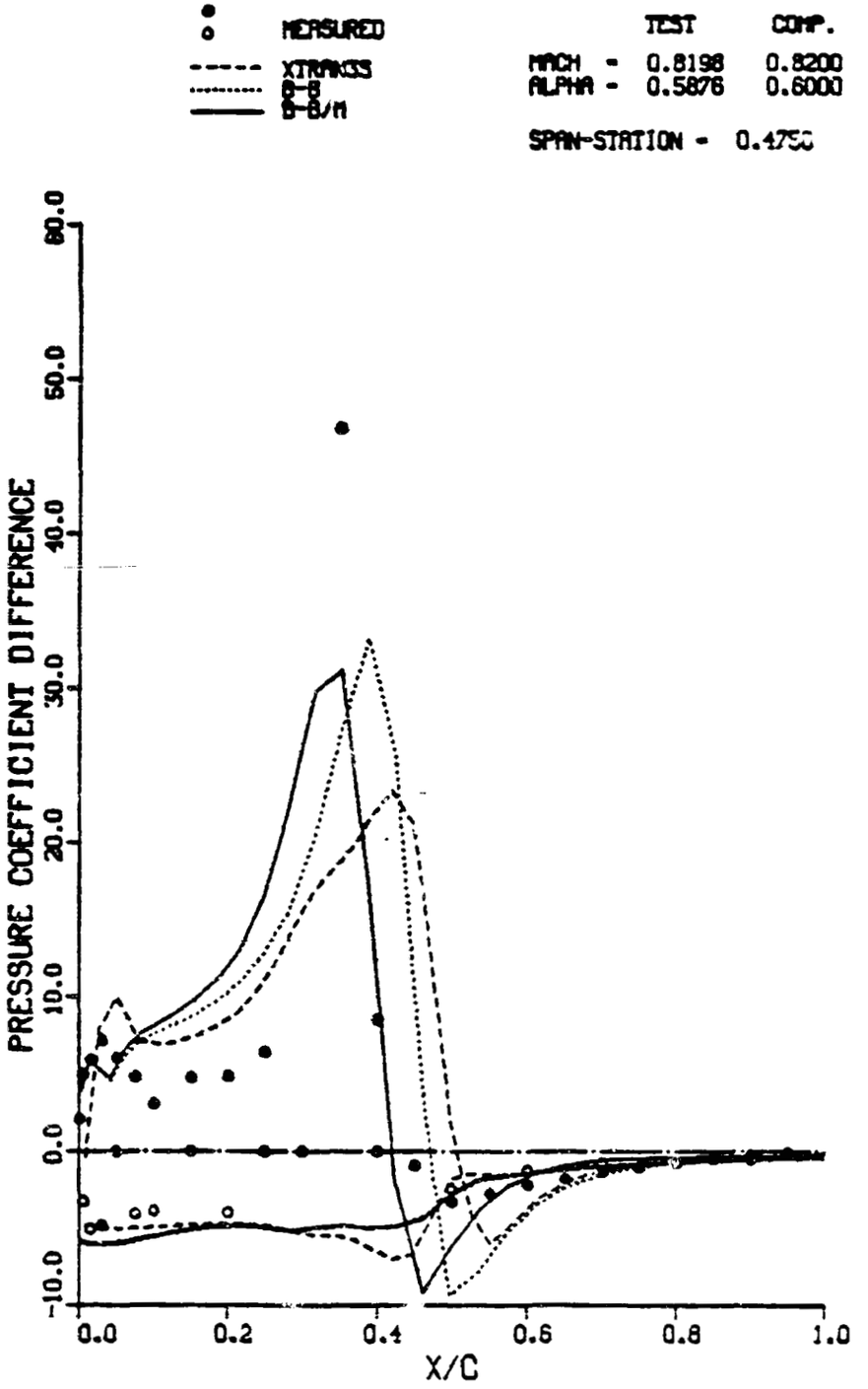

(e) SPAN-STATION = 0.475

Figure 31. Comparison of Computed and Measured Quasi-Steady Pressure Difference at Several Span-Stations (Sheet 3 of 6)

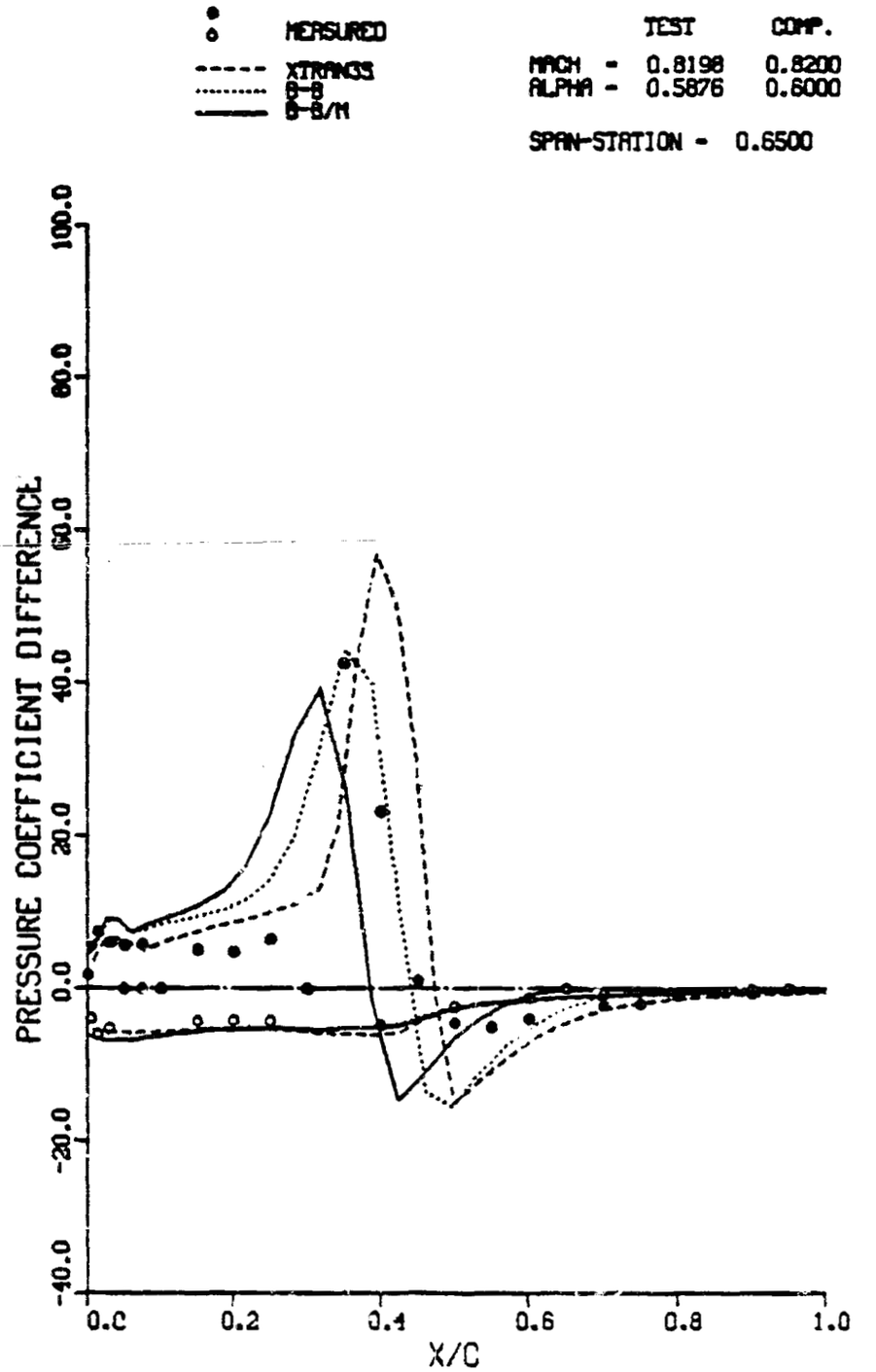

(d) SPAN-STATION = 0.650

Figure 31. Comparison of Computed and Measured Quasi-Steady Pressure Difference at Several Span-Stations (Sheet 4 of 6)

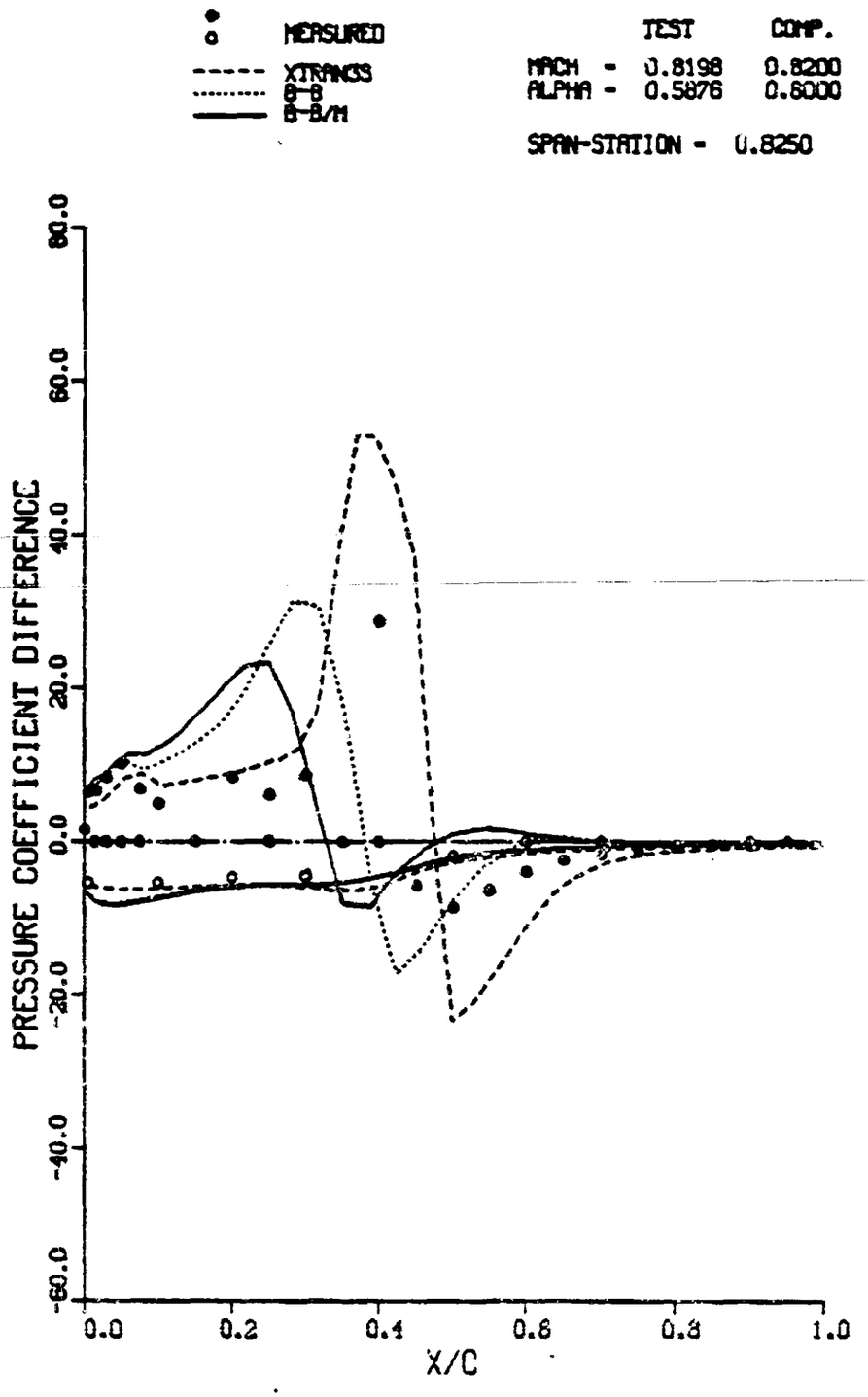

(e) SPAN-STATION = 0.825

Figure 31. Comparison of Computed and Measured Quasi-Steady Pressure Difference at Several Span-Stations (Sheet 5 of 6)

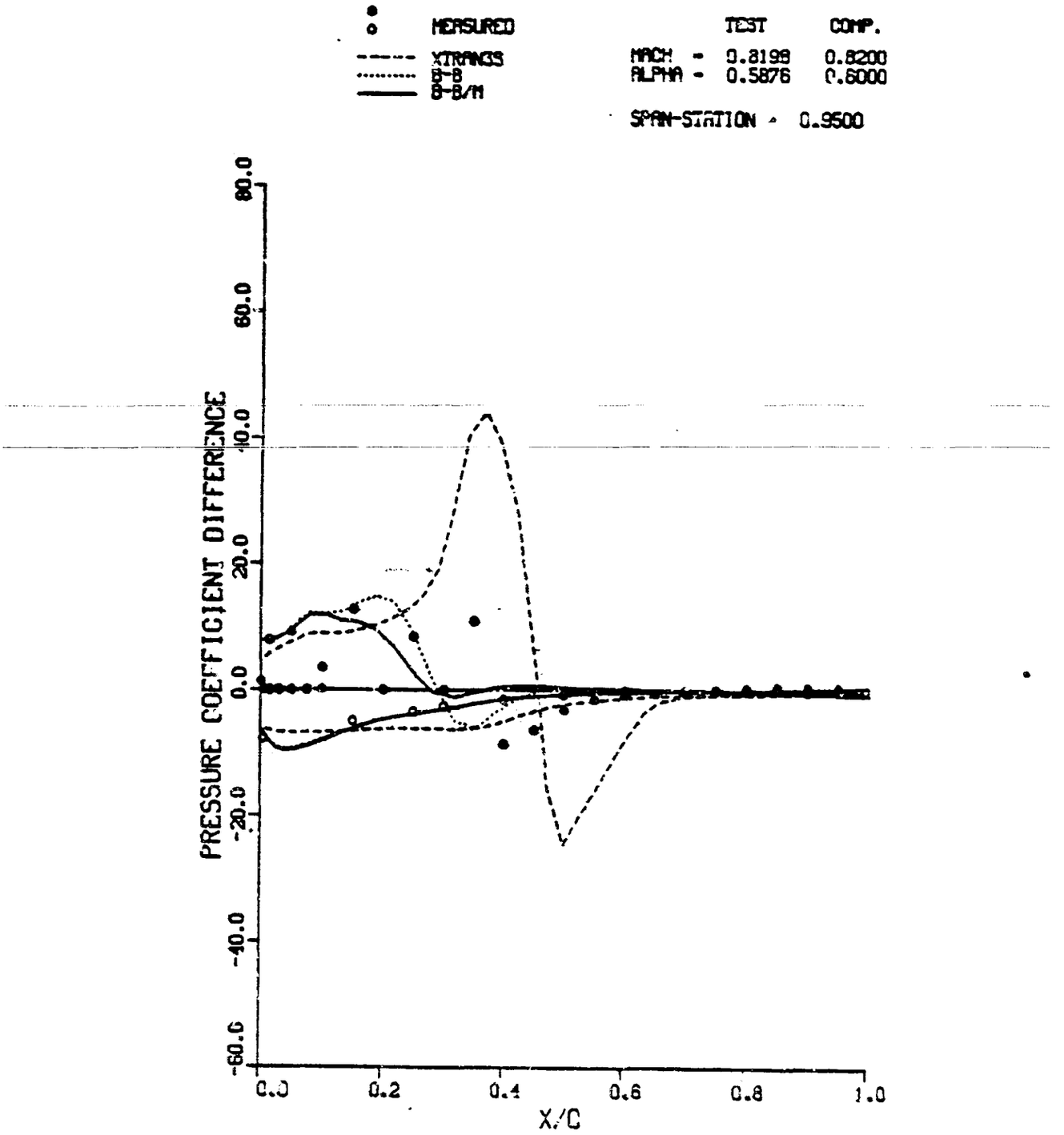

(f) SPAN-STATION = 0.950

Figure 31. Comparison of Computed and Measured Quasi-Steady Pressure Difference at Several Span-Stations (Sheet 6 of 6)

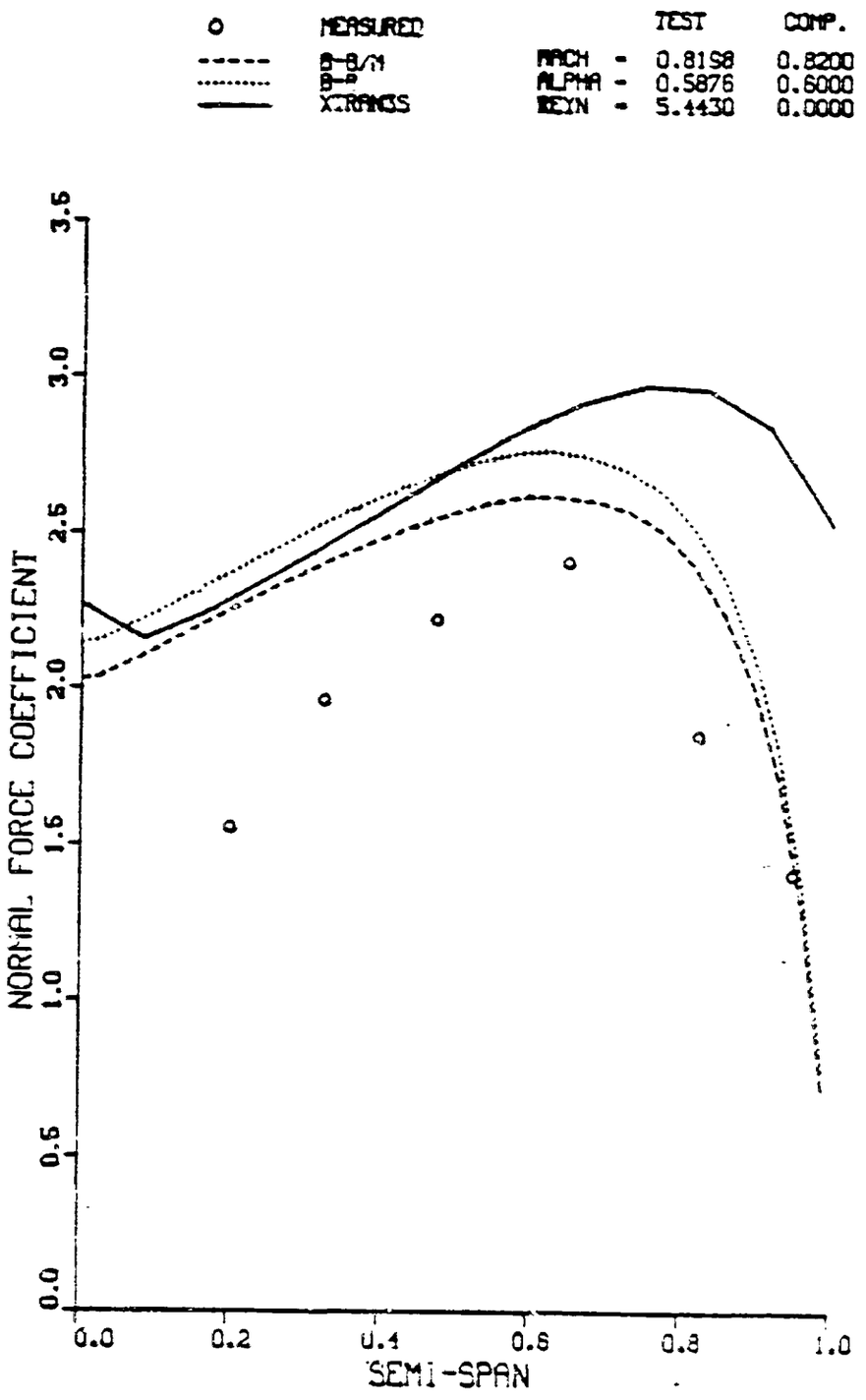

Figure 32. Comparison of Computed and Measured Quasi-Steady Span-Loading

*USGPO: 1983-659-062-1011